# Adaptive CFAR PN Code Acquisition for DSSS Systems

A thesis

By

**Bin Wei**

Director of Studies

**Dr. Mohammad Sharif**

Second Supervisors

**Dr. David Binnie**

**Prof. Abid Almaini**

School of Engineering and Building Environment

Napier University, Edinburgh

March 2008

# ABSTRACT

The communication between transmitter and receiver in Direct Sequence Spread Spectrum (DSSS) systems starts with synchronisation, which can be carried out in two steps: *acquisition* and *tracking*. Acquisition is the coarse searching of the delay of PN code in transmitted signal, and tracking is to find the exact delay of PN code in transmitted signal and maintain the alignment of the two PN codes.

This thesis "*Adaptive PN code Acquisition for DSSS Systems*" presents research on PN code acquisition in DSSS systems. The research focused on the adapitve threshold optimisation with Constant False Alarm Rate (CFAR) techniques in different noise background. Both homogeneous and non-homogeneous noise background are analysed to check the performance of different CFAR techniques, in the terms of Probability of detection ( $P_d$ ), Probability of false alarm ( $P_{fa}$ ) and Mean Acquisition Time (MAT). The limitations of general CFAR techniques in non-homogeneous noise background are disclosed in the research, and adaptive censoring technique is applied into general CFAR techniques, showing significant improvement in performance. In the research, MATLAB is used for mathematical simulations, and Monte Carlo simulation is used for independent validation of the theoretical results obtained. ISE, Modelsim, and System generator are used for the hardware implementation in Field Programmable Gate Array (FPGA).

Results show that all the kinds of CFAR techniques perform well in homogeneous noise background, with high $P_d$ and short MAT, however, the general CFAR techniques without automatic censoring suffer serious degradation in non-homogeneous noise background. In this thesis, after disclosing the limilation of general CFAR techniques, Greatest-Of/ Smallest-Of CFAR (GO/SO-CFAR) was introduced to solve the problem in non-homogeneous noise background. The simulation results show that GO/SO-CFAR has much better performance than the general CFAR in non-homogeneous noise background, especially in noise background with high interferences, GO/SO-CFAR can maintain high $P_d$ and short MAT. FPGA is used to analyse the complexity of achievement for GO/SO-CFAR detector, and the results illustrate that GO/SO-CFAR is only slightly more complex and slower than the CA-CFAR and OS-CFAR detectors. Therefore, GO/SO-CFAR is much more suitable than general CFAR techniques in non-homogeneous noise background, when the noise condition is unknown.

# DECLARATION OF ORIGINALITY

I hereby declare that this thesis together with the work contained was composed and originated entirely by myself except where due acknowledgement to others has been made.

Edinburgh, UK

March 2008

Bin Wei

# ACKNOWLEDGEMENT

First, I wish to give thanks to my father Mr. Hanqi Wei and my mother Mrs. Guizhu Yu. They gave me the best upbringing and the sweetest family I could ever wish for. In the last 20 years of my study, they worked hard to support me, and encouraged me when I was frustrated.

I also would like to thank my Director of studies, Dr. Mohammad Y. Sharif for the help since my study in MSc in Napier University. He gave me direction in the beginning of my research for PhD and lots of support and encouragement. Also, I would like to thank Dr. David Bennie and Prof. Abid Almaini for their support to my research work.

This is also an opportunity for me to give thanks to my wife Mrs. Mingjia Liu. During the past three years of my research, she made her best to support me, and made the life much easier for me. Also, thanks to all my friends in Edinburgh, you are important in my life.

Finally, I would like to acknowledge that my research programme was fully funded by Napier University. And I also received lots of help and support from the staff of the University.

# LIST OF ABBREVIATIONS AND SYMBOLS

| | |
|---|---|
| $A$ | Amplitude of signal |
| ADT | Average Detection Threshold |
| AMPS | Advanced Mobile Phone System |
| ASIC | Application-Specific Integrated Circuits |
| AWGN | Additive White Gaussian Noise |
| $B$ | Bandwidth |
| BER | Bit-Error Rate |
| BPF | Band-Pass Filter |
| BPSK | Binary Phase Shift Keying |
| $C$ | Channel capacity |
| CA-CFAR | Cell-Averaging CFAR |
| CDF | Cumulative Density Function |
| CDMA | Code Division Multiple Access |
| CDMA2000 | 3G standard for North America |
| CFAR | Constant False Alarm Rate |
| CNR | Clutter-to-thermal Noise Ratio |
| COTS | Commercial Off-The-Shelf |
| CST | Chi-Square Target |
| CUT | Cell Under Test |
| $c(t)$ | Spreading signal |
| DLL | Delay Lock Loop |
| $d_o$ | Reference distance |
| DSP | Digital Signal Processing |

| | |
|---|---|
| DSSS | Direct Sequence Spread Spectrum |
| $\Delta$ | Signal delay time in channel |
| $\Delta_1$ | Hypothesised delay time at receiver |
| EDGE | Enhanced Data rate for GSM Evolution |
| $\varepsilon_r$ | Dielectric of free space |
| $f_c$ | Operation frequency |
| FCC | Federal Communications Commission |
| FDMA | Frequency Division Multiple Access |
| FHSS | Frequency-Hopping Spread Spectrum |
| FM | Frequency Modulation |
| FPGA | Field Programmable Gate Array |
| FSK | Frequency Shift Keying |
| $F_u$ | Frequency uncertainty |
| $\gamma(.)$ | Lower incomplete gamma function |
| $\Gamma(.)$ | Gamma function |
| GO-CFAR | Greatest-Of CFAR |
| GO/SO-CFAR | Greatest-Of/Smallest-Of CFAR |
| GPRS | General Packet Radio Service |
| GSM | Global System for Mobile communications |
| 1G | First Generation |
| 2G | Second Generation |
| 3G | Third Generation |
| $H_0$ | No target present |
| $H_1$ | Target present |

| | |
|---|---|
| I.I.D | Independent and Identically Distributed |
| I-Q | In-phase and Quadrature-phase |
| IMT-2000 | International Mobile Telecommunication 2000 |
| INR | Interference-to-thermal Noise Ratio |
| I/O | Input and Output |
| ISDN | Integrated Services Digital Network |
| ISM | Industrial, Scientific, and Medical |
| IS-95 | Interim Standard 95 (first CDMA standard) |
| $K$ | Power ratio in specular component to multi-path components |
| $L$ | Order of M-sequence |
| LOS | Line-Of-Sight |
| $\lambda$ | Total noise power |
| MAI | Multiple Access Interference |
| MAT | Mean Acquisition Time |
| MF | Matched Filter |
| ML | Maximum-Likehood |
| M-sequence | Maximum-length sequence |
| MSB | Most Significant Bit |
| $N$ | Length of PN code sequence ( Length of reference window for CFAR detectors) |
| NLOS | Non-Line-Of-Sight |
| NMT | Nordic Mobile Telephone |
| OEM | Original Equipment Manufacturer |
| OS-CFAR | Order-Statistics CFAR |

| | |
|---|---|
| PN | Pseudo-Noise |
| PTSN | Public Switched Telephone Networks |
| $P_d$ | Probability of detection |
| $P_{dc}$ | Probability of clutter edge detection |
| $P_{fa}$ | Probability of false alarm |
| $P_{fc}$ | Probability of false alarm in clutter edge detection |
| $P_m$ | Probability of miss |
| $pn_i$ | Received PN code sequence |
| $pn_j$ | Locally generated PN code sequence |
| $r$ | Number of interfering targets |
| RASE | Rapid Acquisition by Sequential Estimation |
| $R_a(\tau)$ | Autocorrelation value |
| $r_{a,a}(\tau)$ | Continuous-time periodic autocorrelation function of c(t) |
| $R_c(\tau)$ | Cross-correlation value |
| RF | Radio Frequency |
| RSC | Radar Cross-Section |
| $r(t)$ | Received signal |
| SNR | Signal-to-Noise Ratio |
| SO-CFAR | Smallest-Of CFAR |
| SRG | Shift Register Generator |
| SS | Spread Spectrum |
| $\sigma$ | Absolute value of the specified standard deviation |
| $T$ | Scaling factor for CFAR detectors |

| | |
|---|---|
| THSS | Time-Hopping Spread Spectrum |
| TDMA | Time Division Multiple Access |
| $T_c$ | Chip duration |
| $t_d$ | Dwell time |
| $T_h$ | Detection threshold |
| $T_k$ | Scaling factor for clutter edge detection |
| $T_u$ | Time uncertainty |
| $\tau$ | Delayed phase in channel |
| $\tau_1$ | Hypothesised phase on receiver |
| UMTS | Universal Mobile Telephone System |
| $\mu$ | Variance of noise |
| VHDL | Very High Speed Integrated Circuit Description Language |
| VSAT | Very Small Aperture Terminal |
| $W$ | Number of uncertainty cells |
| W-CDMA | Wideband CDMA |
| WGN | White Gaussian Noise |
| $x(t)$ | Transmitted signal |
| $y$ | Output of correlator |

# TABLE OF CONTENTS

# LIST OF FIGURES

## LIST OF TABLES

# CHAPTER 1

## General Overview

### 1.1 General introduction about wireless communications

Communication is the process of transmission of information from one point to another, normally named transmitter and receiver. The information transmitted can be analogue or digital depending on different types of communication. The message is transmitted through a channel. This could be wire between the transmitter and receiver, just like in Public Switched Telephone Networks (PTSN) system. Also, the channel can be free space between the transmitter and receiver, i.e. wireless channel. Wireless communication has been growing rapidly in the past decade, as the techniques in Digital Signal Processing (DSP), digital Radio Frequency (RF) and circuit integration significantly advanced.

As the number of users increasing, the wireless communication industry faces some challenges in quality of services. While most of the services being demanded are still voice, there is a growing need in multimedia services. Based on the additional services, the International Telecommunications Union laid out the framework of the third generation of mobile systems (3G) under the umbrella of International Mobile Telecommunication 2000 (IMT-2000) [1-2].

The first generation wireless telephone technology (1G) is analogue cell phone standard. It is firstly developed in the late 1970's. One of 1G standard is Nordic Mobile Telephone (NMT), used in Nordic countries, Eastern Europe and Russia. Another is Advanced Mobile Phone System (AMPS) used in the United States. 1G system is based on Frequency Division Multiple Access (FDMA), in which the available frequency spectrum is divided among the users. The second generation of mobile system (2G) is digital, and this is the main difference between the 1G and 2G [3]. 2G techniques are divided into two types of standards: Time Division Multiple Access (TDMA)-based or Code Division Multiple Access (CDMA)-based. Global System for Mobile communications (GSM) is a TDMA-based technique, it is originally from Europe, but later it is used worldwide. The CDMA technique was firstly commercialised by Qualcom®. In CDMA, instead of dividing the time or frequency spectrum, all users are allowed into the same spectrum but with different Pseudo-Noise (PN) code. This means that the users interfere with each other in the system, and the capacity is determined by the interference that the system can tolerate [4]. In [5], it shows that CDMA can provide much more capacity than FDMA and TDMA. Interim Standard 95 (IS-95) is the first CDMA system, which is used by Americas and parts of Asia. There are mainly two types of 3G standards, Universal Mobile Telephone System (UMTS) and CDMA2000. UMTS also known as Wideband CDMA (W-CDMA), is the solution generally preferred by countries that used GSM, centred in Europe. UMTS is managed by the 3GPP organization also responsible for GSM, General Packet Radio Service (GPRS) and Enhanced Data rate for GSM Evolution (EDGE). CDMA2000 is the standard in North America, which grew out of the earlier 2G CDMA standard IS-95 [1].

The development of spread spectrum technique makes CDMA possible. It is a technique that spread the information signal to a bandwidth in excess of the minimum bandwidth to

transmit that signal. Compared with the other techniques, CDMA has capacity advantage, however, it is challenging in implementation. *PN code synchronisation* and *power control* are the two important parts of CDMA implementation [6-9]. The implementation of PN code synchronisation is researched later in this thesis.

## 1.2 Advantage of digital communication Systems

Digital communications systems usually represent an increase in complexity over the equivalent analogue systems. Some of the reasons are listed to show why digital communication is better [10].

a) Increased demand for data transmission
b) Increased scale of integration, sophistication and reliability of digital electronics for signal processing, combined with decreased cost.
c) Facility to source code for data compression
d) Possibility of channel coding to minimise the effects of noise and interference
e) Ease with which bandwidth, power and time can be traded off in order to optimise the use of these limited resources.
f) Standardisation of signals irrespective of their type, origin or the services they support, leading to an Integrated Services Digital Network (ISDN).

## 1.3 Synchronisation in digital communication systems

Many of the digital communication systems need accurate synchronisation for correct operation. This means some locally generated parameters must be properly aligned to those in the received signal. Normally, the parameters include carrier frequency; carrier phase; bit duration; symbol time and so on [11]. These types of synchronisation are necessary in digital communication systems, as the output of the demodulator must be

sampled periodically in order to recover the transmitted information. Therefore, the synchronisation work in digital communication is actually to estimate the delay between the transmitter and receiver. Knowing the delay, the demodulator in receiver side can be sampled at the right sampling instant. For coherent communication, all the above types of synchronisation are necessary, especially for the carrier frequency and phase synchronisation. But for non-coherent communication systems, carrier phase synchronisation is not necessary.

There are two major ways to achieve synchronisation: *hardwire synchroniser* and *recovery synchroniser*. In hardwire synchroniser, there are two separate channels. One channel is used to transmit the information for demodulation of the received signal. Another channel is used to transmit the modulated signal. In recovery synchroniser, the information signal and reference information is transmitted together. In CDMA system with a hardwire synchroniser, the spread signal and PN code are transmitted in a different channels. Therefore, the PN code in spread signal and the separately transmitted PN code have same delay. The received signal can be directly despread with the received PN code to obtain the original information signal. However, the cost of such application will be expensive, because it can be considered as two separate communications. Also, it lacks security that the system was designed to achieve in the first place, as PN code is not masked [9]. To implement recovery synchroniser, the same PN code sets are generated at both transmitter and receiver. That is, an unmodulated PN signal is initially transmitted using a pilot channel, then the receiver synchronises the PN signal and the locally generated PN code. When the delay in the received PN signal is found, the locally generated PN code with same delay can be used to despread the received signal, and the original message can be recovered.

## 1.4 Motivation of this Thesis

There are already extensive publications about PN code acquisition, and the studies were based on different methods for performance improvement. Some of the published results are based on the search strategy: serial, parallel or hybrid search schemes. In terms of trade-off between complexity and acquisition speed, parallel approach is the fastest of all the three search schemes, but it has highest complexity. Serial search is the one with the lowest complexity, thus it is suitable for portable equipments [9]. The number of dwells is another important issue in many studies. In a multiple dwell search, multiple tests of the phase are performed before the declaration of the acquisition. It is quite similar as the serial, parallel, and hybrid search schemes in the trade-off between complexity and acquisition [10]. Many of the other publications are about the estimation of noise in channel for wireless communications. Noise always affects signal transmission over channel. If fixed threshold is applied without knowing the magnitude of noise in channel, it will leads to either bigger Probability of false alarm ( $P_{fa}$ ) or lower Probability of detection ( $P_d$ ). Constant False Alarm Rate (CFAR) is very popular in the field of radar detection. In CFAR detectors, the threshold is adaptively set up by estimating the noise level in the channel. This can be found by taking a block of cells around the Cell Under Test (CUT) and calculating the average power in a mean level detector like, Cell-Averaging CFAR (CA-CFAR). Many other CFAR techniques have been developed, like Order-Statistics CFAR (OS-CFAR), Greatest-Of CFAR (GO-CFAR) and Smallest-Of CFAR (SO-CFAR) [12-15]. The differences between them are in the method of noise level estimation.

Noise background is a quite important factor in wireless communication channel. Basically, there are two types of noise background: homogeneous and non-homogeneous.

In homogeneous noise background, with constant Additive White Gaussian Noise (AWGN), many types of CFAR techniques were proved effective [15-16]. Non-homogeneous noise background is much more complex than homogeneous noise background; however it is more likely to exist in real communication channel. Therefore, the many studies relate to PN code acquisition are for non-homogeneous noise background [14, 17-19]. Multiple targets and clutter noise are the two types of non-homogeneous noise background. Multiple targets are caused by multiple paths in communication, with different delays in different paths, there will be more correlation peaks, and they will affect the correct PN code detection. Clutter is represented by returns from diffuse features, and when trying to find a target return in clutter area, the clutter acts as noise. Therefore, in transmission with clutter noise, some output from the correlator are with higher Signal-to-Noise Ratio (SNR). Except CA-CFAR, all the other CFAR techniques are aimed to solve problems caused by non-homogeneous background, like OS-CFAR is developed for multiple targets environment, and GO-CFAR and SO-CFAR are for clutter environment. However, they can not maintain at a high level of $P_d$ and Mean Acquisition Time (MAT) for all the situations [17]. In the multiple target environment, the number of interfering targets will affect the performance of CFAR detectors, and in clutter environment, the performance of CFAR detectors is highly dependent on the position of clutter edge.

The objectives of the research works in this thesis are shown in the figure 1.1, illustrating how the objectives were developed.

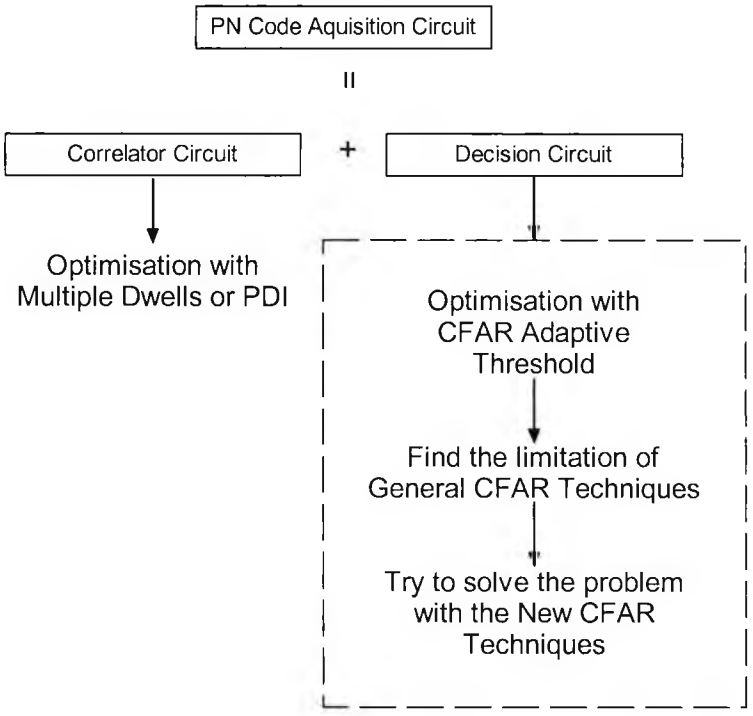


Figure 1.1: Research objectives in PN code acquisition

PN code acquisition circuit has two parts: correlator circuit and decision circuit, both can be optimised with different methods. Correlator circuit can be optimised with multiple dwells or Post Detection Intergration (PDI) as shown in my friend Obiebi's thesis [36]. My research focused on the decision circuit, because general CFAR techniques suffer poor performance in non-homogeneous noise background, some other techniques are needed to solve the problem.

The main aim of this thesis is to design a CFAR technique that will automatically change the method of noise level estimation for different noise background. For this kind of CFAR technique, clutter edge detection is needed, in which the CFAR detector will automatically censor the cells with different SNR as the CUT. The clutter edge detection technique is firstly referred in [20], where the CFAR technique use clutter edge detection is called GO/SO-CFAR. Considering the acquisition speed and the complexity of

application in Field Programmable Gate Array (FPGA), GO/SO-CFAR detector is much better than other CFAR detectors for mobile communication channels with unknown noise conditions.

## 1.5 Contribution of this Thesis

In order to study the performance of CFAR detectors in PN code acquisition, the theory of PN code acquisition was studied, and the circuits of CFAR detectors were modelled mathematically. The communication channels for performance analysis were separated as homogeneous noise background and non-homogeneous noise background. Non-homogeneous noise background is where we should pay attention to, as multiple targets or clutter noise exist in this background. The equation for $P_d$, $P_{fa}$ and MAT of CFAR detectors were derived for both homogeneous and non-homogeneous noise background, and simulations were carried for different parameters. Numerical results showed that in homogeneous noise background all the general CFAR detectors like CA-CFAR, OS-CFAR have good performance. However, in non-homogeneous noise background all the CFAR detectors without adaptive censoring suffer rapid degradation in $P_d$ and MAT. Knowing the limitation of general CFAR techniques, GO/SO-CFAR technique with adaptive censoring is introduced to solve the problem, and the circuit was mathematically modelled. The sets of equations for GO/SO-CFAR detector in non-homogeneous noise background were derived. The simulation results indicated that GO/SO-CFAR detector can maintain good performance in non-homogeneous noise background with unknown noise condition, and it is especially suitable for background strong interfering targets. From industrial point, the complexity and cost of realisation the circuit is another important factor. Therefore, the implementation of GO/SO-CFAR circuit in FPGA was also carried out in this thesis with detailed structure analysis, and

results indicated that GO/SO-CFAR is not complex and expensive in implementation. From academic point of view, this thesis will present the reader with an understanding of how to carry out mathematical analysis of a circuit and how it can be implemented into hardware. Also, some research topics were shown at the end of the thesis, which can give the reader some direction for research works.

# CHAPTER 2

## Spread Spectrum and CDMA

### 2.1 History of Spread Spectrum

Spread Spectrum (SS) was firstly described in 1941. It has been used in military systems since 1950s. The initial commercial use of SS began in the 1980s in USA with three systems: Equatorial Communications System's Very Small Aperture Terminal (VSAT) system for newspaper newswire services, Del Norte Technology's radio navigation system for navigation of aircraft for crop dusting and similar applications, and Qualcomm's OmniTRACS system for communications to trucks. Later in the 1980s, the US Federal Communications Commission (FCC) opened the Industrial, Scientific, and Medical (ISM) frequency bands for unlicensed spreading spectrum communications and since then, SS has been widely used in wireless communication. In 1990s, the 2G standard IS-95 was applied in North America. This was the first standard of CDMA. In the year 2000, a historic decision was made, that the UMTS/IMT-2000 standard will be used in the 3G systems. And, it is expected to provide higher transmission rate than the 2G [7-8].

### 2.2 Basic concepts of Spread Spectrum

SS is apparent in the Shannon and Hartley channel-capacity theorem:

$$C = B \times \mathrm{Log}_2 (1+ S/N) \quad (2.1)$$

In (2.1), *C* is the Channel capacity in Bits Per Second (BPS), which is the maximum data rate for a theoretical Bit-Error Rate (BER). *B* is the required channel bandwidth in Hz, and S/N is the SNR. To be more explicit, one assumes that *C*, which represents the amount of information allowed by the communication channel, also represents the desired performance. Bandwidth (*B*) is the price to be paid, because frequency is a limited resource. S/N ratio expresses the environmental conditions [9, 21].

An elegant interpretation of this equation, applicable for difficult environments (low S/N ratio caused by noise and interference), says that one can maintain or even increase communication performance (high *C*) by allowing or injecting more bandwidth (high *B*), even when signal power is below the noise floor. Modify the above equation by changing the log base from 2 to *e* (the Napierian number), and by noting that $\mathrm{Ln} = \mathrm{Log}_e$:

$$C/B = (1/\mathrm{Ln}2) \times \mathrm{Ln}\,(1+S/N) = 1.443 \times \mathrm{Ln}(1+S/N) \quad (2.2)$$

Applying the MacLaurin series development for

$$\mathrm{Ln}\,(1+x) = x - x^2/2 + x^3/3 - x^4/4 + \ldots + (-1)^{k+1}x^k/k + \ldots: \quad (2.3)$$

Equation (1.2) can be written as

$$C/B = 1.443 \times (S/N - 1/2 \times (S/N)^2 + 1/3 \times (S/N)^3 - \ldots) \quad (2.4)$$

S/N is usually low for SS applications. (As just mentioned, the signal power density can be even below the noise level.) Assuming a noise level such that S/N <<1, Shannon's expression becomes roughly:

$$C/B \approx S/N \quad (2.5)$$

To send error-free information for a given noise-to-signal ratio in the channel, therefore, we need only perform the fundamental SS signal-spreading operation: increase the transmitted bandwidth.

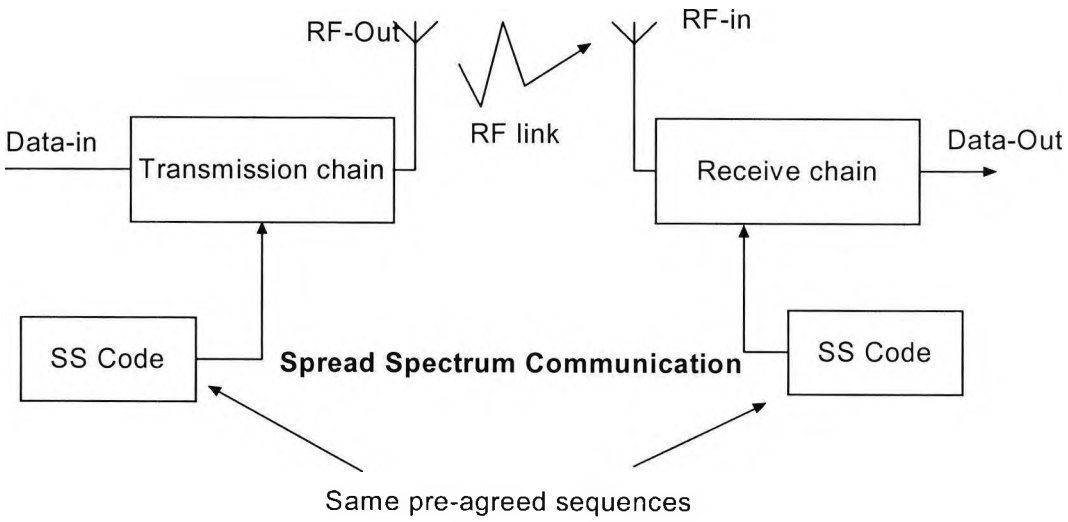


Figure 2.1: Block diagram of Spread Spectrum communication systems

Figure 2.1 shows the block diagram of SS communication systems. It shows that before the signal is transmitted by RF, the original data is spread by SS code, which is generally PN code. Because the PN code signal is much higher in frequency compared with the original data, the spread data will be much higher in bandwidth, this makes the transmitted signal resistant to noise and anti-jamming as shown in section 2.2.1. The effect of spreading is shown in figure 2.2, where the energy of the original data is spreaded over a bigger bandwidth after the spreading process.

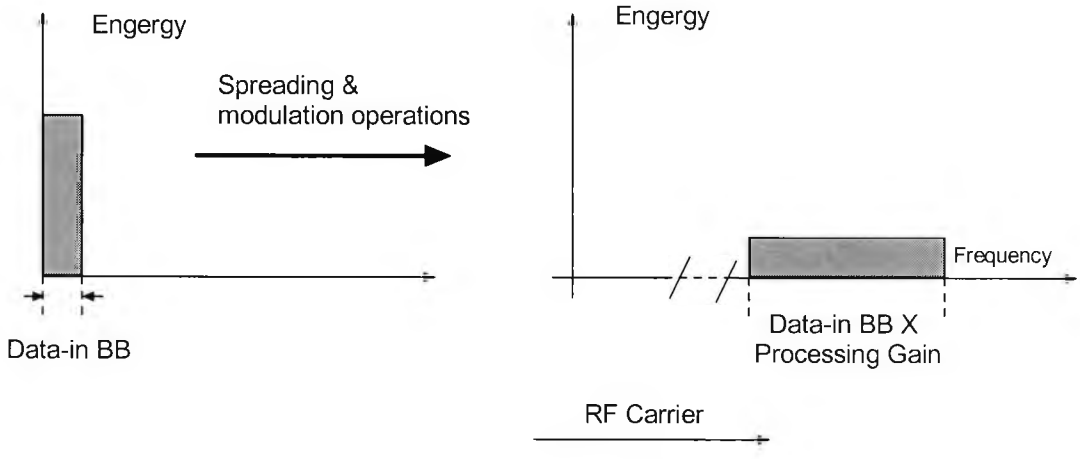


Figure 2.2: Spreading and modulation on transmitter side

On the receiver side, the same SS code can be used to despread the received data. The despreading process is shown in figure 2.3. The SS codes can be generated by same PN code generator on both transmitter and receiver sides, but to despread the received data correctly, the PN code used in spreading and despreading must be synchronised before the despreading process.

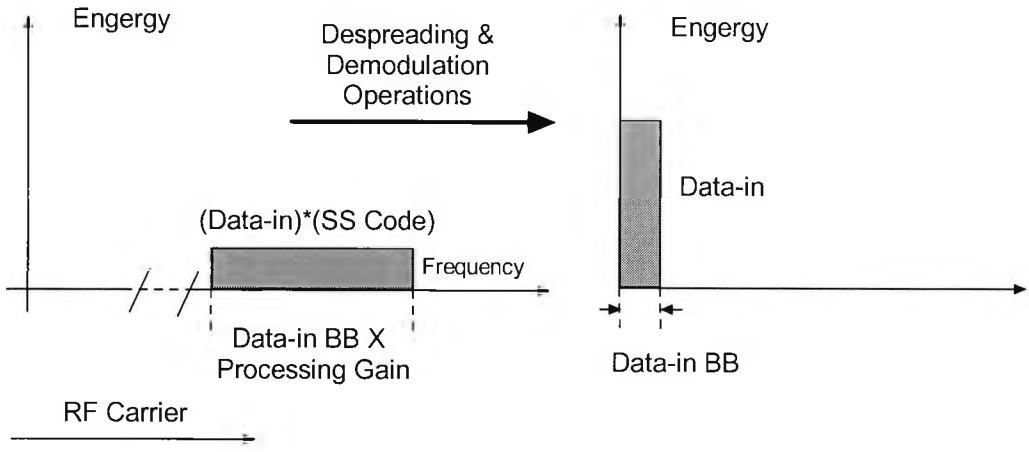


Figure 2.3: Despreading and demodulation on receiver side

### 2.2.1 Why Spread Spectrum

There are several advantages to using SS communication systems, mainly based on its characteristics of high security and immunity to interference [8].

a) Resistance of interference and anti-jamming

The characteristic of resistance of interference and anti jamming is the most interested advantage of SS systems. Because the interference and jamming don't have the spreading key, they will be rejected by the receiver. Figure 2.4 illustrates the rejecting of interference in SS systems, in this figure it can be observed that the noise-like spread signal which contains spreading key is restored after dispreading. And the interference from the channel is spread over a wide band with low energy density, which means nothing to the receiver.

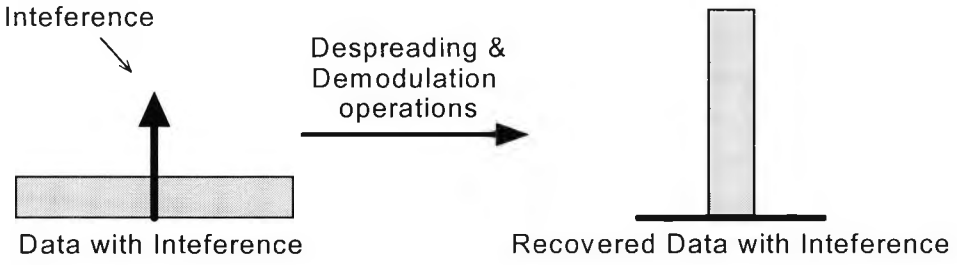


Figure 2.4: Resistance of interference in SS systems

b) Resistance to interception

Resistance to interception is another important advantage of SS system. Without the correct spreading key, the received signal is similar to noise. Also, as the energy of signal is spread over a wide band, the signal level can be below the noise level. This makes the communication invisible to the other receivers.

## 2.3 Different types of Spread Spectrum techniques

### 2.3.1 THSS

In Time-Hopping Spread Spectrum (THSS) communications, there is a short pulse named chirp. Chirps are transmitted either with a pseudorandom duration or position. Figure 2.5 shows the signal of THSS with equal chirp chip durations. In this method, the position of the chirp pulse is determined by a PN code generator, and each bit of the original data is transmitted as a short pulse. This technique seeks to accomplish uncertainty in the communication channel for any unwanted receiver by varying the time intervals between the transmitted pulses [9, 22].

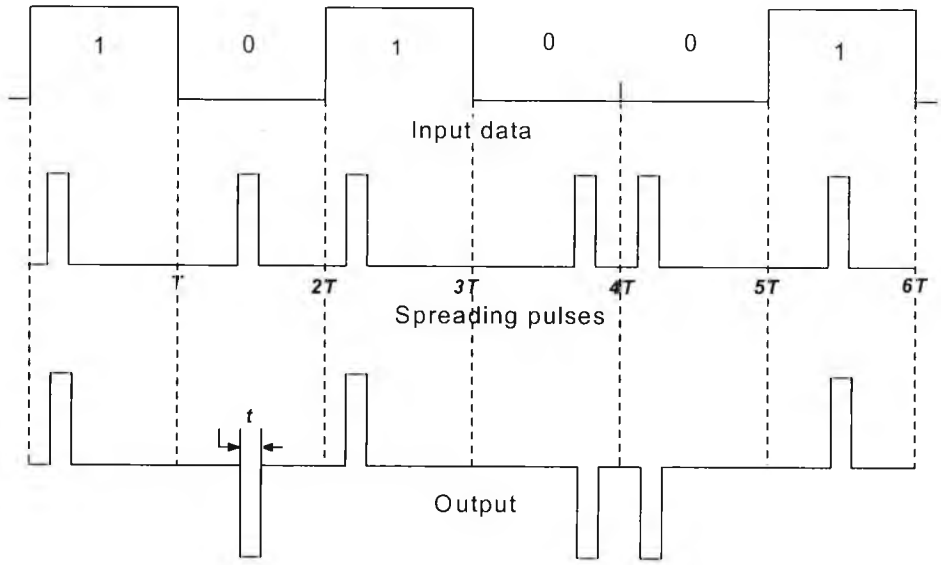


Figure 2.5: Time hopping method with equal chirp durations

In figure 2.6, it shows the method of THSS with different chirp durations. In this method, the starts of chirp pulses are same with the input bit. And the duration of each chirp pulse is determined by the PN code generator.

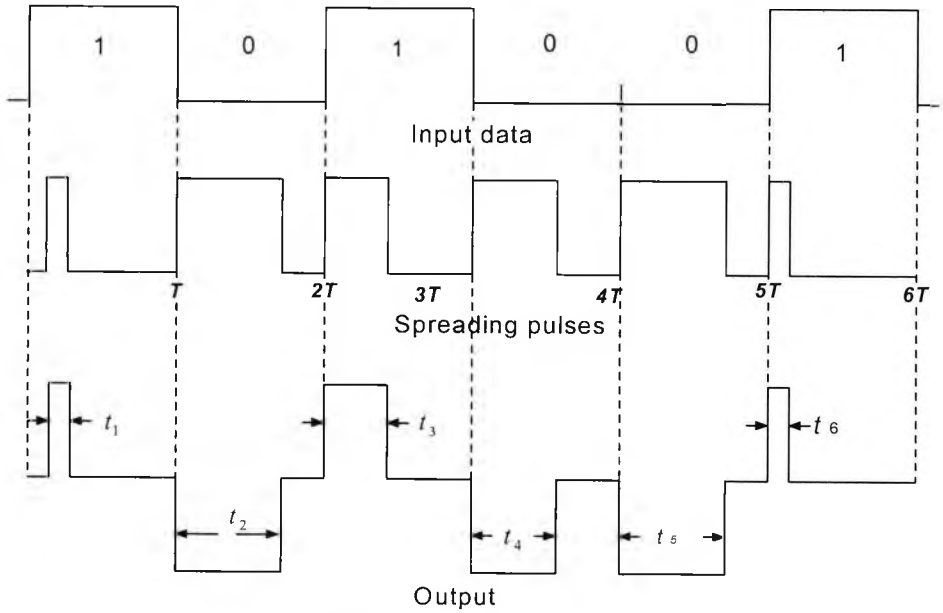


Figure 2.6: Time hopping method with varying chirp durations

### 2.3.2 FHSS

Frequency-Hopping Spread Spectrum (FHSS) is a method of transmitting radio signal by rapid switching of a carrier among frequency channels, using a pseudorandom sequence known to both transmitter and receiver [22]. In this method, Frequency Shift Keying (FSK) is used. Figure 2.7 and 2.8 demonstrate the block diagrams of FHSS transmitter and receiver.

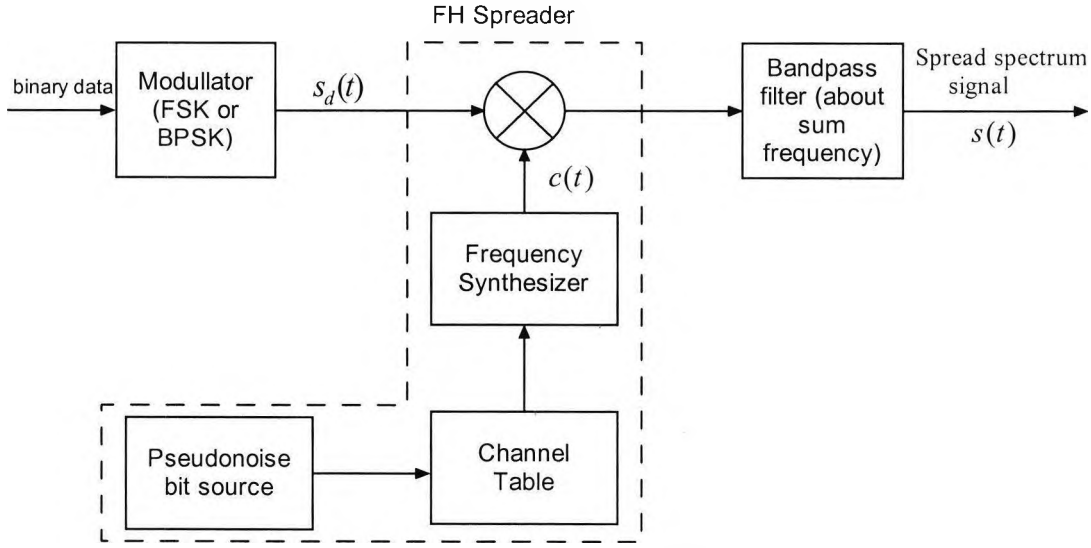


Figure 2.7: Block diagram for a FHSS transmitter

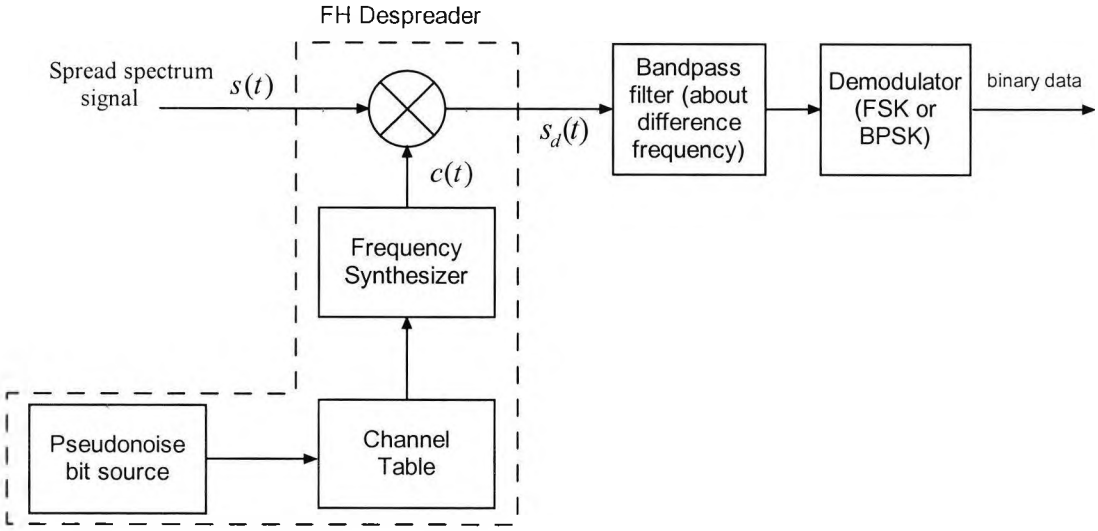


Figure 2.8: Block diagram for a FHSS receiver

There are the three important parameters for a FHSS system:

a) Hop set: This is the number of channels used by the system

b) Dwell time: This the length of time that the system transmits on a channel (frequency)

c) Hop rate: How fast the system changes from one frequency to another.

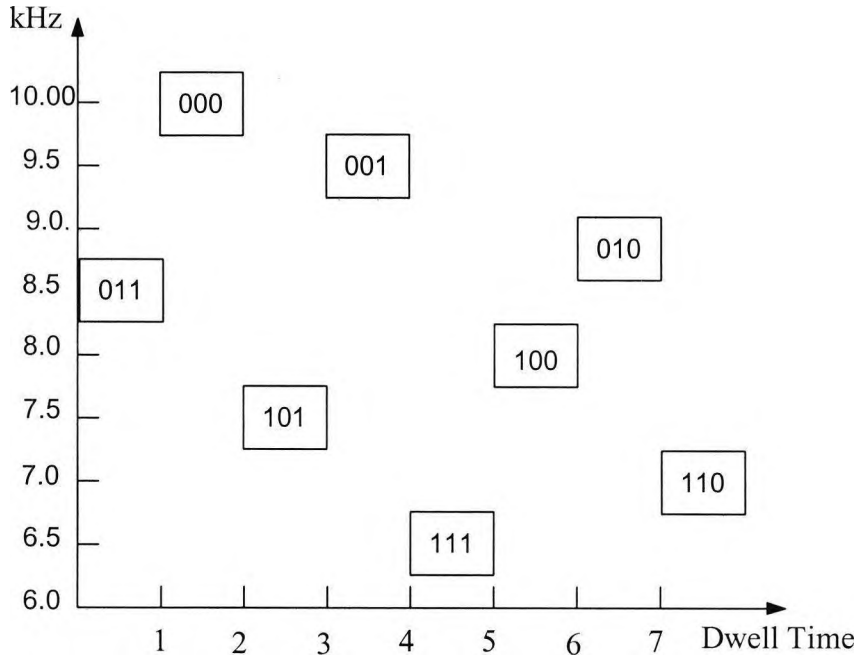


Figure 2.9: Frequency hopping system with 3-bit control codes

Figure 2.9 shows the FHSS systems with 3-bit PN code generator for hopping control. There are eight channels in this system, and the carrier frequency is 8 kHz. According to the control code, the receiver automatically switches the channels for communication.

### 2.3.3 DSSS

Direct Sequence Spread Spectrum (DSSS) is the best known SS technique. In DSSS, the widening of message bandwidth is accomplished by mixing the message with a pseudorandom signal which is much wider in bandwidth. This is the spreading process on the transmitter side, and at the receiver side, to demodulate the spread signal the receiver

must know the pseudorandom sequence. Figures 2.10 and 2.11 show the block diagrams of DSSS transmitter and receiver.

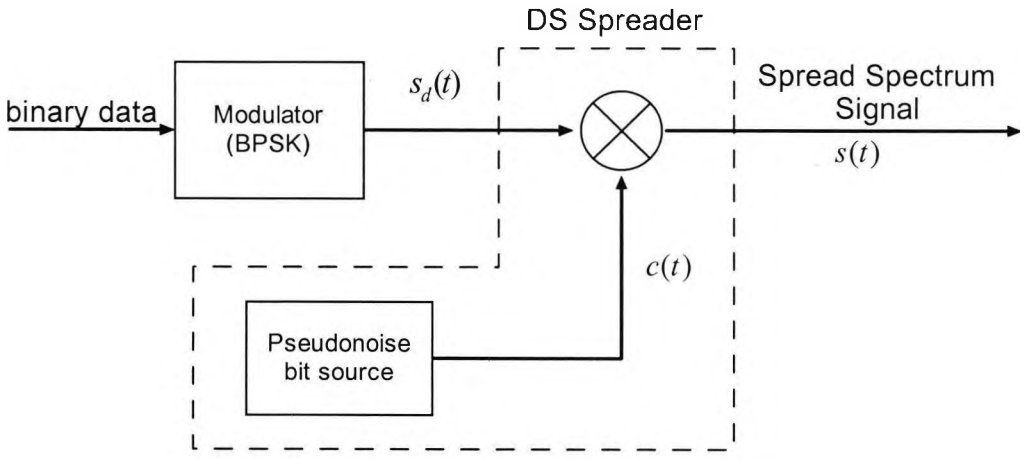


Figure 2.10: Block diagram of DSSS system transmitter

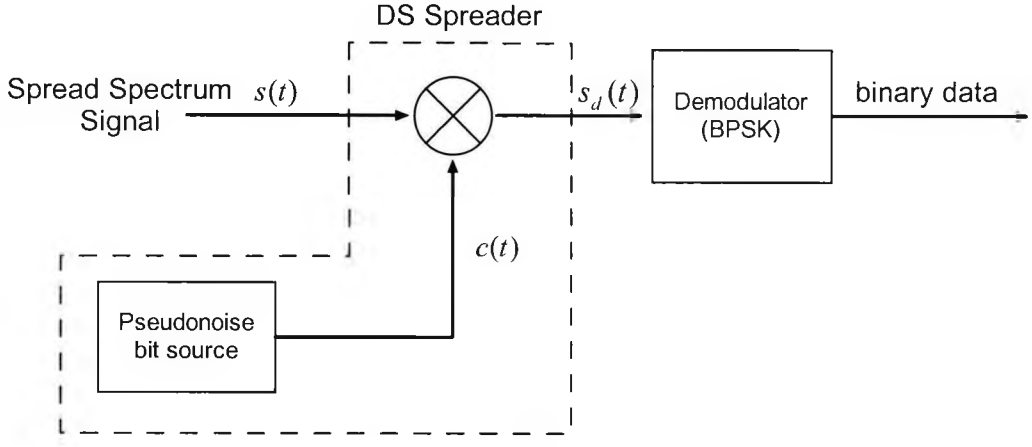


Figure 2.11: Block diagram of DSSS system receiver

In figure 2.12, it shows an example of spreading the original signal on the DSSS transmitter side.

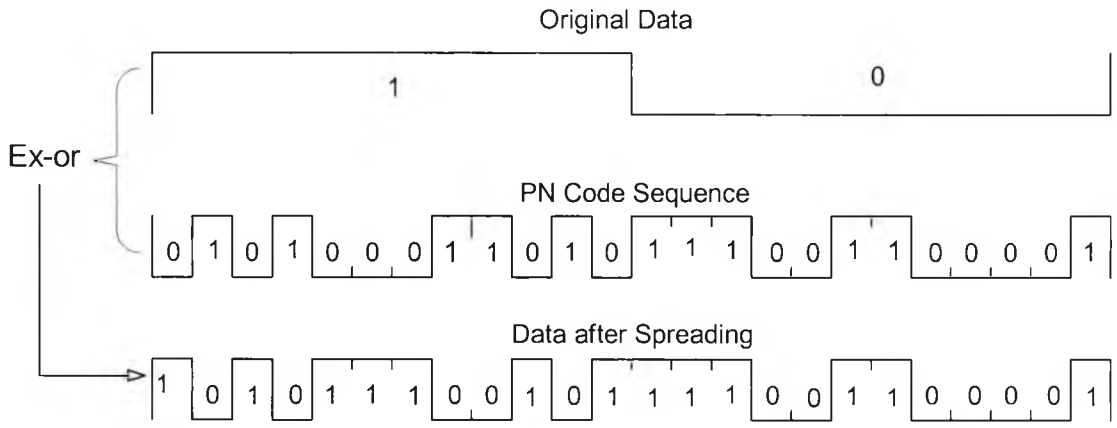


Figure 2.12: Spreading in DSSS transmitter

On the receiver side, knowing the PN code sequence, the original data can be restored by despreading (Ex-or the received signal and synchronised PN code sequence). Figure 2.13 shows the despreading process to restore the original data in figure 2.12.

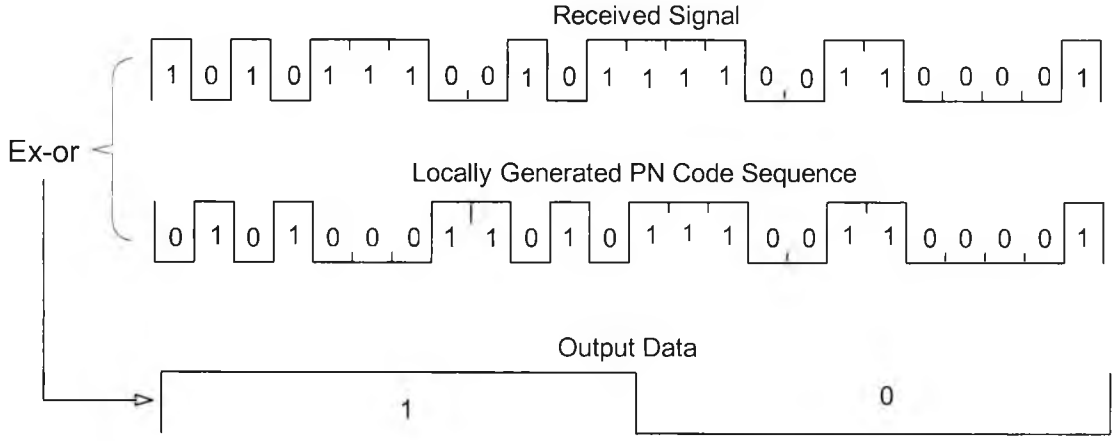


Figure 2.13: Despreading in DSSS receiver

### 2.3.4 Comparisons between FHSS and DSSS

The major disadvantage of THSS system is that code synchronisation takes a long time and it also needs a frequency synthesiser, which makes it more complex. So, in practice, THSS is not widely used. The following comparison is concentrated on the two most popular techniques: FHSS and DSSS.

Frequency hopping does not employ any processing gain, since there is no spreading of the signal. Processing gain, which provides the decrease in power density when a signal is despread, improves the received signal's SNR. Because FHSS does not use any processing gain, the frequency hopper needs to transmit using more power in order to have the same SNR as a DS radio. However, since the unlicensed RF bands have the same overall power limit defined for both types of radio, the FHSS systems cannot achieve the same SNR as DSSS system [22].

Using frequency hopping, it is also more difficult to synchronise the receiver to the transmitter because both the time and frequency need to be tuned. A direct sequence device on the other hand, needs only the timing of the chips to be synchronised. As a result, FHSS system must spend more time to search for the signal, and then lock on to it. This greatly increases the latency time between data transmissions.

Because DSSS systems can lock in the chip sequence in just a few bits, and only requires this exercise one time after power up, DSSS devices will have a much lower latency for all data transmissions. This lower latency is one of the reasons that DS provides higher bandwidth utilisation compared to FH systems.

## 2.4 Pseudo-Noise code

### 2.4.1 Noise-like code sequences

A PN code acts as a noise-like carrier used for bandwidth spreading of signal energy. It is like zero-mean White Gaussian Noise (WGN) with same power spectral density for all frequency. And the amplitude of a WGN has the Probability Density Function (PDF) as in equation (2.6) [23, 24]:

$$P = \frac{1}{\sigma\sqrt{2\pi}} e^{\left[-\frac{1}{2}\left(\frac{x}{\sigma}\right)^2\right]} \tag{2.6}$$

where σ is the absolute value of the specified standard deviation. Figure 2.14 illustrates the probability density of a WGN for varying amplitude with σ = 1.

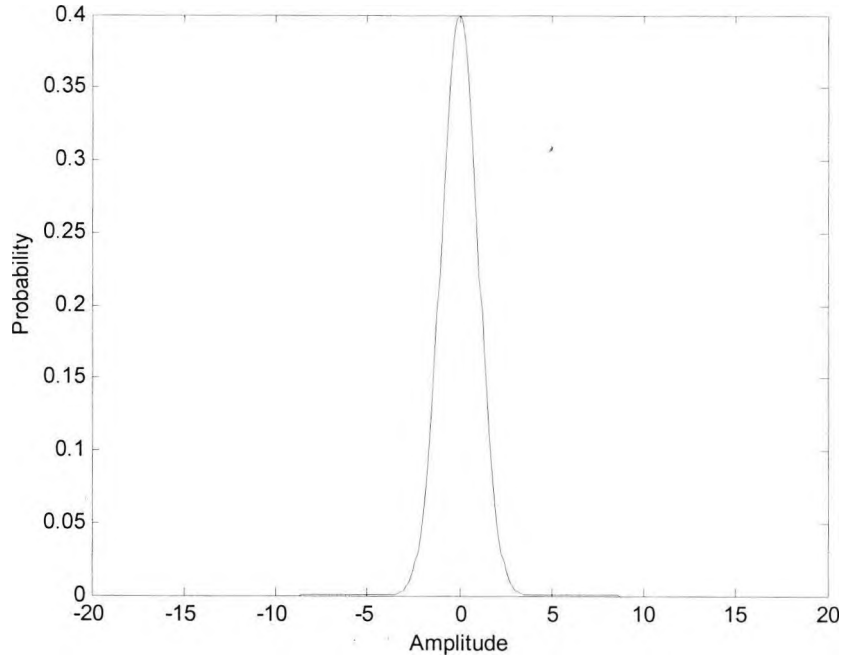


Figure 2.14: Probability density of a WGN in varying amplitude with σ = 1

The PN code is a Pseudo-Random sequence of 1s and 0s. It is not real random, because it is periodic and can be predicted if knowing how it is generated. In DSSS applications, the binary sequence with elements {0, 1} is mapped into a corresponding binary sequence with elements {-1, 1}.

### 2.4.2 Special properties of PN code sequences

There are some properties that PN code sequence follows [9, 25]:

a) Balance Property

For any period, the difference between the number of 1s and 0s should be at most one bit.

b) Run-length distribution

A run is a sequence of 1s or 0s. In each period of PN code sequence, one-half of the runs are 1 bit, about one-fourth of the runs are 2 bits, and one-eighth of those are 3 bits, etc.

c) Autocorrelation

The autocorrelation result of a PN code sequence is quite like that of a white noise, which is pulse like at synchronisation point and quite low at other condition.

$$R_a(\tau) = \int_{-NT_c/2}^{NT_c/2} pn(t).pn(t+\tau)dt \qquad (2.7)$$

Equation (2.7) shows the autocorrelation function. Autocorrelation is the process of correlate a single sequence with the delayed version of same sequence. For a PN code sequence *pn(t)*, if $\tau \neq NT_c$, the output would be best to be less than 1. But when $\tau = NT_c$, the output goes to maximum, which is the length of PN code sequence. The autocorrelation output of two PN sequences is in figure 2.15.

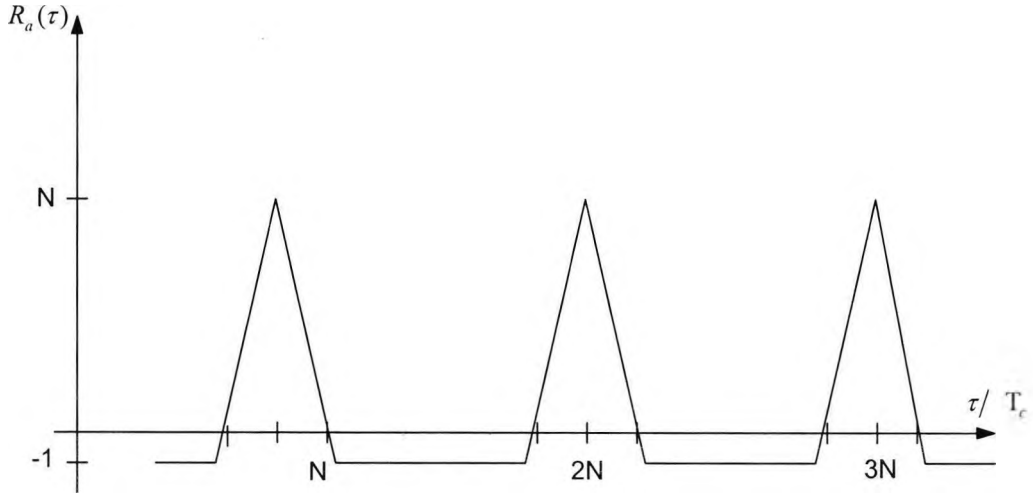


Figure 2.15: Autocorrelation output of two PN sequences

d) Cross-correlation

Cross-correlation is used to analyse the interference caused by other PN code sequence. Equation (2.8) can be used to measure the agreement between code $pn_i$ and $pn_j$.

$$R_c(\tau) = \int_{-NT_c/2}^{NT_c/2} pn_i(t).pn_j(t+\tau)dt \tag{2.8}$$

If for all $\tau$, $R_c(\tau)$ is zero, the two codes are called orthogonal. In some applications the cross-correlation properties of PN sequences are as important as the autocorrelation properties. For example, in CDMA communications, all users occupy same bandwidth and transmit simultaneous, if the codes used are not orthogonal, there will be interference between them. So, in practice, the maximum number of simultaneous users is limited.

### 2.4.3 Types of PN code sequences

It is very important to select a good PN code sequence for a DSSS system. The length of PN code determines the capacity of the system; also it will affect the speed of synchronisation. There are many different types of codes that are suitable for DSSS systems, and the most popular ones are Maximum-length sequence (M-Sequence) and Gold code [25-29]. The generation of PN code sequences are normally based on shift registers.

M-Sequences are with period of $2^L$-1, where $L$ denotes the order of the M-Sequence or the length of the shift register used in generator. M-Sequences have good property in autocorrelation, with peak value $2^L$-1, and -1 when not synchronised. Figure 2.16 shows the Shift Register Generator (SRG) for the M-Sequence.

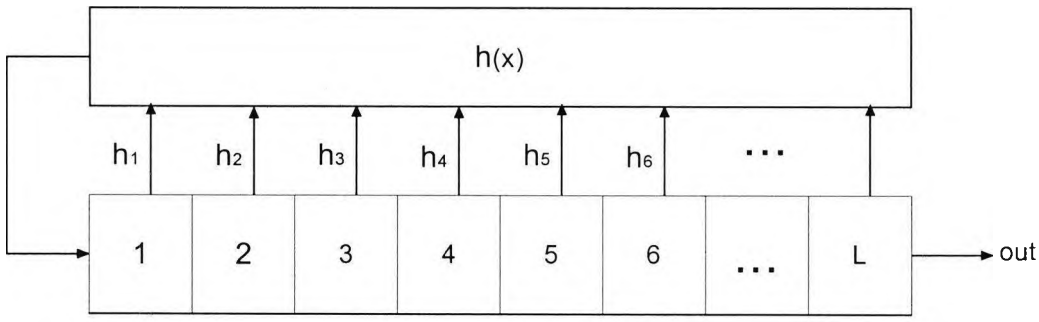


Figure 2.16: Shift register generator for M-Sequence [30]

The SRG implements a primitive polynomial *h(x)*:

$$h(x) = 1 + h_1 x + h_2 x^2 + \cdots + h_{L-1} x^{L-1} + x^L \tag{2.9}$$

In the polynomial *h(x)*, $h_i$ either takes value 1 or 0 depending on whether there is a feedback connection or not. So, the polynomial can be simply written as [$L$, $h_{(L-1)}$, ... , $h_{(1)}$], where the zero entries are not explicit, as no feedback exist on this tap.

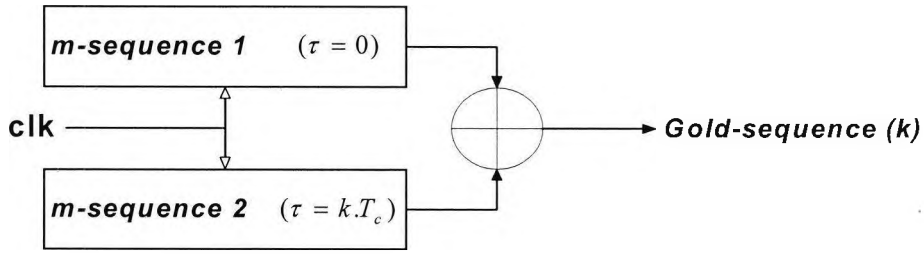


Figure 2.17: Gold-Sequence generator by two M-Sequences [30]

Generation of Gold code can be achieved by exclusive or-ing two M-Sequences with same length, also the two M-Sequences must be synchronised in clock phase. The length of the Gold code is the same as both M-Sequences, because it is obtained by adding two code sequences; also it is non-maximal, which makes it worse in autocorrelation. Because every change in the phase of the two M-Sequences will generated a new Gold code, for two M-Sequences with length $2^L$ -1, totally $2^L$+1 different Gold codes can be generated

including the two base M-Sequences. For large $N$ and $L$ odd, the maximum value of the cross-correlation function between any pair of Gold sequence is $R_{max} = \sqrt{2L}$. And for $L$ even, $R_{max} = \sqrt{L}$. Specified M-Sequences (called preferred M-Sequences) can be selected to generate Gold code with 3-value cross-correlations. The examples of preferred M-Sequences pairs are shown in table 2.1 [30]. Bound is the percentage of highest cross-correlation peak to the autocorrelation peak, it represents the probability for wrong detection. Therefore, for Gold sequence, bound is the lower the better.

Table 2.1: Preferred pairs of M-Sequences for Gold codes

| | $N_c = 2^L - 1$ | Preferred pairs of M-Sequences | 3- value Cross-correlations | | | bound |
|---|---|---|---|---|---|---|
| 5 | 31 | [5,3] [5,4,3,2] | 7 | -1 | -9 | -29% |
| 6 | 63 | [6,1] [6,5,2,1] | 15 | -1 | -17 | -27% |
| 7 | 127 | [7,3][7,3,2,1] [7,3,2,1][7,5,4,3,2,1] | 15 | -1 | -17 | -13% |
| 8 | 255 | [8,7,6,5,2,1][8,7,6,1] | 31 | -1 | -17 | +12% |

## 2.5 Summary

In this chapter, SS communications and CDMA were introduced. Three different types SS named THSS, FHSS and DSSS were briefly explained and compared. The application of SS in commercial mobile communications in the form known as CDMA was briefly discussed. The importance of PN code in SS systems is stated, and the different types of PN codes and their generation method are explained. Code synchronisation between the received and locally generated PN code will be introduced in chapter 3.

# CHAPTER 3

## PN Code Acquisition

### 3.1 Introduction

All spread spectrum techniques require the timing information of the transmitted signal to be obtained in order to despread the received signal and demodulate the despread signal. For a DSSS system, if it is not aligned even by single chip duration, it will be unable to despread the received spread spectrum signal, since the spread sequence is designed to have a small *out-of-phase* autocorrelation magnitude. Therefore, the process of acquiring the timing information of the transmitted spread spectrum signal is essential to the implementation of any form of spread spectrum technique [31].

Usually the problem of timing synchronisation is solved via a two-step approach:

- *Code acquisition (coarse acquisition or coarse synchronization)*: Synchronizes the transmitter and receiver to within an uncertainty of $\pm Tc$.
- *Code tracking*: Performs and maintains fine synchronization between the transmitter and receiver.

Given the initial acquisition, code tracking is a relatively easy task and is usually accomplished by a Delay Lock Loop (DLL) [9]. The tracking loop keeps on operating

during the whole communication period. If the channel changes abruptly, the DLL will lose track of the correct timing and initial acquisition will be re-performed. Sometimes, initial code acquisition is performed periodically no matter whether the tracking loop loses track or not.

Compared to code tracking, code acquisition in a spread spectrum system is usually very difficult. First, the timing uncertainty, which is basically determined by the transmission time of the transmitter and the propagation delay, can be much longer than a chip duration. As initial acquisition is usually achieved by a search through all possible phase delays of the sequence, a larger timing uncertainty causes a larger search area. Beside timing uncertainty, we may also encounter frequency uncertainty which is due to Doppler shift and mismatch between the transmitter and receiver oscillators. Thus, this necessitates a two-dimensional search in time and frequency. Moreover, in many cases, initial code acquisition must be accomplished in low signal-to-noise-ratio environments and in the presence of jamming. The possibility of channel fading and the existence of multiple access interference in CDMA environments can make initial acquisition even harder to accomplish [9-11].

Considering that BPSK is used in spreading and period of the T, we can express the transmitted spread spectrum signal as $\sqrt{2P}c(t)$, where *c (t)* is a periodic spreading signal given by

$$c(t) = \sum_{l=-\infty}^{\infty} c_l p_T(t - lT_C) \tag{3.1}$$

Where $c_l$ is the components of $c(t)$, and $P_T$ is the power of it. Neglecting the present of noise in channel, the received signal is given by (3.2), which is delayed version of transmitted signal with delay time $\Delta$.

$$r(t) = \sqrt{2P}c(t-\Delta) \tag{3.2}$$

The receiver hypothesized a phase $\Delta_1$ for the despreading sequence generator. The signal for despreading can be expressed as $c(t-\Delta_1)$. Since only initial acquisition is needed, $\Delta_1$ is the integer times of the chip duration $T_c$. Multiplying the received signal and the despreading signal, the despread signal can be written as $\sqrt{2P}c(t-\Delta)c(t-\Delta_1)$.

Integrate the despread signal for $T$ seconds, and use the square of the integrated value as decision statistic, the decision statistic becomes

$$z = \frac{1}{2T^2}\left|\int_T \sqrt{2P}c(t-\Delta)c(t-\Delta_1)dt\right|^2$$

$$= \frac{P}{T^2}\left|r_{a,a}(\Delta-\Delta_1)\right|^2 \tag{3.3}$$

In (8), $r_{a,a}(\tau)$ is the continuous-time periodic autocorrelation function of spreading signal $c(t)$, where $\tau$ equal to $|\Delta-\Delta_1|$. For an M-Sequence with period $T = NT_c$, where $N$ is the length of PN code, the result continuous-time periodic autocorrelation is

$$r_{a,a}(\tau) = \begin{cases} T-(N+1)\tau & for \quad \tau < T_c \\ -T_c & for \quad \tau \geq T_c \end{cases} \tag{3.4}$$

From equation (3.4), it is easy to note that when $\tau = 0$, the decision statistic has a maximum output $T$, and when the $\tau$ is bigger than $T_c$, the output is very small.

Figure 3.1 shows the stage diagram of for PN code acquisition. The received signal $r(t)$ is correlated with the locally generated PN sequence $c(t-\Delta_1)$ for the dwell time. The output

of the detector is compared with threshold $T_h$ to decide whether the PN codes are aligned. In figure 3.1, $H_1$ is the hypothesis of target in present, $H_0$ is the hypothesis of no target, $P_{fa}$ is the probability of false detection, and $P_d$ is the probability of detection.

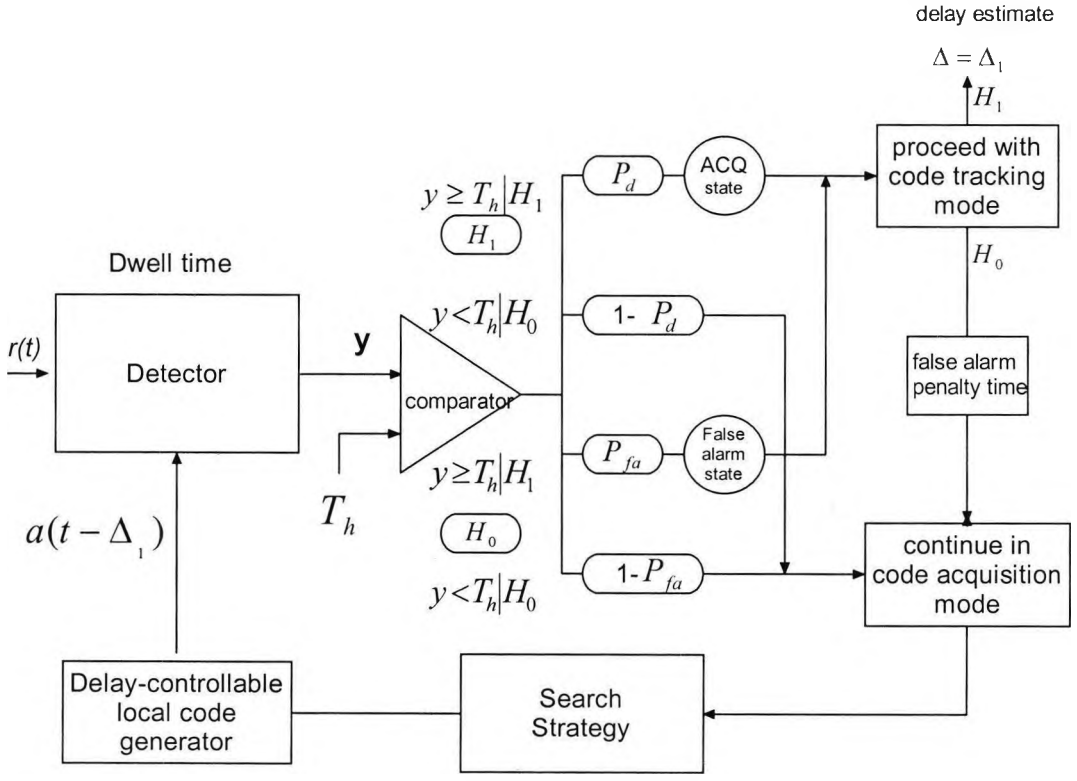


Figure 3.1: Stage diagram for PN code acquisition

In a real mobile communication, with the presence of noise, two kinds of errors may exist in the acquisition process as shown in figure 3.1, named *false alarm* and *miss*. A false alarm occurs when the detector output exceeds the threshold for an incorrect hypothesized phased while a miss occurs when the detector output falls below the threshold for a correct hypothesized phase. A false alarm will cause an incorrect phase to be passed to the tracking process, but as the phase is incorrect, it will not be able to lock on the signal and will return to the acquisition process. The false acquisition will add penalty time to the overall acquisition time. On the other hand, a miss will cause the circuit to neglect the

current correct hypothesized phase, therefore the acquisition will not be earlier than the next correct phase. The probability of miss ($P_m$) can be obtained by $1 - P_d$, and the penalty time for a miss depends on the different search strategies.

## 3.2 Detector Structures

### 3.2.1 Coherent or non-coherent detectors

In principle, there are two types of detectors, coherent and non-coherent [7-8]. Normally, the carrier phase mismatch is caused by two reasons: propagation delay and non-phase locked oscillator at the receiver. And, in a coherent detector, carrier phase needs to be recovered at the receiver. For a non-coherent detector, it doesn't need carrier phase recovery and hence it has less complexity at the price of high error rate. Figure 3.2 shows the structures of the block diagram of a coherent detector, where carrier phase needs to be recovered.

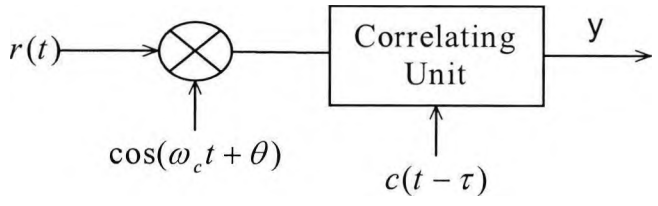


Figure 3.2: Basic block diagrams of a coherent detector

The non-coherent detector with I and Q branches are presented in figure 3.3. This enable the effect of the carrier phase to be ignored since the non-coherent combining after squaring will eliminate the phase error.

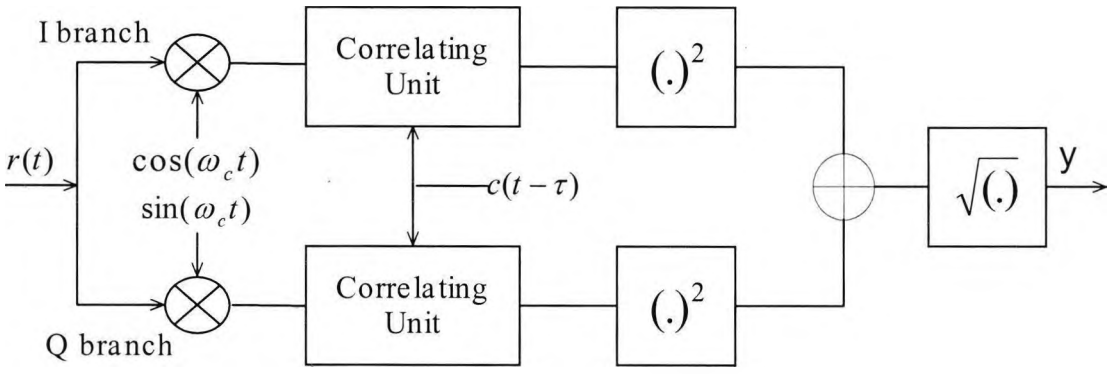


Figure 3.3: Block diagram of I-Q non-coherent detector

Figure 3.4 shows the basic structure of a non-coherent square-law detector. In this circuit, the receiver hypothesises a phase and if it matches the phase of the received signal, the wideband signal will be despread to narrowband. A Band-Pass Filter (BPF) with same bandwidth as the narrowband signal can be used to collect the power of the despread signal. If the wideband signal is despread to narrowband, the BPF will collect the complete signal power and the decision device will decide that the acquisition has been made. On the other hand, if the phases are not matched, the BPF will only collect a small portion of the signal, the decision device will decide that the hypothesised phase is not correct, and hypothesise another.

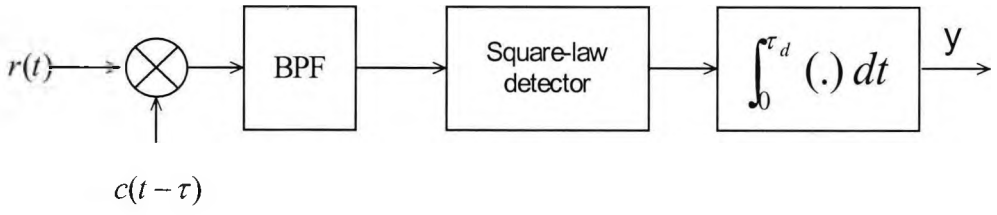


Figure 3.4: Block diagram of non-coherent square-law detector

### 3.2.2 Active Correlator

In an active correlater, the received signal and the locally generated PN code are multiplied chip by chip and accumulated for a dwell time $t_d$. So, the decision is made every $t_d$. If $N$ chips are used in correlation, then the $t_d$ is $NT_c$, where $T_c$ is the chip duration. The active correlator is shown in figure 3.5. The advantage of using an active correlator is that it consumes less hardware and therefore less power. However, for a long code length $t_d$, it takes long time to test each single chip, and the acquisition speed is slow.

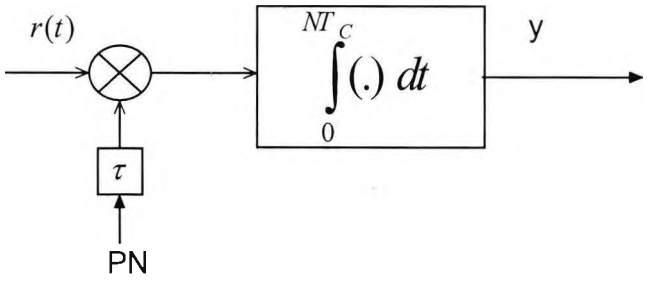


Figure 3.5: Active correlator [32]

### 3.2.3 Passive Correlator

Passive correlator is based on the principle of Matched Filter (MF) [33-35]. A MF is a filter whose frequency response is designed to match the frequency spectrum of input signal. In CDMA systems, MF is used to find out a code sequence within the received signal. When the code sequence is matched, the output of MF will give a peak. Figure 3.6 shows the operation of a MF.

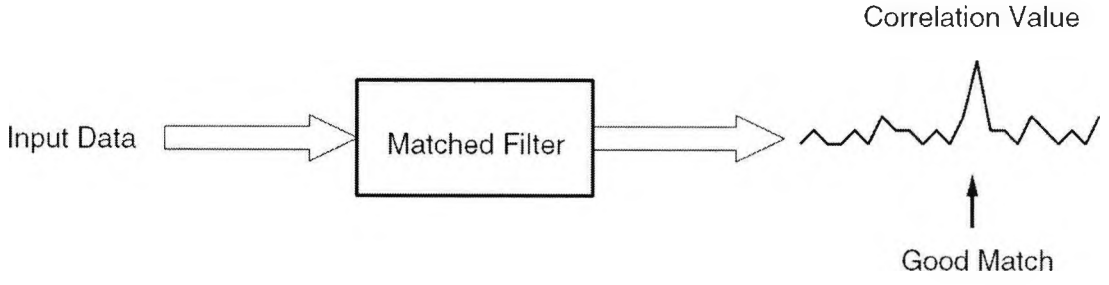


Figure 3.6: Basic operation of a MF [35]

Given a transmitted signal $x(t)$ of duration $T$, the impulse response of the MF is given as:

$$h(t) = \begin{cases} x(T-t); & 0 \le t \le T \\ 0; & otherwise \end{cases} \tag{3.5}$$

The output of MF is given by:

$$\begin{aligned} y(t) &= \int_{\tau=0}^{T} x(t-\tau)h(\tau)d\tau \\ &= \int_{\tau=0}^{T} x(t-\tau)x(T-\tau)d\tau \end{aligned} \tag{3.6}$$

When $t = NT$ ($N$= 0, 1, 2 ...), the MF is matched to the input signal. A MF generally applies the structure of a Finite Impulse Response (FIR) filter with coefficients -1 or +1. The coefficients are in the reverse order, for example, with PN code (+1, +1, -1, -1, -1, +1, -1, +1, +1, -1, +1, -1, +1, -1, +1, +1), the MF is showing in figure 3.7.

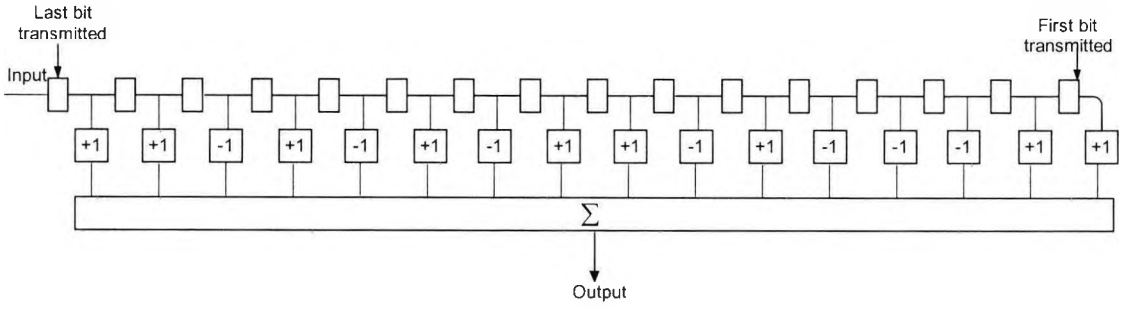


Figure 3.7: Matched filter with FIR structure [35]

In a MF, the output duration of correlation is $T_c$. Compared with the duration $NT_c$ of an active correlator, a MF is $N$ times faster than an active correlator.

### 3.2.3.1 Transposed form FIR structure

The MF showing in figure 3.7 has a traditional structure. There is another structure named transposed form FIR, which can be used for MF. The basic structures of traditional FIR and transposed form FIR are shown in figure 3.8.

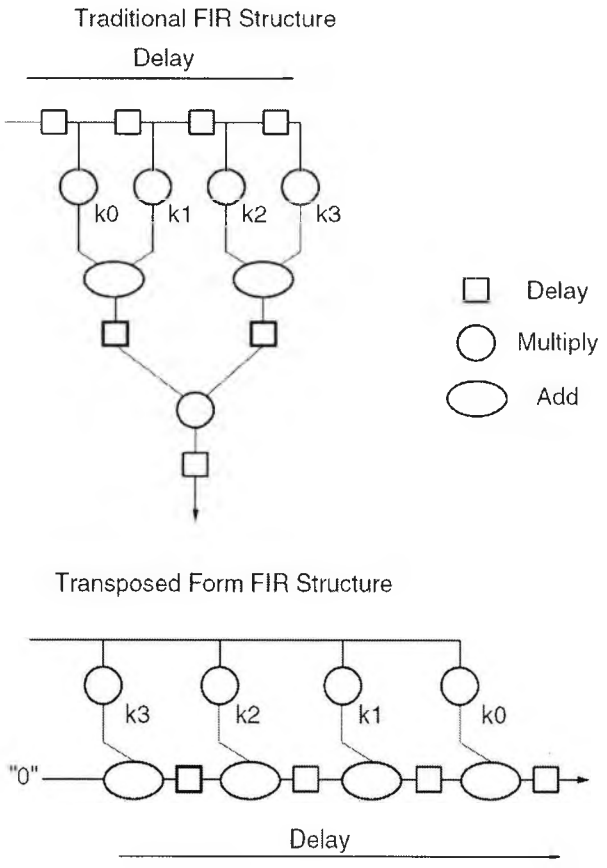


Figure 3.8: FIR and transposed FIR structure [35]

In a traditional FIR filter, the input samples are piped in the delay line, and all the taps are added at one time to get the output. But in a transposed form FIR filter, the input samples are firstly multiplied with the coefficients, then piped. Thus, compared with the traditional FIR structure, the transposed form FIR structure has lower input to output latency.

## 3.3 Search Strategies

In the receiver, each relative position between the codes is called a *cell*, and the uncertainty region is defined as the total number of cells is searched. The procedure to explore the uncertainty region is referred as the search strategy. The delay in time and offset in frequency, normally called *time* and *frequency uncertainties*, which are denoted

as $T_u$ and $F_u$, must be estimated if the despreading of the signal is to be done. The uncertainties in time and frequency are usually bounded into a specified interval or region, which is named uncertainty region like shown in the following figure 3.9.

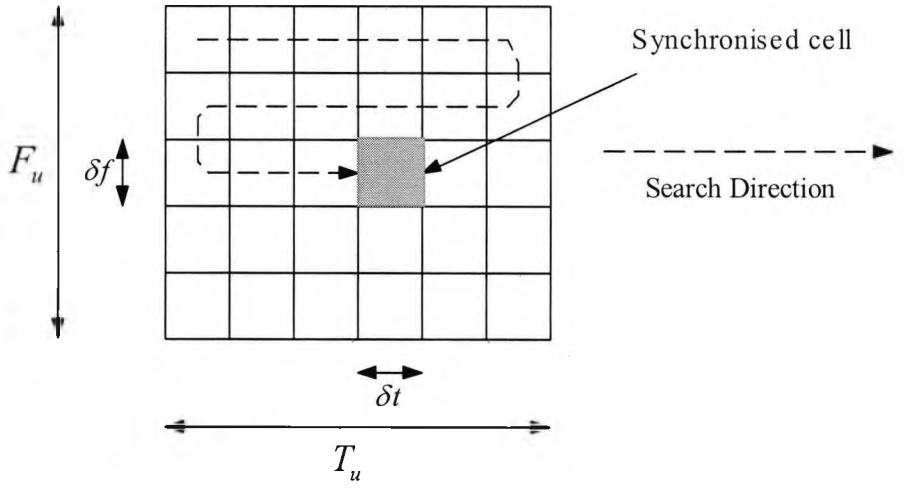


Figure 3.9: Two-dimensional serial search strategy of the PN code uncertainty region [36]

In figure 3.9, the uncertainty region is divided into sub-regions by $\delta t$ and $\delta f$, and this is referred to as a *cell*. For now, it is assumed that only one cell has correct delay of the received PN signal. This cell is called the *synchronised cell*. The remaining *out-of-phase* cells are *non-synchronised cells*.

The synchronisation work can be also done only in the time uncertainty region. This means that a one-dimensional search in the time uncertainty region can be carried out and the frequency uncertainty neglected [8-9]. This is also used in this thesis. It is obvious, that the performance of the circuit will be affected if doing that. In the situation of small frequency uncertainty, the circuit performance only suffers small degradation, but for large frequency uncertainty, the performance of the circuit is seriously affected.

In this thesis, the number of uncertainty cells ($W$) is same as the PN code length. Because $\delta t$ is chosen as $T_c$, and $\delta f$ is chosen to be $F_u$, and $W$ can be calculated with the following equation.

$$W = \frac{T_u \times F_u}{\delta t \times \delta f} \tag{3.7}$$

Here $T_c$ is used as the step-size of the search. The step-size can be chosen as half, quarter or even smaller portion of $T_c$. The smaller step-size makes the acquisition more accurate, but it is more complex to achieve. Some types of search strategies are introduced in the following.

### 3.3.1 Maximum-likehood

Normally in the Maximum-likehood (ML) detector, it requires parallel correlation of all the possible cells in the uncertainty region with received the signal and choosing the one with largest correlation cell. If there are $W$ cells in the uncertainty region, the number of such detectors will equal to $W$. Alternatively, firstly the $W$ cells can be correlated serially and stored, and then the cell with largest correlation value is chosen as the synchronised cell [6, 9]. The block diagram of a ML detector is shown in figure 3.10.

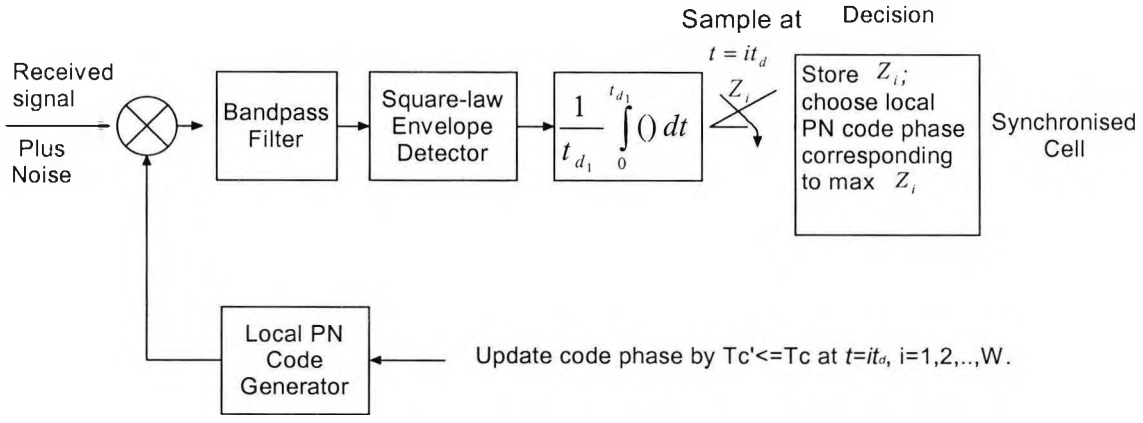


Figure 3.10: Block diagram of ML detector [9]

The advantage of using ML detector is that a definite decision will be made with only one search of the uncertainty region. But there are some disadvantages that cannot be accepted for a SS system. Because the PN sequence used in SS systems are normally very long, the application of a parallel ML detector will be very complex, and if serial ML detector is applied, the processing time will be long.

### 3.3.2 Serial Search

A popular strategy for the acquisition of PN sequence is to use a single correlator or match filter to serial search for the correct phase of received signal [9]. Figure 3.11 illustrates the basic configuration for a DSSS schemes. In a stepped serial acquisition scheme for a DS system, the code uncertainty region is searched cell-by-cell until the synchronised cell is determined. The correlation and sample implementation of serial search detector are quite similar to the ML detector, and the only difference is that the serial search detector uses a threshold. At each sampling instant, the output after a dwell time is compared with the predetermined threshold. If the output is greater than the threshold, acquisition is declared. Otherwise, the detection will continue. Compared with the ML detector, the noticeable advantage of a serial search detector is that when acquisition is achieved during the early cells being tested, the acquisition time can be quite short. But in a detector with ML strategy, all the cells in uncertain region need to be correlated. On the other hand, there is a disadvantage of using serial search strategy that the circuit may have false detection or miss the correct cell. However, this technique is simple to implement and thus generally is used in most acquisition circuits.

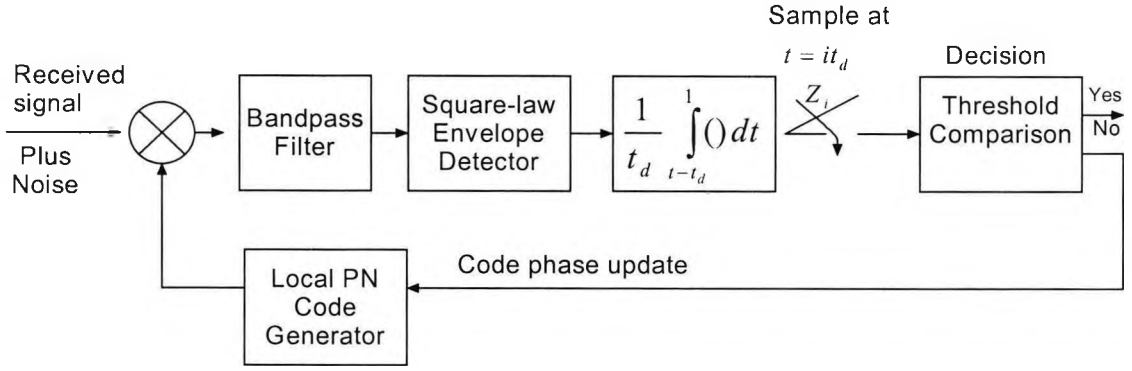


Figure 3.11: Block diagram of serial search strategy [9]

### 3.3.3 Parallel Search

Parallel search technique is a combination of several correlators. As shown in figure 3.12, there are three correlators, the biggest output of the three correlators are compared with the threshold. If the value is greater than the threshold, acquisition is declared, otherwise, the search is continued by hypothesising another phase.

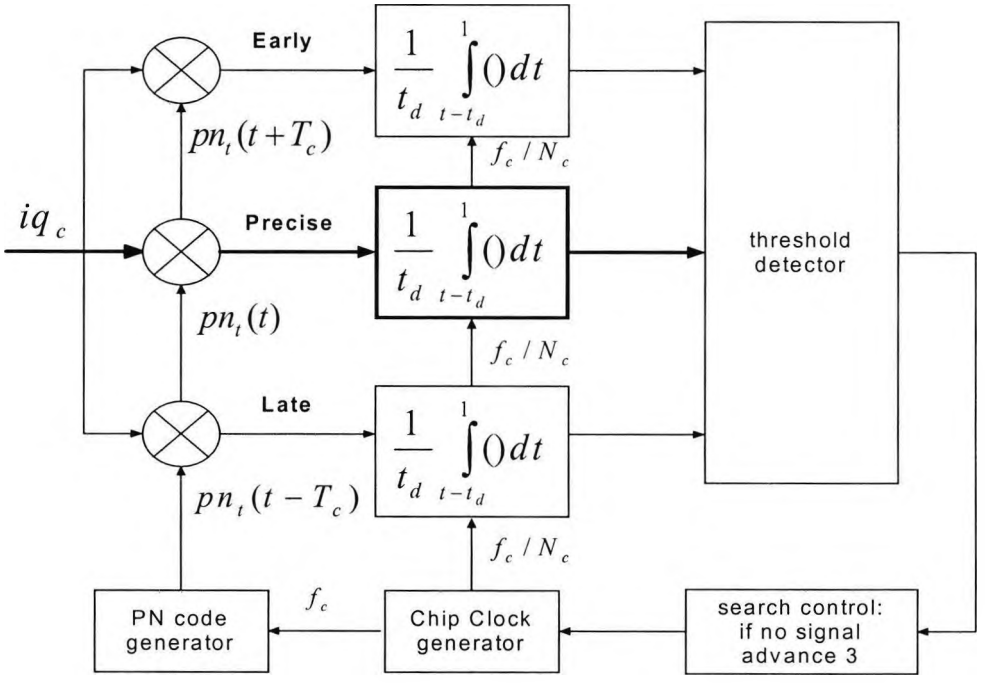


Figure 3.12: Parallel search with three correlators [11]

As with serial search strategy, the detector with parallel search strategy may have false and miss acquisition. The advantage of applying parallel search is the speed. Assuming $M$ correlators are used in the detector, the time taken to search the uncertainty region is less than the serial search by a factor $M$. As the factor $M$ increases, the acquisition time reduces, but it is more complex in implementation. If $M = W$, it is similar to the ML technique, but no threshold is needed.

### 3.3.4 Sequential Estimation

The technique called *rapid acquisition by sequential estimation* (RASE) is proposed by Ward [37].

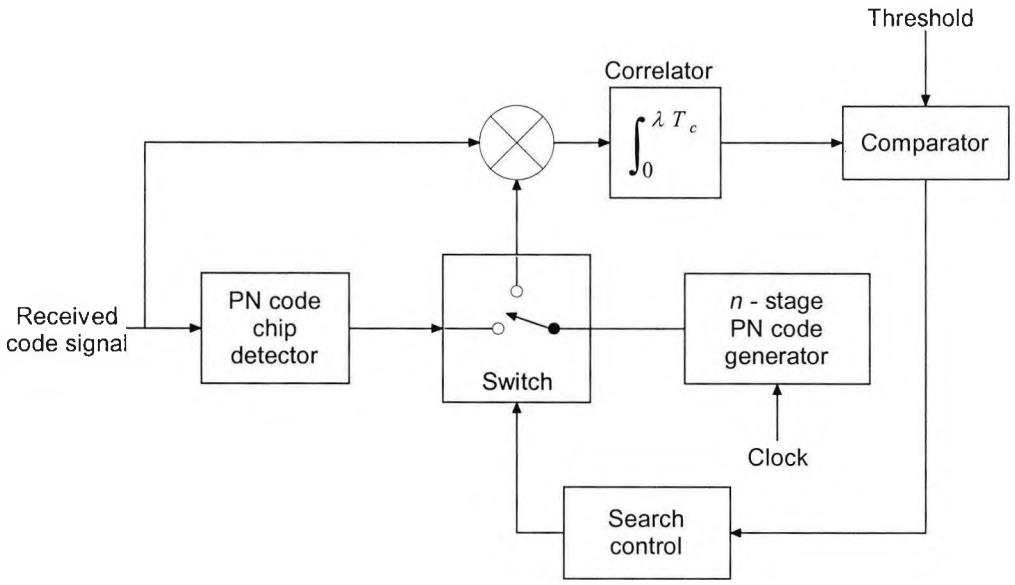


Figure 3.13: Block diagram of RASE receiver [37]

The switch is initially in position 1. The RASE receiver enters its best estimate of the first $n$ received code chips into the $n$ stages of its local PN generator. When the register is fully loaded, it starts operation. A PN sequence has the property that the next combination of register states depends only on the present combination of states. The switch is next

thrown to position 2. Therefore, if the first $n$ received chips are correctly estimated, all the following chips from the local PN code generator will be correct. After a dwell time, if the output is greater than the threshold, acquisition is declared. Otherwise, the switch is turned back to position 1 [37]. The system will repeat until it finds the synchronised cell. The advantage of RASE is that it is rapid, but on the other hand, it is highly vulnerable to noise and interferences.

### 3.3.5 Hybrid Search Strategy

It is normally a combination of parallel and serial search strategies. In the acquisition speed, it can be faster than the serial search, but it is less complex than the parallel search [38].

## 3.4 Single- and multiple-dwell detectors

In a single-dwell acquisition system, whenever the output is above the threshold, then the acquisition is declared and tracking model is started. There is another system named multiple-dwell system, where multiple tests of the same phase are carried out before the declaration of acquisition. Figure 3.14 shows the diagram of an $N$-Dwell detector. In the detector, there is a trigger for each decision circuit, which is controlled by the decision of previous dwell. If the $K_{th}$ dwell fails in detection, then the process will start again from the first dwell.

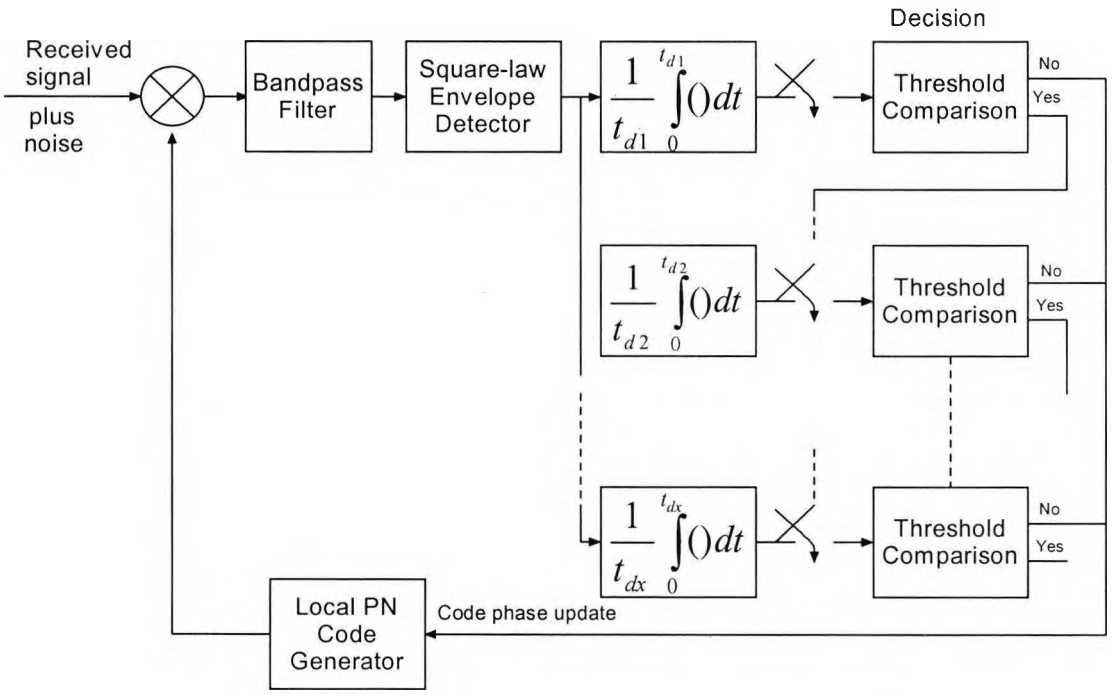


Figure 3.14: Multiple-dwell PN code acquisition circuit [9]

In a multiple-dwell detector, normally, the first dwell is made very short so it takes a short time to identify a possible synchronised cell. The second dwell is longer and so on, in order to ensure a reliable detection. When CFAR techniques are used in decision circuit, and with same designed false alarm rate, the time spent in non-synchronised cells is longer for a single dwell than a multiple-dwell as the time for the first dwell of multiple-dwell is shorter [36]. However, as the first dwell of multiple-dwell detector is shorter, it has a bigger probability to miss the synchronised cell, because the SNR is smaller. In this thesis, the research is focused on the comparison of CFAR techniques, and single dwell detector is selected in analysis.

## 3.5 Parameters for performance measurement

The delay of the received signal is random. Therefore, the code acquisition process has to be modelled probabilistically. There are several probability parameters that can be used

for performance analysis: Probability of detection, $P_d$; the probability of false alarm, $P_{fa}$; the probability of miss, $P_m$. However, as it is difficult to determine whether their performance by using three parameters, the mean acquisition time, MAT is introduced as the most important factor for performance measures.

In code acquisition, there are two hypotheses: $H_1$ and $H_0$ [9]. $H_1$ is the hypothesis that the target is present, and $H_0$ is used when there is no target present. Under $H_1$, there are two probabilities: detection or miss.

$$P_d = \Pr(y \geq T_h) \tag{3.8}$$

$$P_m = \Pr(y < T_h) \tag{3.9}$$

Under $H_0$, there is probability of false alarm:

$$P_{fa} = \Pr(y \geq T_h) \tag{3.10}$$

To calculate the MAT of acquisition circuit, a penalty time for a false detection needs to be set. As shown in [39], if the penalty time is set to be $MT_c$, the MAT for a single dwell detector can be calculated as

$$MAT = \sum_{L=0}^{\infty} \{[(L+0.5) \times N + M \times P_{fa} / (1 - P_{fa})] \times P_d \times P_m^{L-1} \times T_C\} \tag{3.11}$$

## 3.6 Summary

The purpose of this chapter was to make a briefly explanation about PN code acquisition techniques. It showed that the work of PN code acquisition is to correlate two sets of PN codes. Different types of detectors can be used in PN code acquisition: active correlator or passive correlator, single dwell or multiple-dwell. The structures of detectors can be trade off between speed and complexity. The parameters for performance measurement

can be $P_d$, $P_{fa}$, or $P_m$. However, the MAT calculated using them is more suitable, as it directly represents the speed of acquisition.

# CHAPTER 4

## Noise and Interference in Mobile Communication Channels

### 4.1 Introduction

Unlike the landline telephones, in mobile communication, the signal is transmitted through the atmosphere. This gives the mobile communication most important advantage: 'anywhere-anytime'. But on the other hand, mobile communication is limited on the data rate and quality due to propagation environment and mobility of users. A radio wave is an electromagnetic wave propagating from the transmitter antenna through the atmosphere to the receiver antenna. The dielectric of space in real wireless channel is $\sqrt{\varepsilon_r}$ [8]. Thus, the transmitted wave will undergo reflection, absorption, refraction, diffraction depending on the type of objects they contact which include building, trees and so on. The presence of these objects may block the direct path between the transmitter and the receiver, which is also known as line-of-sight (LOS) path. In the urban environment, as many objects exist between the transmitter and receiver, the radio wave received at the receiver will be mainly non-line-of-sight (NLOS). In the rural area, it will be mainly by LOS [40]. When the radio waves received at the receiver are from different paths, the mode of communication is multi-path. The present of multi-path makes PN code synchronisation much more difficult, as signals with same information arrive at receiver at different times, due to different delay of paths.

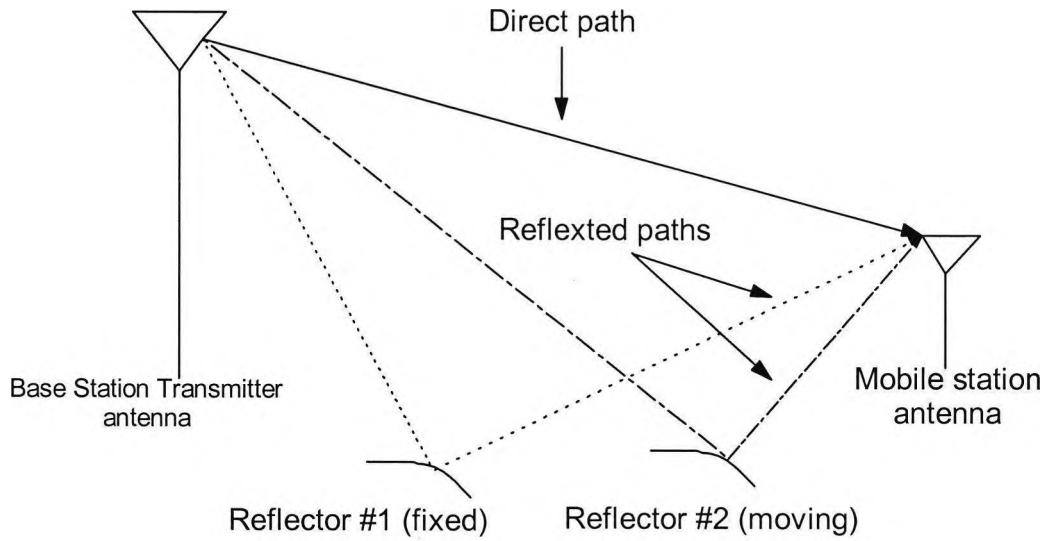


Figure 4.1: A multi-path mobile communication channel

Fading is about the phenomenon of loss of signal in telecommunication. It refers to the distortion that a carrier-modulated telecommunication signal experiences over certain propagation media. A fading channel is a communication channel where the signal transmitted experiences attenuation in power. In wireless communication, fading is due to multi-path propagation and sometimes is referred to as multi-path induced fading. Fading results in a fluctuation of the average power of the received signal.

Noise plays a crucial role in wireless communication systems. It determines the performance in the communication. In the communication, the level of noise is always described by SNR, and it is unknown to the receiver. Noise can be constant and also may be with clutter, and the types of noise have large influence to the performance of PN code acquisition.

Wireless systems also suffer from interferences like jamming, Multiple Access Interference (MAI), inter- and intra-cell interference, and so on. The presence of interference will directly result the decrease of SNR.

Research focuses on the performance of PN acquisition circuits for different environment, like multi-path, fading, and different types of SNR.

## 4.2 Fading in the mobile communication channels

In wireless communications, the presence of reflectors in the environment surrounding a transmitter and receiver create multiple paths that a transmitted signal can traverse. As a result, the receiver sees the superposition of multiple copies of the transmitted signal, each traversing a different path. Each signal copy will experience differences in attenuation, delay and phase shift while travelling from the source to the receiver. This can result in either constructive or destructive interference, amplifying or attenuating the signal power seen at the receiver. Strong destructive interference is frequently referred to as a deep fade and may result in temporary failure of communication due to a severe drop in the channel SNR.

A common example of multi-path fading is the experience of stopping at a traffic light and hearing an FM broadcast degenerate into static, while the signal is re-acquired if the vehicle moves only a fraction of a meter. The loss of the broadcast is caused by the vehicle stopping at a point where the signal experienced severe destructive interference. Cellular phones can also exhibit similar momentary fades.

Fading channel models are often used to model the effects of electromagnetic transmission of information over the air in cellular networks and broadcast communication. Fading channel models are also used in underwater acoustic communications to model the distortion caused by the water. Mathematically, fading is usually modeled as a time-varying random change in the amplitude and phase of the transmitted signal. There are basically two types of fading: *large-scale* and *small-scale fading*. Large scale fading represents the average signal power attenuation or path loss due to motion over large areas. The phenomenon is affected by prominent terrain contours between the transmitter and receiver. The statistics of large-scale fading calculates the path loss by function using distance. It is often described in terms of a mean-path loss and a log-normally distributed variation about the mean. Small-scale fading refers to the changes in signal amplitude and phase that can be experienced as a result of small changes in propagation delay [41]. Small-scale fading is called *Rayleigh fading*, if there is large number of multiple reflective paths, and no LOS signal exists. The envelope of such signal is statistically described by a Rayleigh PDF.

### 4.2.1 Large-Scale Fading

In large-scale fading propagation models, the mean path loss $\overline{L_p}(d)$, as a function of distance $d$ between the transmitter and receiver is proportional to an $n$th-power of $d$ relative to a reference distance $d_0$. This is shown as

$$\overline{L_p}(d) \propto (\frac{d}{d_0})^n \tag{4.1}$$

In dB, the mean path loss can be stated

$$\overline{L_p}(d) = 10\log L_s(d_0) + 10n\log(\frac{d}{d_0}) \tag{4.2}$$

Typically, the value $d_0$ is taken to be 1 km for large cells, 100 m for microcells, and 1 m for indoor channels. The value of the path-loss exponent $n$ in (4.2) depends on the frequency, antenna heights, and the propagation environment. In free space where signal propagation follows an inverse-square law, $n$ is equal to 2. In the presence of a very strong guided wave phenomenon, $n$ can be lower than 2, and when obstruction exists, $n$ is larger. $L_s(d_0)$ is the *free space loss*, and can be expressed as

$$L_s(d_0) = (\frac{4\pi d}{\lambda})^2 \tag{4.3}$$

In this equation, λ is the wavelength of the propagating signal.

When variations are provided to describe a particular path, the path loss $L_p(d)$ can be expressed in terms of $\overline{L_p}(d)$ and a random variable $X_\sigma$ [41].

$$L_p(d) = 10\log L_s(d_0) + 10n\log(\frac{d}{d_0}) + X_\sigma \tag{4.4}$$

In equation (4.4), $X_\sigma$ denotes a zero-mean Gaussian random variable with standard deviation σ. In the calculation of path loss due to large-scale fading, the following parameters are needed:

(1) The reference distance between the transmitter and receiver

(2) The path loss exponent

(3) The standard deviation $X_\sigma$.

### 4.2.2 Small-Scale Fading

Small-scale fading is the fluctuation in signal envelope due to multi-path and the speed at which the mobile is moving. Assume that the propagation delay is $\tau_n(t)$, and the attenuation factor is $\alpha_n(t)$, then received signal *r (t)* can be expressed as

$$r(t) = \sum_n \alpha_n(t) s[t - \tau_n(t)] \tag{4.5}$$

For any real bandpass waveform, $s(t)$ can be represented using complex notation as

$$s(t) = \mathrm{Re}\{g(t)e^{j\omega_0 t}\} \tag{4.6}$$

Where $g(t)$ is known as the complex envelope, expressed as

$$g(t) = x(t) + jy(t) = |g(t)|e^{j\theta(t)} \tag{4.7}$$

Using complex notation, the equation (4.6) can be written as

$$\begin{aligned} r(t) &= \mathrm{Re}(\{\sum_n \alpha_n(t) g[t - \tau_n(t)]\} e^{j2\pi fc[t-\tau_n(t)]}) \\ &= \mathrm{Re}(\{\sum_n \alpha_n(t) e^{j2\pi fc[t-\tau_n(t)]} g[t - \tau_n(t)]\} e^{j2\pi fct}) \end{aligned} \tag{4.8}$$

The equivalent received signal is

$$z(t) = \sum_n \alpha_n(t) e^{-2\pi f_c \tau_n(t)} g[t - \tau_n(t)] \tag{4.9}$$

Consider $g(t) = 1$ for an unmodulated carrier at frequency $f_c$, the equation can be reduces to

$$z(t) = \sum_n \alpha_n(t) e^{-j2\pi f_c \tau_n(t)} = \sum_n \alpha_n(t) e^{-j\theta_n(t)} \tag{4.10}$$

Where $\theta_n(t) = 2\pi f_c \tau_n(t)$ .If $\tau_n$ changes by $1/f_c$, $\theta_n(t)$ will change $2\pi$, which will cause a big change in $z(t)$. Assume that a mobile system is operating at $f_c$ = 900 MHz and the delay is $1/f_c$ =1.1 nanoseconds, this is a very big value.

Figure 4.2 shows the causes of fading in multi-path channels. The reflected signals have two components $x_n(t)$ and $y_n(t)$, where $x_n(t) + y_n(t) = \alpha_n(t)e^{-j\theta_n(t)}$.

$$r_0(t) = \sqrt{x_r^2(t) + y_r^2(t)} \tag{4.11}$$

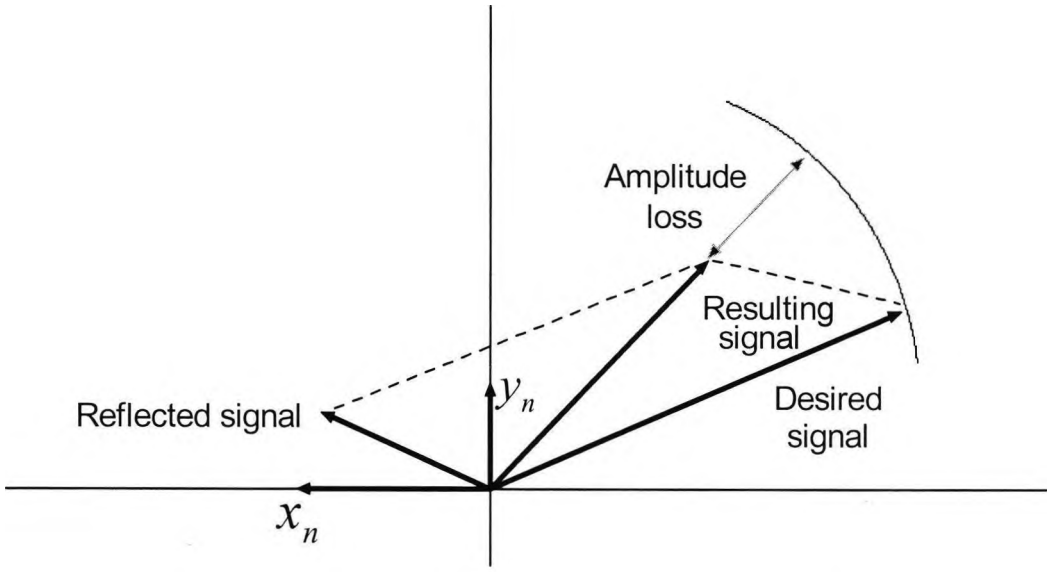


Figure 4.2: Cause of fading in multi-path channels [42]

For a selected time, if the variables are $x_r(t)$ and $y_r(t)$, where $x_r(t)$ and $y_r(t)$ are the cumulated value of $x_n(t)$ and $y_n(t)$ correspondingly. For the magnitude $r_0(t)$ of an unmodulated signal, the equation can be expressed as

#### 4.2.2.1 Power density function for Rayleigh fading channel

When the components of $z(t)$ are independent the probability density function for a amplitude $r_0$ can be expressed as Rayleigh PDF [42]

$$p(r_0) = \frac{r_0}{\sigma^2} e^{-\frac{r_0^2}{2\sigma^2}} \qquad (r_0 \geq 0) \tag{4.12}$$

The parameter $\sigma^2$ is the predetection mean power of the multi-path signal. The Rayleigh PDF presents the worst case of fading. It has no specular signal component and no density for a single link, as no LOS is considered. In a Rayleigh channel, the power is exponentially distributed. The phase is uniformly distributed and independent from the amplitude. Figure 4.3 shows the PDF of Rayleigh distributed amplitude for different standard deviation σ.

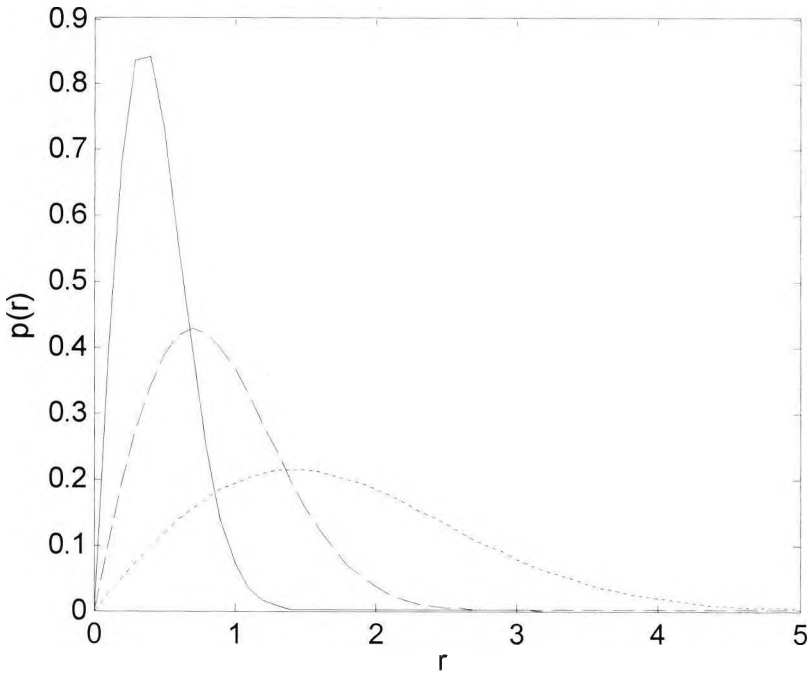


Figure 4.3: Rayleigh probability density. (-) σ = 0.5, (- -) σ =1, (.) σ =2.

#### 4.2.2.2 Power density function for Ricean fading channel

In the case, that there is non-zero mean (presence of LOS and other NLOS signals), the target envelope is Ricean distributed. The received envelope amplitude has a Ricean PDF as shown in the following equation [42-43]:

$$p(r_0) = \frac{r_0}{\sigma^2} e^{-\frac{r_0^2 + A^2}{2\sigma^2}} I_0\left(\frac{r_0 A}{\sigma^2}\right) \qquad (r_0 \geq 0, A \geq 0) \tag{4.13}$$

In (4.13), $A$ denotes the amplitude of the specular component and $I_0$ is the modified Bessel function of the first kind and zero order. The Ricean distribution can be also described with parameter $K_r$, which is the ratio of the power in the specular component to the power in the multi-path signal, expressed in equation, it is

$$K_r = A^2 / (2\sigma^2) \tag{4.14}$$

Figure 4.4 depicts the Ricean PDF. And we can see that when there is no LOS signal ($K_r \rightarrow \infty$), the Rayleigh PDF and Ricean PDF are same.

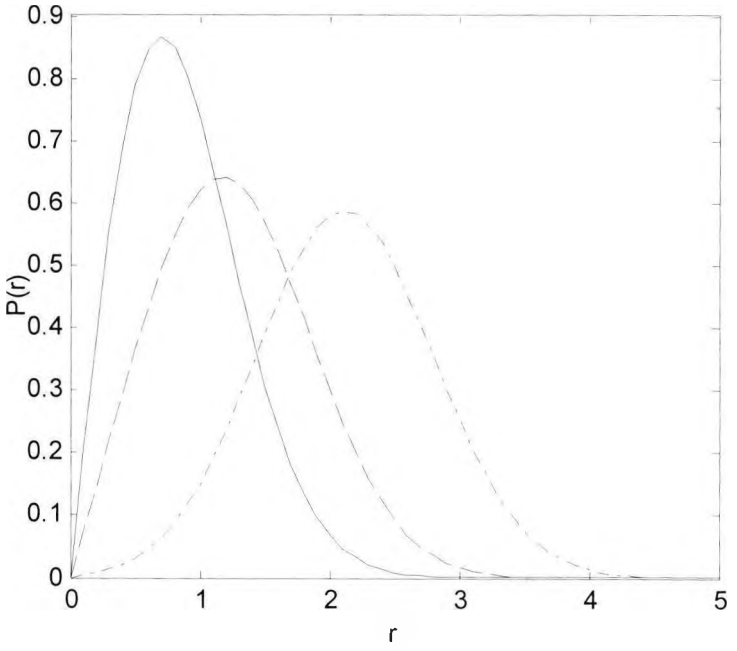


Figure 4.4: Ricean probability density, (-) $K_r$ = -∞, (- -) $K_r$= 1 dB, (-.-) $K_r$=6 dB

## 4.3 Target models in detection envelope

Chi-Square Target (CST) models were firstly introduced by Peter Swerling to describe the statistical properties of the Radar Cross-Section (RCS) of complex objects. The general models of CST models are Swerling models, which apply Chi-square probability density function [43].

In probability theory and statistics, Chi-square distribution is one of the widely used theoretical probability distributions in inferential statistics. It is useful, because when the *null hypothesis* is true, the calculated quantities will have distributions approximate to the chi-square distribution.

If $X_i$ are $K$ independent, normally distributed random variables with mean 0 and variance 1, then the Chi-square distributed random variable Q can be obtained by

$$Q = \sum_{i=1}^{K} X_i^2 \tag{4.15}$$

The PDF of the chi-square distribution is expressed as follow

$$f(x,k) = \begin{cases} \frac{1}{2^{k/2}\Gamma(k/2)} x^{(k/2)-1} e^{-x/2} & for \quad x > 0 \\ 0 & for \quad x \le 0 \end{cases} \tag{4.16}$$

where $\Gamma(.)$ is the gamma function. And its Cumulative Density Function (CDF) is [44]

$$F(x,k) = \frac{\gamma(k/2, x/2)}{\Gamma(k/2)} = P(k/2, x/2) \tag{4.17}$$

where $\gamma(.)$ is the lower incomplete gamma function.

### 4.3.1 General target models

Based on the chi-square PDF, the RCS of Swerling models can be obtained from equation (4.15)

$$p(\sigma) = \frac{m}{\Gamma(m)\sigma_{av}} (\frac{m\sigma}{\sigma_{av}})^{m-1} e^{-\frac{m\sigma}{\sigma_{av}}} \tag{4.18}$$

Where $\sigma_{av}$ refers to the mean value of sigma. This is not always easy to determine, as certain objects may be viewed most frequently from a limited range of angles. For instance, a sea-based radar system is most likely to view a ship from the side, the front, and the back, but never the top or the bottom. $m$ is the number of degrees of freedom divided by 2. While the number of degrees of freedom used in the chi-square PDF is an integer value in statistics, it can assume any positive real number in the target model. Values of $m$ between 0.3 and 0.2 have been found to closely approximate certain simple shapes, such as cylinders or cylinders with fins. Since the ratio of the standard deviation to the mean value of the chi-square PDF is equal to $m^{-1/2}$, larger values of $m$ will result in less fluctuation. If $m$ equals infinity, the target's RCS is non-fluctuating.

### 4.3.2 Swerling target models

Swerling target models are special case of CST model with special degree of freedom. There are five types of Swerling models [43-44]:

A. Swerling I

A model where the RCS varies according to a Chi-square probability density function with two degrees of freedom ($m$ = 1). This applies to a target that is made up of many independent scatterers of roughly equal areas. As little as half a dozen scattering surfaces can produce this distribution. Swerling I describes a target whose radar cross-section is constant throughout a single scan, but varies independently from scan to scan. In this case, the PDF reduces to

$$P(\sigma) = \frac{1}{\sigma_{av}} e^{-\frac{\sigma}{\sigma_{av}}} \tag{4.19}$$

B. Swerling II

Swerling II is similar to Swerling I model, but the RCS values are independent from pulse to pulse.

C. Swerling III

A model where the RCS varies according to a Chi-square probability density function with four degrees of freedom ($m$ = 2). It is like Swerling I, that only one scan is used. The PDF can be expressed as

$$P(\sigma) = \frac{4\sigma}{\sigma^2_{av}} e^{-\frac{2\sigma}{\sigma_{av}}} \tag{4.20}$$

D. Swerling IV

Similar as Swerling III, but it is varies from pulse to pulse.

E. Swerling V

Constant RCS with $m \to \infty$.

## 4.4 Homogeneous and non-homogeneous noise background

Homogeneous is the simplest noise background. In analysis, there are no interfering targets, and the SNR maintains constant. However, it is unlikely to exist in real mobile communications.

In non-homogeneous noise background with clutter or multiple targets, the performance of CFAR detectors will be seriously affected, which is shown in the chapter 5.

a) In the transmission with clutter, when the clutter edge enters the reference window, the noise power of the masked cells increases abruptly. When the CUT is not covered by the clutter region (less than half cells covered), the false alarm rate will be excessive. On the other hand, if the CUT is covered by the clutter, it will be masked, thus there will be a high probability of miss.
b) In multiple targets environment, when there are more than two close targets. The interfering targets may exist in the reference window together with the primary target. Thus, the threshold will be raised and may be higher than the primary target.

Multiple targets environment is easier than clutter environment to analyse. Because, in clutter transmission, both CUT under cover and not under covered need to be considered. If the CUT is in clear region, clutter transmission can be considered as multiple targets transmission, and the cells covered by clutter region can be treated as interfering targets.

## 4.5 Summary

In this chapter, the channel models for mobile communication channels were studied. Fading is a important source of performance degradation for acquisition circuits. For the case of fading, the large-scale fading is mainly characterised as path loss, and for small-

scale fading, it results in multiple signals on the receiver side. For the analysis of CFAR detectors in chapter 5 and 6, the mobile communication channels are divided into homogeneous noise background and non-homogeneous noise background. In homogenous noise background, the noise level is constant, and in non-homogeneous noise background, multiple targets or clutter exist.

# CHAPTER 5

## CFAR Techniques for PN Code Acquisition

### 5.1 Introduction

CFAR detection can refer to a common form of adaptive algorithm used in radar systems to detect target returns against a background of noise, clutter and interference [45]. In the PN code detection, the system determines a threshold, above which a target is detected. If pre-determined without any power information about the received signal, the threshold maybe too high or too low. In the case that the threshold is too low, more targets will be detected in a trade of with more false alarms. On the other hand, if the threshold is too high, fewer targets will be detected, but the false alarm numbers also decrease. If the noise background of the communication is constant with PDF of the noise, a fixed threshold can be set to provide specified $P_{fa}$. In the practical communication channels, the noise level changes both spatially and temporally. So, the threshold also needs to be changing to maintain a constant false alarm rate. And this is the technique named CFAR. The following figures demonstrate the benefits of using adaptive threshold instead of fixed threshold in non-constant noise environment.

Figure 5.1 illustrates the PN code detection in a communication with constant noise power. The green line is the adaptive threshold and blue line represents the output of

correlator. Red line in the figure shows a proper level of fixed threshold, it is chosen by the receiver depend on the noise level. Obviously, the targets detected by both thresholds are same in this condition. Range bin represents number of PN code chips that have been correlated.

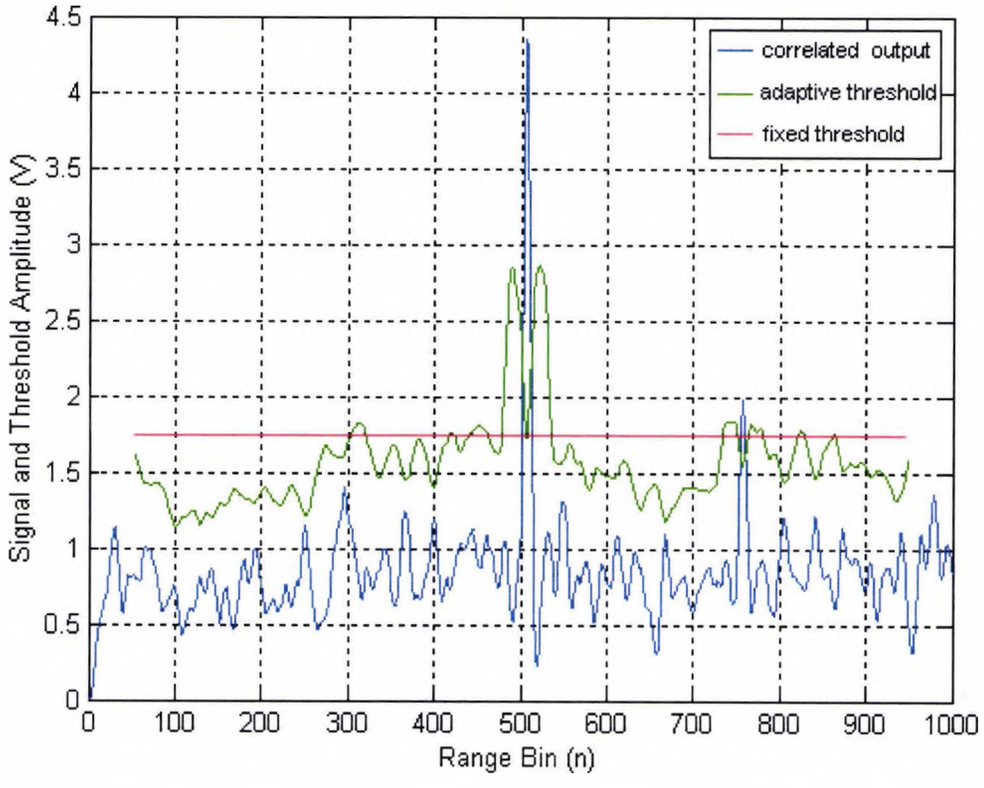


Figure 5.1: MF output and threshold levels for constant noise [46]

However, when the noise is non-constant, no suitable fixed threshold can be chosen. As shown in figure 5.2, in the case of transmission with non-constant noise, the adaptive threshold (green line) can still detect the peak of correlation, and avoid the false targets cause by high noise power. But when fixed threshold is used, like shown in the figure 5.2, to detect the both correct correlation peaks, many false targets within range bin 0 to 300 will be detected.

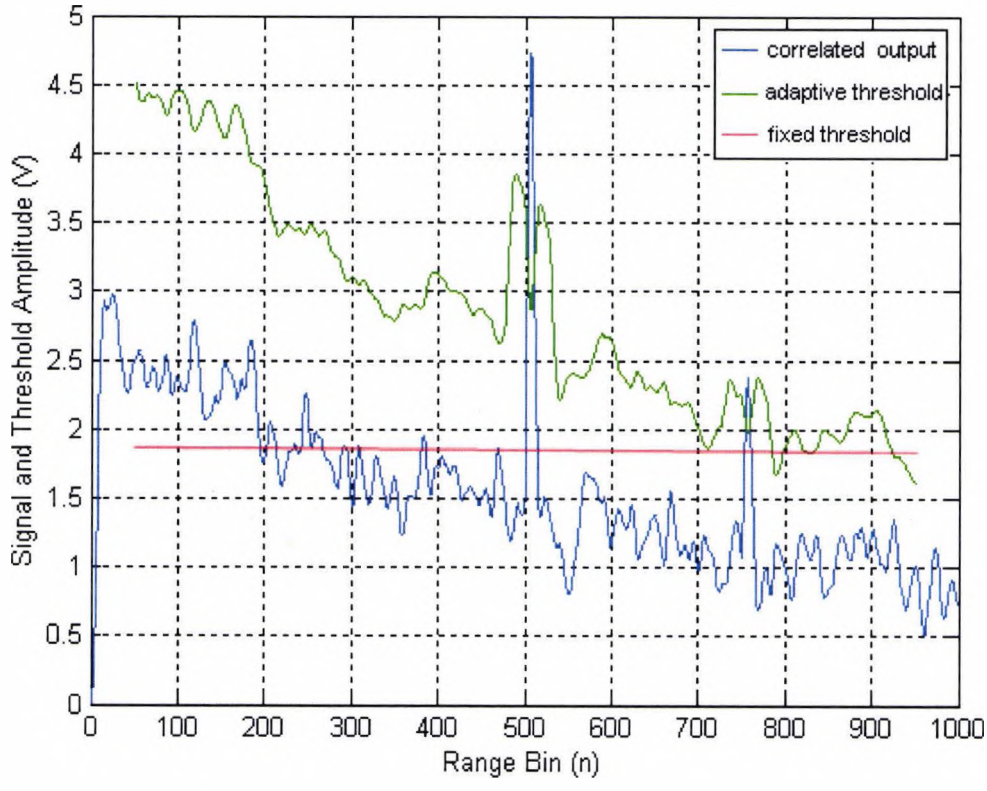


Figure 5.2: MF output and threshold levels for non-constant noise [46]

In the CFAR detectors, the threshold is set adaptively based on the local noise power. Based on the method to obtain the noise power, CFAR detectors can be divided into two types: *mean-level detectors* and *order-statistics (OS) detectors.* In a mean-level detector, the noise level is estimated by calculating the average power of the cells in reference window. An example is CA-CFAR detector [47], in which the noise power is estimated as the mean level of $N$ reference cells around the CUT. The CA-CFAR detector is the one with maximum detection probability in homogeneous noise background, when all the cells in reference window are Independent and Identically Distributed (I.I.D) and exponential distributed. But in non-homogeneous noise background, with clutter or multiple targets, the performance of CA-CFAR is seriously affected. Therefore, some other CFAR techniques were developed to overcome the problem caused by non-homogeneous noise background. Greatest-of CFAR (GO-CFAR) and Smallest-of CFAR

(SO-CFAR) were modified from CA-CFAR technique [48-50]. Both of them are mean-level detectors, but not like CA-CFAR, in GO-CFAR and SO-CFAR detectors only reference cells on one side is used in estimating the mean level. In non-homogeneous noise background, by using only one side of reference cells for noise level estimation, the interfering targets and clutter region may be separated from the CUT.

In OS-CFAR detectors, only the *K-th* biggest cell is selected and considered as the mean noise level [51]. When there are interfering targets existing in reference window, and if the $K$ is properly selected to avoid them, the noise level of CUT can be still estimated correctly. But in clutter transmission, the highly selected $K$ will lead to big $P_m$, and if it is low, there will be big $P_{fa}$.

Full analysis for the CFAR detectors is shown in chapter 6.

## 5.2 General model descriptions of CFAR techniques

The decision segment of an adaptive PN code acquisition circuit is normally based on CFAR techniques. Figure 5.3 shows the basic model of a CFAR detector.

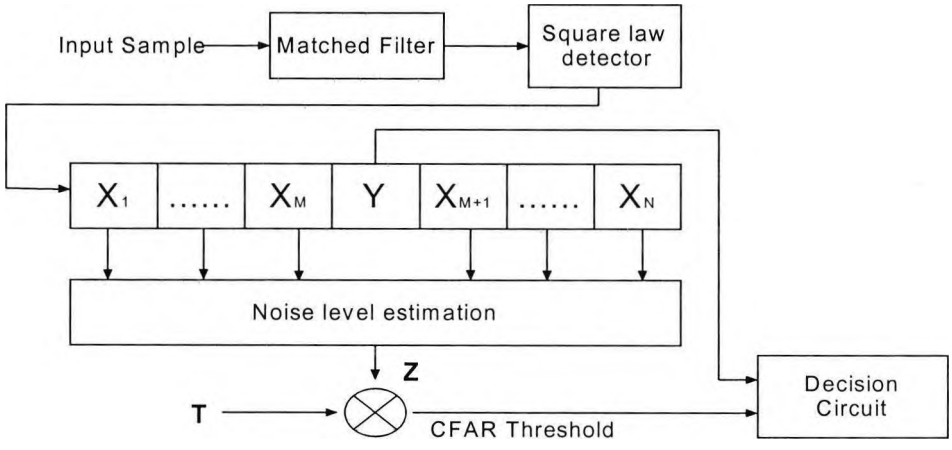


Figure 5.3: Basic model for a CFAR detector

In a CFAR processor, there are $N$ cells in the reference window. The outputs from the MF are sampled and stored in the reference window, and the middle one is the cells being tested. The noise level in the reference window can be obtained by different algorithm. $T$ is the scaling factor. When the $P_{fa}$ is chosen, $T$ can be calculated, and it is a fixed value. The CUT $Y$ is compared with $TZ$ to decide whether there is a target.

A. CA-CFAR

Figure 5.4 shows the noise level estimator part of a CA-CFAR detector. In a CA-CFAR detector, all the $N$ reference cells are summed, and the average value of the $N$ reference cell is considered as the mean noise power.

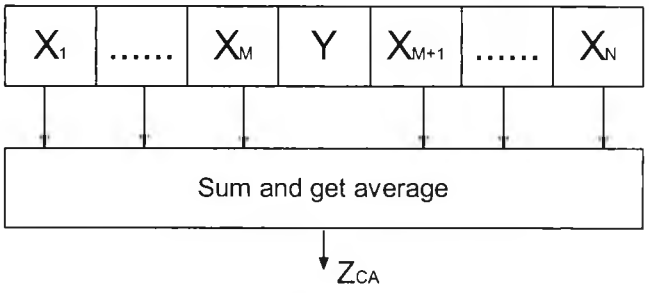


Figure 5.4: CA-CFAR noise level estimator

B. OS-CFAR

In an OS-CFAR detector, firstly all the cells are sorted, and then the *K-th* largest cell is selected for threshold calculation. The model for noise level estimation is shown in figure 5.5.

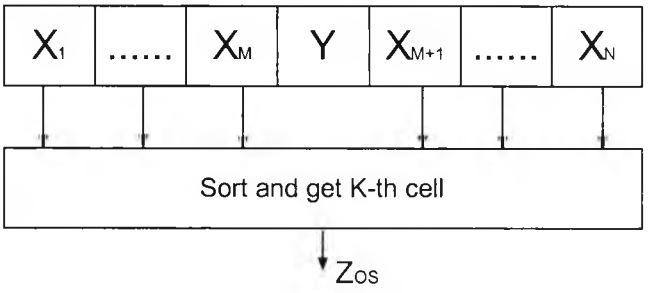


Figure 5.5: OS-CFAR noise level estimator

C. GO-CFAR and SO-CFAR

Figure 5.6 illustrates the method of noise power estimation in GO-CFAR and SO-CFAR detectors. The reference window is separated into two parts on each side of the CUT, and the average noise power of each is $Z_1$ and $Z_2$. In GO-CFAR and SO-CFAR, the noise level is the larger or smaller of $Z_1$ and $Z_2$, respectively.

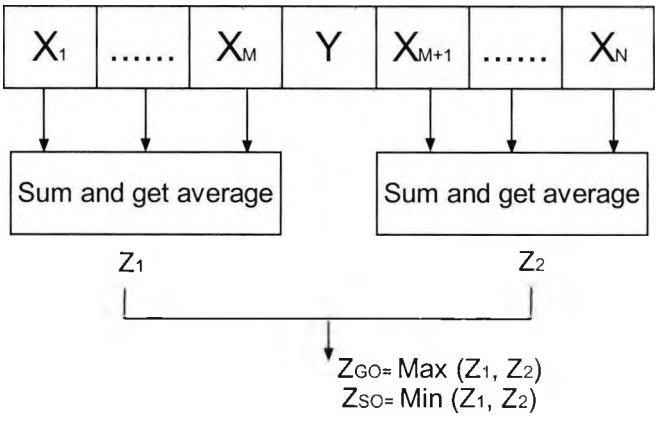


Figure 5.6: GO- and SO-CFAR noise level estimators

### 5.2.1 Basic assumptions and mathematical descriptions

In homogeneous noise background, if the output of square-law detector is assumed to be exponentially distributed, the output signal has PDF as [10]

$$f(x) = \frac{1}{\lambda}\exp(\frac{-x}{\lambda}) \tag{5.1}$$

Under the hypothesis of null targets ($H_0$), λ can be expressed as in equation (5.2).

$$H_0 : \lambda = u, \tag{5.2}$$

Under the hypothesis of presence of target ($H_1$):

$$H_1 : \lambda = u(1+S), \tag{5.3}$$

Where λ is the total noise power, $\mu$ is the variance of noise and $S$ is the SNR of the output signal, under the assumption of Swerling I model and Gaussian noise background. $P_d$ and $P_{fa}$ are the two important factors used to analyse the performance of an acquisition circuit. Under the above assumptions, the general equation for $P_{fa}$ can be expressed as

$$\begin{aligned} P_{fa} &= P[Y > TZ | H_0] \\ &= \int_{TZ}^{\infty} (1/\mu)\exp(-y/\mu)dy \\ &= M_Z(-T/\mu) \end{aligned} \tag{5.4}$$

where $M_Z(.)$ is the moment generating function (MGF) [17]. And for $P_d$, with hypothesis $\lambda = \mu(1+S)$ , it can be expressed as

$$\begin{aligned} P_d &= P[Y > TZ | H_1] \\ &= \int_{TZ}^{\infty} [1/\mu(1+S)]\exp[-y/\mu(1+S)]dy \\ &= M_Z[-T/\mu(1+S)] \end{aligned} \tag{5.5}$$

In the non-homogeneous noise background, the assumption is different. For multiple targets transmission, the interfering targets have $\lambda = u(1+I)$, where $I$ is the Interference-to-Thermal Noise Ratio (INR). Although it is still correct to use the assumption $\lambda = u(1+S)$, the threshold calculation will be affected by the reference cells, consequently the $P_{fa}$ and $P_d$ will be affected. In the case of clutter transmission, the cells

covered by the clutter region have power $\lambda = u(1+C)$, where $C$ is the Clutter-to- thermal Noise Ratio (CNR). If the CUT is covered, it will have $\lambda = u(1+S)/(1+C)$.

## 5.3 Analysis of CFAR detectors in homogeneous noise background

The performance of CFAR detectors in the presence of homogeneous noise background are analysed and compared in the following sections.

### 5.3.1 CA-CFAR detectors

In the CA-CFAR detector, all the $N$ cells are summed and the average value is considered to be the mean noise power. Therefore

$$Z_{CA} = \frac{1}{N}\sum_{i=1}^{N} X_i \tag{5.6}$$

Under the assumption of exponentially distributed homogeneous noise background, the PDF of $Y$ can be expressed as the special case of gamma density with $\alpha = 1$.

$$f(y) = \beta^{-\alpha} y^{\alpha-1} \exp(-y/\beta)/\Gamma(\alpha) \tag{5.7}$$

$\Gamma(.)$ is the gamma function. The MGF of $Y$ can be derived as follow:

$$M_Y(u) = \int_0^{\infty} e^{uy} \frac{e^{-y/\beta} y^{\alpha-1}}{\Gamma(\alpha)\beta^{\alpha}}$$

$$= \int_0^{\infty} \frac{e^{-y(1-\beta u)/\beta} y^{\alpha-1}}{\Gamma(\alpha)\beta^{\alpha}} \tag{5.8}$$

Let $x = y(1-\beta u)/\beta$

$$M_Y(u) = \int_0^{\infty} e^{uy} \frac{e^{-x}}{\Gamma(\alpha)\beta^{\alpha}} \left(\frac{\beta x}{1-\beta u}\right)^{\alpha-1} \left(\frac{\beta}{1-\beta u}\right) dx$$

$$= \frac{1}{(1-\beta u)^{\alpha}} \int \frac{x^{\alpha-1} e^{-x}}{\Gamma(\alpha)} du$$

$$= (1-\beta u)^{-\alpha} \tag{5.9}$$

For $X_i$, the CDF is $G\ (1,\ \mu)$, and for $Z_{CA}$, the CDF can be expressed as $G\ (N,\ \mu/N)$ [17]. Substitute (5.9) into (5.4) with $\alpha=N$, $\beta=\mu/N$. The equation for $P_{fa}$ can be obtained by

$$P_{fa}(CA) = \frac{1}{(1+T/N)^N} \tag{5.10}$$

By replacing $T$ with $T/(1+S)$, the $P_d$ of CA-CFAR detector can be expressed as

$$P_d(CA) = \frac{1}{(1+T/N(1+S))^N} \tag{5.11}$$

Derived using (5.10), the scaling factor $T$ can be obtained by

$$T = N(P_{fa}^{-1/N} - 1) \tag{5.12}$$

Figure 5.7 shows the $P_d$ of CA-CFAR detectors with different value of $N$, at with the assumption that $P_{fa} = 10^{-4}$.

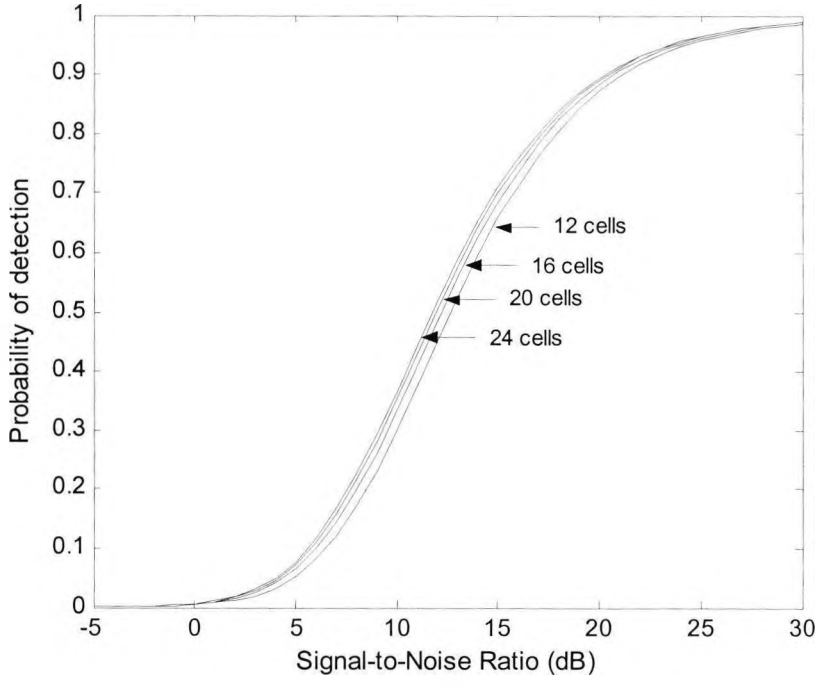


Figure 5.7: $P_d$ for CA-CFAR with different lengths of reference window

It can be seen that, in homogeneous noise background, CA-CFAR detectors have better performance when more reference cells are used. However, the trend of improvement is decreasing when $N$ becomes larger. Thus, it is no need to choose a very big $N$ for good performance, and in this thesis, 20 is chosen as the number of reference cells.

### 5.3.2 OS-CFAR detectors

In OS-CFAR detectors, the $N$ reference cells are sorted in increasing order:

$$X_{(1)} \leq X_{(2)} \leq \ldots \leq X_{(K)} \leq \ldots \leq X_{(N)} \tag{5.13}$$

and

$$Z_{OS} = X_{(k)} \tag{5.14}$$

The PDF of $Z_{OS}$ can be calculated by

$$f_k(Z_{OS}) = K\binom{N}{K}[P(z)]^{K-1}[1-P(z)]^{N-K}\, p(z) \tag{5.15}$$

where $P(z)$ is the CDF of signal in reference window with $\lambda = 1$ in (5.1), and $p(z)$ is corresponding PDF [14]. Therefore, the PDF of $Z_{OS}$ can be written as

$$f_k(Z_{OS}) = K\binom{N}{K}[1-\exp(-Z_{OS})]^{K-1} \times \exp[-Z_{OS}(N-K+1)] \tag{5.16}$$

Substitute (5.15) into (5.4) and (5.5), then the $P_f$ and $P_d$ of OS-CFAR can be obtained by

$$P_{fa}(OS) = k\binom{N}{K}\frac{\Gamma(N-K+T+1)\Gamma(K)}{\Gamma(N+T+1)} \tag{5.17}$$

and

$$P_d(OS) = k\binom{N}{K}\frac{\Gamma[N-K+T/(1+S)+1]\Gamma(K)}{\Gamma[N+T/(1+S)+1]} \tag{5.18}$$

where $\binom{N}{K} = \dfrac{N!}{(N-K)!K!}$.

When $P_{fa}$ is set to be $10^{-4}$ and 20 reference cells are used, the $P_d$ for OS-CFAR is shown in figure 5.8.

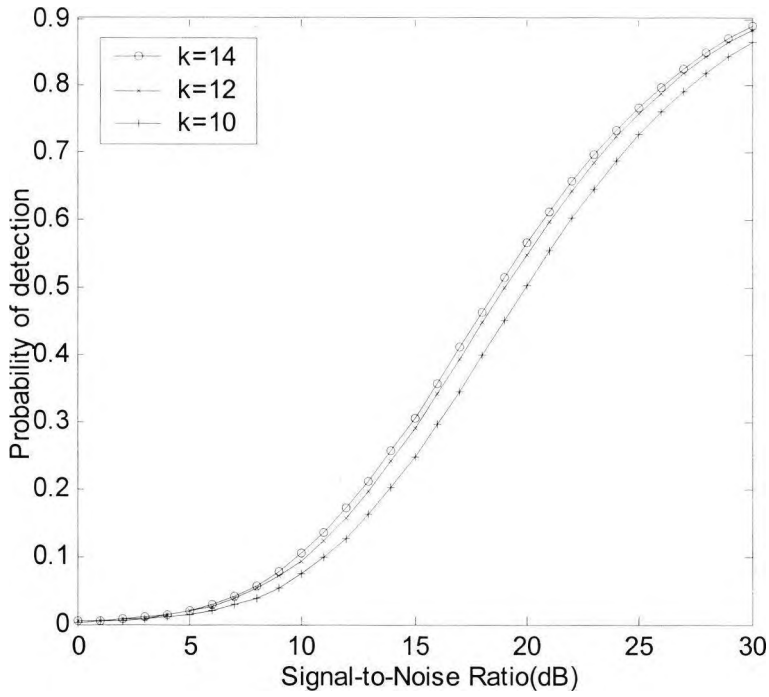


Figure 5.8: $P_d$ of OS-CFAR detector with $N = 20$, $K = 14$, 12, and 10

It is seen that, with homogeneous noise background, the $P_d$ is improved when order parameter $K$ increases. Therefore, in homogeneous noise background, the OS-CFAR with higher parameter $K$ will give better performance. Also, an OS-CFAR detector with higher parameter $K$ is easier to be achieved with bobble sorting technique [55]. Take $K$ = 19 for example, only 19+18 times of comparisons are need to find the $19_{th}$ biggest cell (19 comparisons to find the biggest and 18 comparisons to find the next).

### 5.3.3 GO-CFAR

The GO-CFAR is designed to reduce the false alarm caused by clutter noise, by selecting the half window with interference for noise level estimation. In a GO-CFAR detector, $Z$ can be obtained by

$$Z = \max(Z_1, Z_2) \tag{5.19}$$

Where

$$Z_1 = \frac{2}{N}\sum_{i=1}^{N/2} X_i \; ; \quad Z_2 = \frac{2}{N}\sum_{i=N/2+1}^{N} X_i \tag{5.20}$$

The PDF of $Z$ can be calculated by

$$f_Z(z) = f_1(z)F_2(z) + f_2(z)F_1(z) \tag{5.21}$$

As $Z_1$ and $Z_2$ have same PDF and CDF, equation (5.21) can also be written as

$$\begin{aligned} f_Z(z) &= 2f_1(z)F_1(z) \\ &= 2Z^{N/2-1}e^{-Z}/\Gamma(N/2) \times \int_0^Z y^{N/2-1}e^{-y}/\Gamma(N/2)dy \end{aligned} \tag{5.22}$$

Using equation (5.5), the $P_d$ can be obtained by

$$\begin{aligned} P_d &= \Pr\{Y > TZ | H_1\} \\ &= \int_0^\infty f_Z(z) \int_{TZ}^\infty \frac{1}{\lambda}\exp(\frac{-x}{\lambda})dxdz \\ &= 2\{1 + 2T/N(1+\lambda)\}^{-N/2} - 2\sum_{i=0}^{N/2-1} \binom{N/2+i-1}{i} \times \\ &\quad \{2 + 2T/N(1+\lambda)\}^{-(N/2+i)} \end{aligned} \tag{5.23}$$

By replacing the λ with 0, the equation for $P_{fa}$ can be expressed as

$$\begin{aligned} P_{fa} &= 2(1 + 2T/N)^{-N/2} - 2\sum_{i=0}^{N/2-1} \binom{N/2+i-1}{i} \times \\ &\quad (2 + 2T/N)^{-(N/2+i)} \end{aligned} \tag{5.24}$$

### 5.3.4 SO-CFAR

In a SO-CFAR detector, $Z$ can be obtained by

$$Z = \min(Z_1, Z_2) \tag{5.25}$$

where $Z_1$ and $Z_2$ are shown in (5.20). In this case, the PDF of $Z$ is given by

$$\begin{aligned} f_Z(z) &= f_1(z)(1 - F_2(z)) + f_2(z)(1 - F_1(z)) \\ &= f_1(z) + f_2(z) - pdf^{GO} \end{aligned} \tag{5.26}$$

By using equation (5.4), the $P_{fa}$ of SO-CFAR can be written as

$$\begin{aligned} P_{fa} &= M_{Y1}(-T/u) + M_{Y2}(-T/u) - P_{fa}^{GO} \\ &= 2(1 + 2T/N)^{-N/2} - 2(1 + 2T/N)^{-N/2} - \\ &\quad 2\sum_{i=0}^{N/2-1} \binom{N+i-1}{i} (2 + 2T/N)^{-(N/2+i)} \end{aligned} \tag{5.27}$$

$P_d$ can be obtained by replacing $T$ with $T/(1+\lambda)$.

$$\begin{aligned} P_d &= 2\{1 + 2T/N(1+\lambda)\}^{-N/2} - 2\{1 + 2T/N(1+S)\}^{-N/2} - \\ &\quad 2\sum_{i=0}^{N/2-1} \binom{N+i-1}{i} \{2 + 2T/N(1+S)\}^{-(N/2+i)} \end{aligned} \tag{5.28}$$

### 5.3.5 Comparison of CFAR techniques in homogeneous noise background

The performance of CFAR detectors are firstly compared in the terms of probability of detection. Figure 5.9 shows the detection probability of CA-CFAR, OS-CFAR, GO-CFAR and OS-CFAR, when $P_{fa}$ is set to be$10^{-4}$, and 20 reference cells are used.

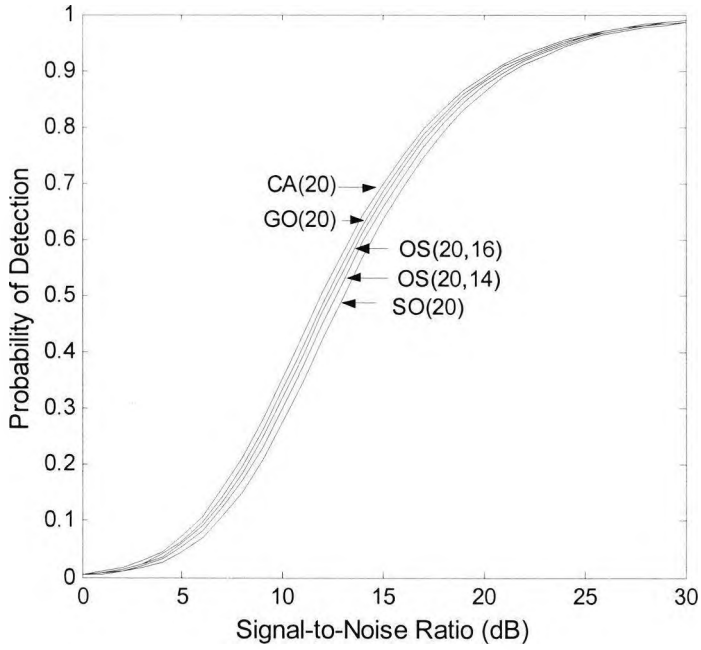


Figure 5.9: $P_d$ for CFAR detectors, $N = 20$, $P_{fa} = 10^{-4}$

The CA-CFAR detector is the one with highest $P_d$, following that is GO-CFAR. GO-CFAR suffers slight degradation compared with CA-CFAR. SO-CFAR is obviously the worst in homogeneous noise background, with lowest $P_d$. The performance of OS-CFAR highly depends on the parameter $K$, when $K$ increases, the performance improves. However it is always better than SO-CFAR and worse than GO-CFAR in homogeneous noise background, this also can be obtained by comparing the Average Detection Threshold (ADT) [17].

The MAT for the four CFAR detectors is shown in figure 5.10. The performance of CFAR detectors can be also compared with MAT, and it confirms the comparison results obtained above.

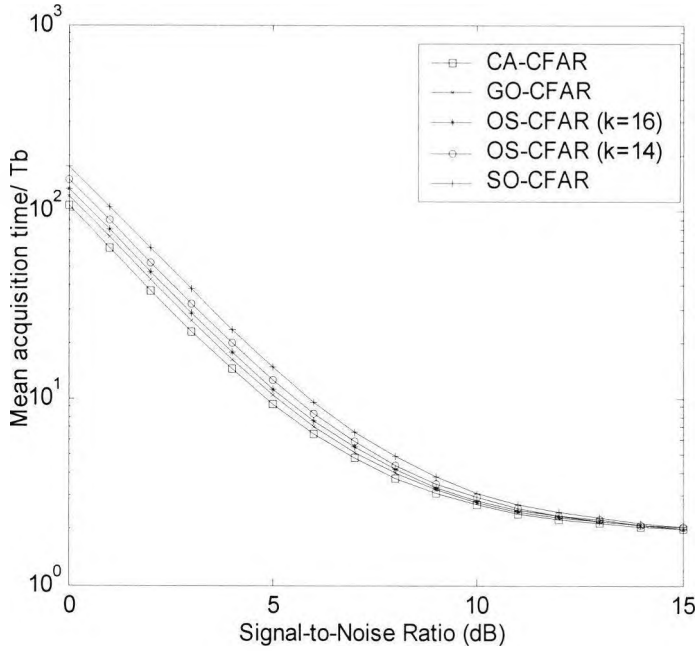


Figure 5.10: MAT for CFAR detectors, $T_b$=256$T_c$, penalty = 2560$T_c$

Some more simulations were done to analyse how the length of reference window will affect the performance of GO-CFAR and SO-CFAR detectors, and the results are shown in figure 5.1.

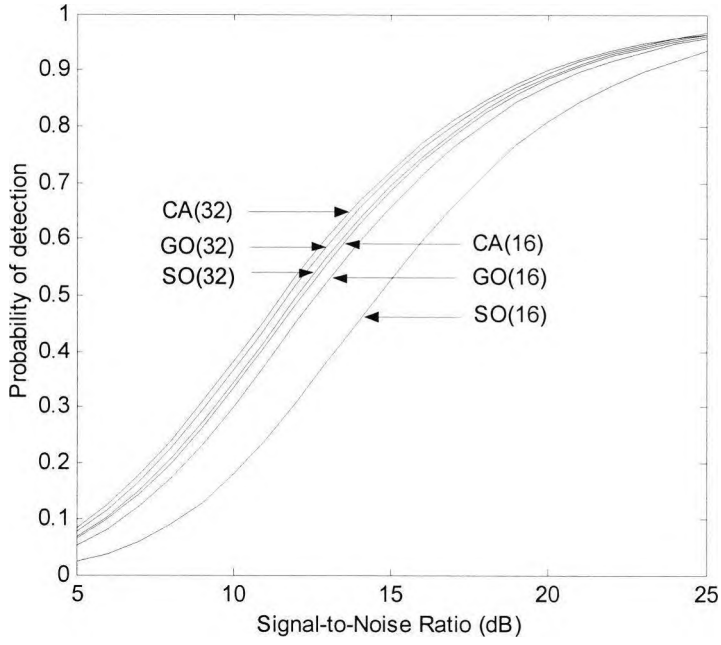


Figure 5.11: $P_d$ for CFAR detectors with different lengths of reference window

It can be seen from figure 5.1, that when the length decrease from 32 to 16, the $P_d$ of CA-CFAR and GO-CFAR detectors both degrade, but in the same scale. However, the $P_d$ of SO-CFAR suffers seriously degradation. It becomes much worse than the CA-CFAR and GO-CFAR detectors. Thus, SO-CFAR is not suitable for the short reference window. No simulation is done for OS-CFAR, because it has one more parameter $K$, which will affect the performance, while the other three CFAR techniques have only one parameter $N$.

## 5.4 Analysis of CFAR detectors in non-homogeneous noise background

Wireless channels in mobile communication systems are distinguished by multi-path wave propagation. Signals arrived at the receiver via different paths bouncing off buildings, the earth's surface, pillars and other scattering objects. The likelihood of a signal passing through the LOS path is small. Signals with same information are transmitted from different paths. Because of different delays of the paths, the signals with same information will cause multiple targets for a matched filter detector as shown in figure 5.12.

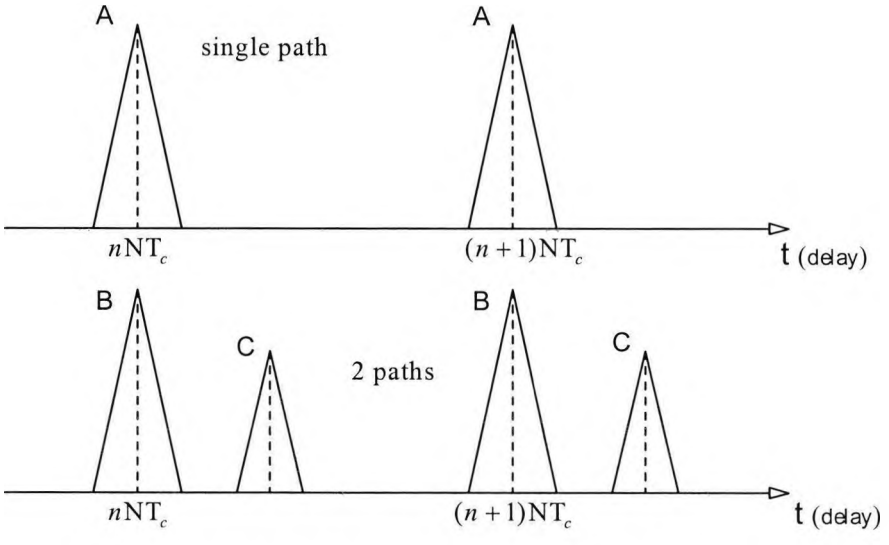


Figure 5.12: Output of MF in multi-path communications

When clutter noise exists in transmission, the CFAR techniques designed for homogeneous background will be affected. It is because that the reference cells are no longer I.I.D when the clutter edge is in the reference window.

### 5.4.1 CA-CFAR detectors in non-homogeneous noise background

In mobile communication with multiple targets, when one or more interfering targets exist in the reference window, the threshold of CA-CFAR will be raised. Therefore, the equations for CA-CFAR need to be derived again for non-homogeneous noise background. When $r$ interfering targets exist in the reference window, and their average INR is $I$, the algorithm for CA-CFAR in multiple targets environment is derived as follow.

The $N$ reference cells can be separated into two groups, one group with $r$ cells of interfering targets, and $N$-$r$ cells from clear background. In the first group, the SNR is $\lambda/(1+I)$, and in second group, the SNR is λ. The cells are I.I.D in their own group. Therefore, the $P_{fa}$ can be obtained by

$$P_{fa}(CA) = \frac{1}{(1+T/N)^{N-r}} \times \frac{1}{[1+T(1+I)/N]^{r}} \tag{5.29}$$

The scaling factor $T$ can be obtained by setting $I$ equal to 0. By replacing $T$ with $T/(1+S)$, the equation for $P_d$ is derived as

$$P_d(CA) = \frac{1}{\{1+T/[(1+S)N]\}^{N-r}} \times \frac{1}{\{1+T\times(1+I)/[(1+S)N]\}^{r}} \tag{5.30}$$

When there is clutter noise in the reference window, if the CUT is from the clear region, the situation is similar as multiple target communication, because the multiple targets can

be regarded as cells with clutter noise. Assuming $r$ cells are covered by the clutter region, and the CNR is $C$, the $P_{fa}$ of CUT in clear region can be expressed as

$$P_{fa}(CA) = \frac{1}{(1+T/N)^{N-r}} \times \frac{1}{[1+T(1+C)/N]^{r}} \tag{5.31}$$

and for $P_d$, it is

$$P_d(CA) = \frac{1}{\{1+T/[(1+S)N]\}^{N-r}} \times \frac{1}{\{1+T\times(1+C)/[(1+S)N]\}^{r}} \tag{5.32}$$

When CUT is from the clutter region, the r cells can be regarded as from the clutter region, but the SNR of the $r$ cells are $\lambda(1+C)$, and SNR of $N$-$r$ cells are λ. Therefore the $P_{fa}$ of CUT in clutter region can be expressed as

$$P_{fa}(CA) = \frac{1}{(1+T/N)^{r}} \times \frac{1}{[1+T/(1+C)N]^{N-r}} \tag{5.33}$$

and for $P_d$ can be calculated by

$$P_d(CA) = \frac{1}{\{1+T/[(1+\lambda)N]\}^{r}} \times \frac{1}{\{1+T/[(1+\lambda)(1+C)N]\}^{N-r}} \tag{5.34}$$

Figure 5.13 illustrates how the interfering targets will affect the performance of CA-CFAR detectors. It is obviously, that even if there is only one interfering target in the reference window, the $P_d$ of CA-CFAR decreases seriously. When there are 2 interfering targets with INR/SNR equal to 2, the $P_d$ dropped below 0.2.

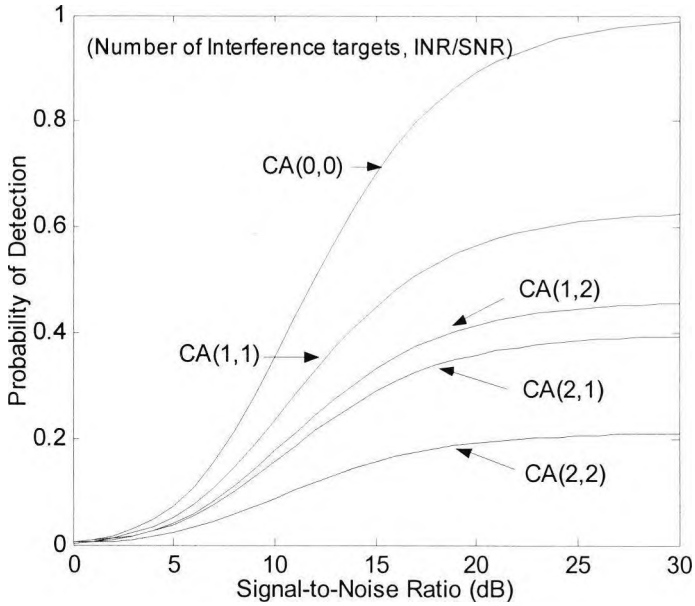


Figure 5.13: $P_d$ for CA-CFAR detectors in multiple targets communications

In clutter transmission, when the cell under test is in the clear, the cells in clutter region can be regarded as interfering targets. It means in clutter transmission, CA-CFAR will also suffer the problem of low $P_d$ .

### 5.4.2 OS-CFAR detectors in non-homogeneous noise background

In order to analyse the performance of OS-CFAR in non-homogeneous background, the PDF of the $K_{th}$ biggest cell is needed. Assuming there are $r$ cells with power level $(1+C)$ and the other $N$-$r$ cells with power level 1.Then, the CDF of the $K_{th}$ cell can be calculated by (5.35) [17]

$$F_Z(z) = \sum_{i=k}^{N} \sum_{L=\max(0,i-r)}^{\min(i,N-r)} \binom{N-r}{L}\binom{r}{i-L} \times e^{-(N-r-L)Z} \times (1-e^{-Z})^{L} e^{-(r-i+L)Z/(1+C)} \times (1-e^{-Z/(1+C)})^{i-L} \tag{5.35}$$

$P_{fa}$ can be obtained by using equation (5.4)

$$
\begin{aligned}
P_{fa}(OS) &= P[Y > TZ | H_0] \\
&= T\int_0^{\infty} F_Z(z)e^{-TZ}dz \\
&= T\sum_{i=k}^{N}\sum_{L=\max(0,i-r)}^{\min(i,N-r)} \frac{\binom{N-r}{L}\binom{r}{i-L}\sum_{j_1=0}^{L}\sum_{j_2=0}^{i-L}\binom{L}{j_1}\binom{i-L}{j_2}(-1)^{j_1+j_2}}{N-r-L+T+j_1+(j_2+r-i+L)/(1+C)}
\end{aligned}
\tag{5.36}
$$

When the CUT is covered by clutter region, $P_{fa}$ can be calculated by replacing $T$ with $T/(1+C)$ in equation (5.36) and $P_d$ can be obtained by replacing $T$ with $T/(1+S)$.

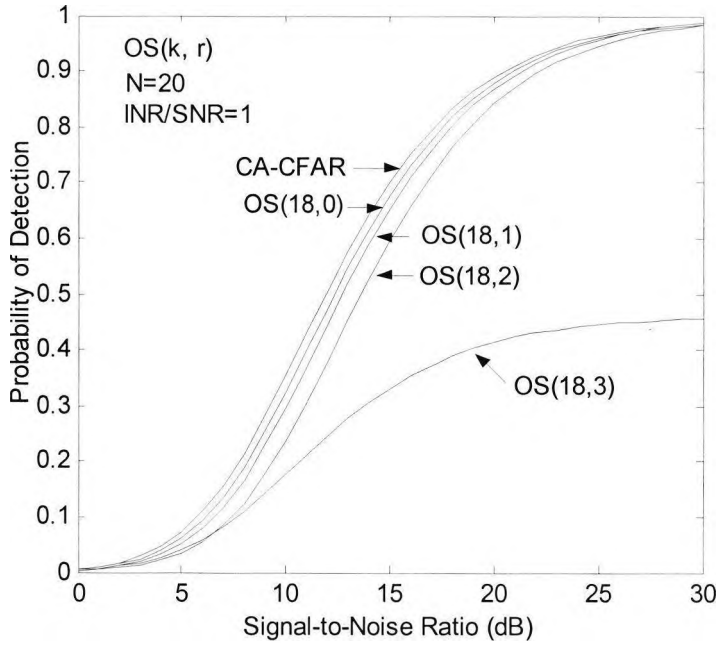


Figure 5.14: $P_d$ for OS-CFAR detectors in multiple targets communications

Figure 5.14 shows the $P_d$ of OS-CFAR as a function of target SNR for different number of interfering targets at $P_{fa} = 10^{-4}$, $N = 20$, and $K = 18$. It can be seen that when there are no more than 2 interfering targets in the reference window, the $P_d$ of OS-CFAR remain

at a high level, but when there are 3 or more interfering targets, the $P_d$ becomes quite low. This is because one of the interfering targets is chosen for the noise level estimation. Therefore, if *N-K* interfering targets exist, they only affect the performance of OS-CFAR slightly. However, if there are more, the OS-CFAR detector suffers rapid decrease in detection probability. In a clutter transmission, the interfering targets can be regarded as clutter cells in the reference window, when the CUT is not covered by clutter region. The situation that CUT is within the clutter region is analysed in section 5.4.4.

### 5.4.3 GO-CFAR and SO-CFAR detectors in non-homogeneous noise background

The derivation of $P_d$ and $P_{fa}$ for GO-CFAR detectors is shown in Appendix A.

In clutter transmission, considering the special case that the leading window has noise from clutter region and the lagging window are from clear region, if CUT is from clear region, the $P_{fa}$ can for a GO-CFAR detector can be calculated by

$$\begin{aligned} P_{fa} &= (1+T/n)^{-n} + (1+(1+C)T/n)^{-n} - \sum_{j=0}^{n-1}\binom{n+j-1}{j} \\ &\times (1+T/n+1/(1+C))^{-(n+j)} \\ &\times \left\{(1+C)^{-n} + (1+C)^{-j}\right\} \end{aligned} \tag{5.37}$$

On the other hand, if the CUT is from the clutter region, the $P_{fa}$ can be calculated by replacing $T$ with $T/(1+C)$ in (5.37).

The special case is not enough for performance analysis. The equations for $P_{fa}$ and $P_d$ in general cases are derived in appendix A. And the results are shown in figure 5.15 and 5.16. Figure 5.15 shows the detection probability of CA-CFAR, GO-CFAR and SO-CFAR detectors with only one interfering target, and figure 5.16 shows the result of

detection probability of CA-CFAR, GO-CFAR and SO-CFAR with two interfering targets in same side of reference window.

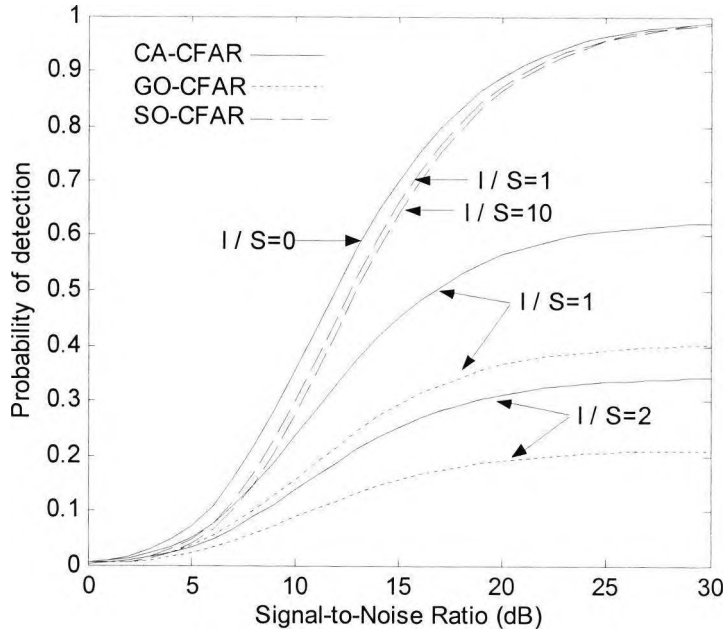


Figure 5.15: $P_d$ for CA-CFAR, GO-CFAR and SO-CFAR detectors with 1 interfering target

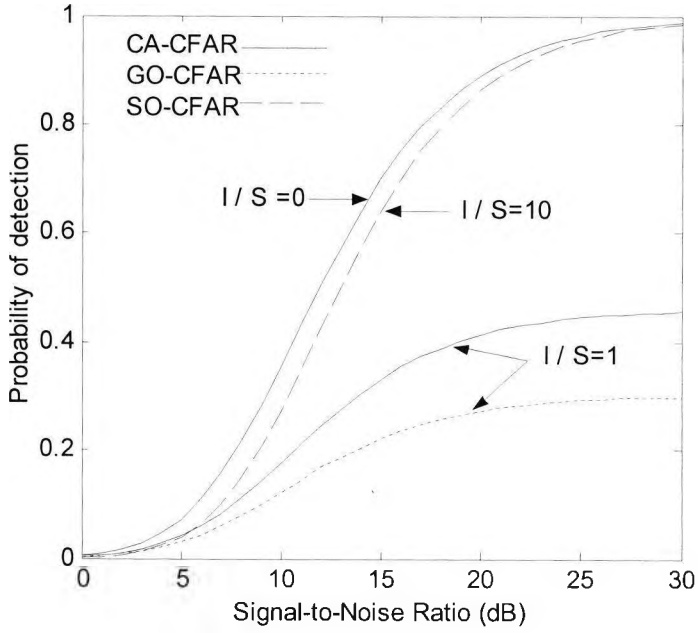


Figure 5.16: $P_d$ for CA-CFAR, GO-CFAR and SO-CFAR detectors with 2 interfering targets on the same side of reference window

Figure 5.15 and 5.16 show that both CA-CFAR and GO-CFAR are seriously affected in multiple targets transmission, with rapid decrease in $P_d$. However, SO-CFAR has much better performance than the other two types of CFAR detectors. Even if high *I/S* and more interfering targets exist, the $P_d$ of SO-CFAR only slightly decreased.

When there are two interfering targets on different sides of the reference window, $Z$ can be expressed by

$$Z_j = \sum_{0}^{N/2-1} X_i + V = U + V \qquad \text{j} = 1, 2 \tag{5.38}$$

Where $U$ has CDF equal to $G\ (N/2\text{-}1,\ \mu)$ and $V$ has CDF equal to $G\ (1,\ \mu\ (1+I))$ [17].

$$f_j(y) = \int_0^y f_U(x) f_V(y-x)dx \tag{5.39}$$

$$f_j(y) = \sigma(1-\sigma)^{-(N/2-1)}(e^{-y\sigma} - \sum_{L=0}^{N/2-2} \frac{(1-\sigma)^L y^L e^{-y}}{L!}) \tag{5.40}$$

Then, the PDF of $Z$ for GO-CFAR and SO-CFAR can be obtained by using equation (5.21) and (5.26), where $F_j(y)$ is the integral of $f_j(y)$. The $P_{fa}$ for GO-CFAR and SO-CFAR with interfering targets on both sides, can be obtained using MGF of $Z$.

Figure 5.17 shows the result of detection probability of CA-CFAR, GO-CFAR and SO-CFAR with two interfering targets on different sides. The performance of SO-CFAR is no longer as good as that with interfering targets on same side. It is even worse than CA-CFAR and GO-CFAR detectors, when the SNR is low. This is because both sides are affected by interfering targets, and the threshold calculation of SO-CFAR can't avoid the interference by selecting the one without interfering targets.

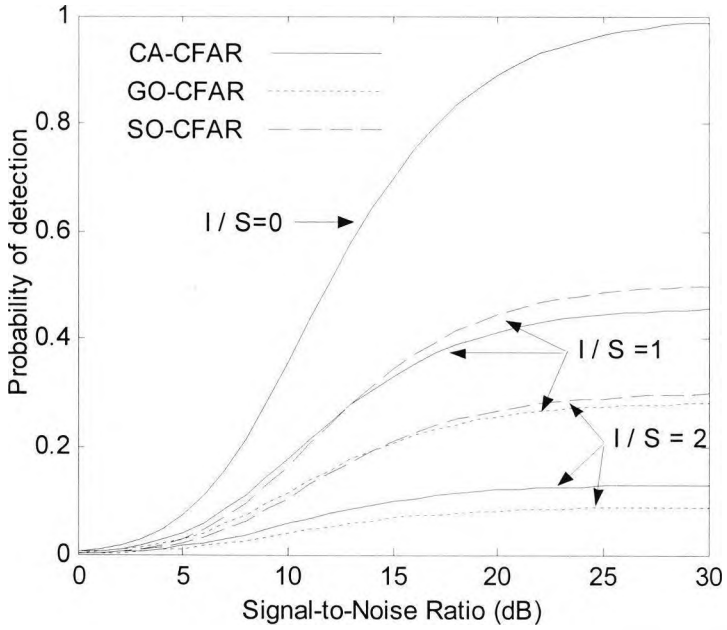


Figure 5.17: $P_d$ for CA-CFAR, GO-CFAR and SO-CFAR detectors with 2 interfering targets on the different side of reference window

### 5.4.4 Comparison of non-adaptive CFAR detectors in non-homogeneous background

To compare the performance of OS-CFAR with other CFAR detectors, $K$ for OS-CFAR detector must be initially chosen. Figure 5.18 shows how the clutter cells will affect the false alarm probability of OS-CFAR with different $K$, at $P_{fa} = 10^{-4}$, $N = 20$, $C = 10$ dB. The alarm probability of OS-CFAR detector is good to be near $10^{-4}$. Otherwise, if the false alarm rate is too high, it will lead to much penalty time in acquisition. On the other hand, if the false alarm rate is too low, it means the threshold is over-estimated, thus the detection probability will be low. The detection probability of OS-CFAR with different $K$, at $P_{fa} = 10^{-4}$, $N = 20$, $C = 10$ dB and SNR=10 dB is shown in figure 5.19.

From figures 5.18 and 5.19, it can be seen that, the position of clutter edge is very important for the performance of OS-CFAR. When the clutter edge is in the middle of the

reference window, the performance of OS-CFAR is the worst, and it improves from middle to the two sides.

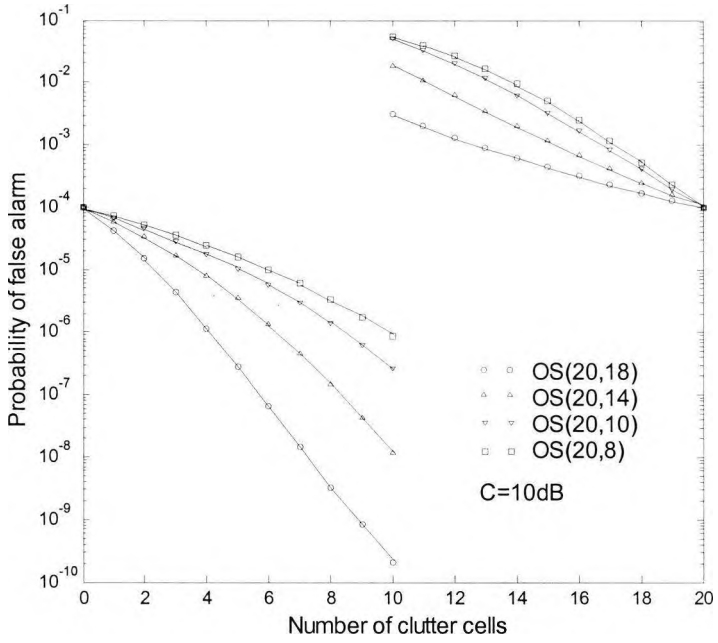


Figure 5.18: $P_{fa}$ for OS-CFAR in clutter transmissions, $K$ = 18, 14, 10, 8, $P_{fa}$ is selected to be $10^{-4}$

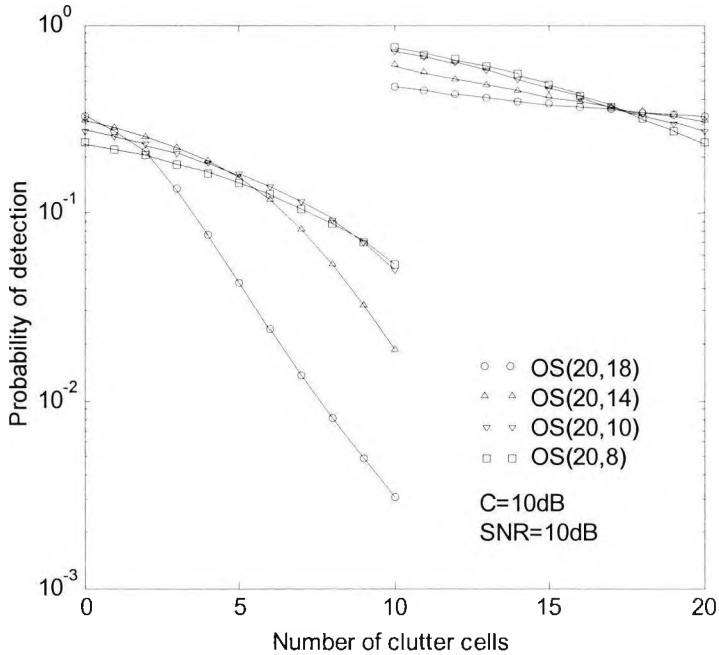


Figure 5.19: $P_d$ for OS-CFAR in clutter transmissions, $K$ = 18, 14, 10, 8, $P_{fa}$ is selected to be $10^{-4}$

As both $P_{fa}$ and $P_d$ of OS-CFAR with different $K$ are different, the best method to compare their performance is to use MAT.

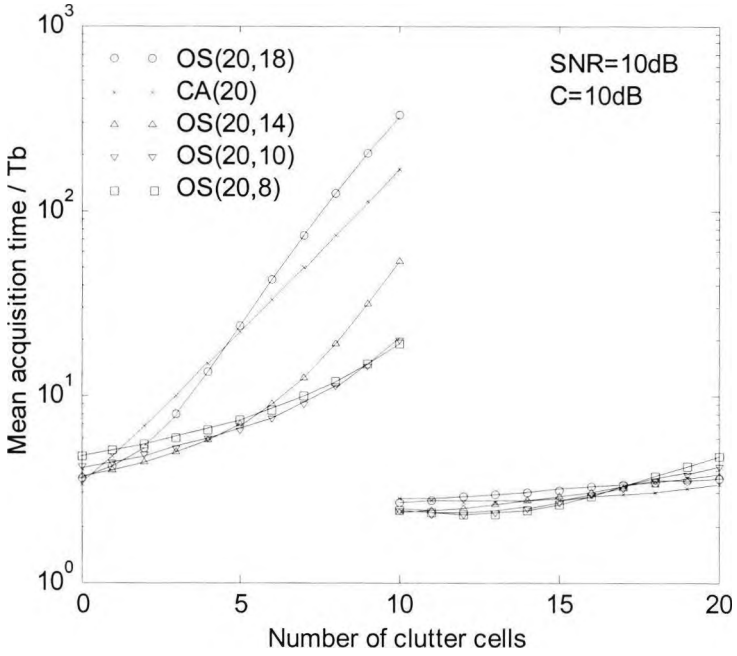


Figure 5.20: MAT for OS-CFAR and CA-CFAR detectors in clutter transmissions

Shown in figure 5.20, when $K$ is chosen to be high (equal to 18), the MAT for CUT in clear region increases rapidly when the number of clutter cells increases, and it is even worse than that of CA-CFAR. When the CUT is covered by clutter region, the MAT of OS-CFAR detectors with different $K$ are very near. As shown in this figure, the MAT of OS-CFAR with $K$ equal to 10 and 8 are the best. However, $K$ equal to 10 is better, because it is only slightly higher than the MAT of $K$ equal to 8 when there are 9 or 10 clutter cells, and it is lower in most situations. Therefore, in clutter transmission, the $K$ of OS-CFAR is best to be chosen as $N$ / 2. In the following, OS-CFAR (20, 10) is used in comparison with other CFAR detectors in clutter transmission.

Figure 5.21 shows the MAT of OS (20, 10), GO (20) and SO (20), at $P_{fa} = 10^{-4}$, $C$ = 10 dB and SNR=10 dB.

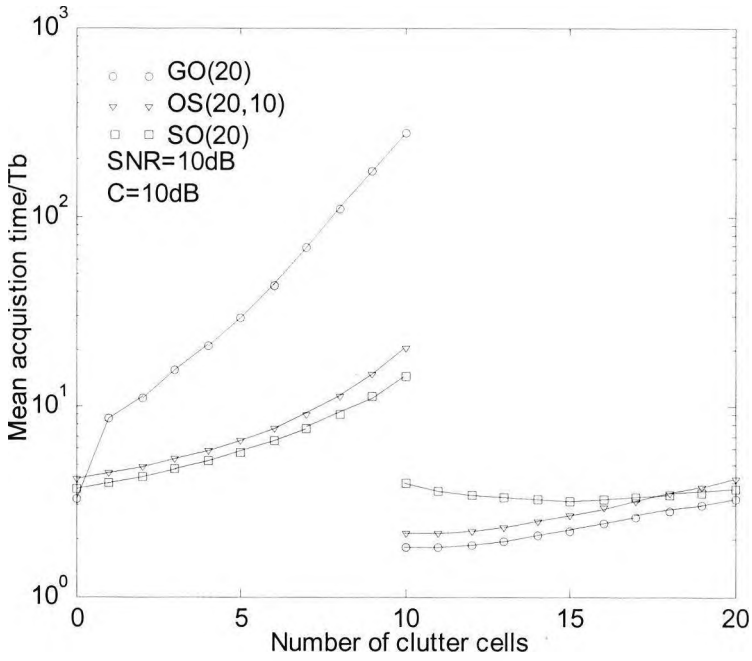


Figure 5.21: Comparison of MAT for OS-CFAR, GO-CFAR and SO-CFAR in clutter transmissions

From figure 5.26, when the CUT is not covered by the clutter region, the MAT of GO-CFAR (20) is the much worse than that of OS-CFAR (20, 10) and SO-CFAR (20). It is like the result shown in figures 5.15 and 5.16, that when the interfering targets are in the same side of the window, the performance of GO-CFAR will be seriously affected, but that of SO-CFAR only has slightly degradated. This is because in GO-CFAR the over-estimated threshold makes the $P_d$ too low. However, in SO-CFAR it remains same as in homogeneous noise background. When the CUT is covered by the clutter region, GO-CFAR has the shortest MAT, the following is OS-CFAR, and SO-CFAR is the worst. For GO-CFAR, the $P_d$ remains the same like in homogeneous noise background, this is

because the $Z$ for threshold calculation is obtained from the clutter region, and the CUT is also covered by clutter. The $P_{fa}$ for GO-CFAR is less than that in homogeneous background, because the clear cells has less probability in false alarm, while the other cells remains the same. For SO-CFAR, when the CUT is covered by clutter region, the $P_d$ increases, however, $P_{fa}$ increases as well.

OS-CFAR is obviously the best choice in clutter transmission compared with GO-CFAR and SO-CFAR, it is only slightly worse than the SO-CFAR when CUT is in clear region and slight worse than the GO-CFAR when CUT is covered by the clutter region.

## 5.5 Summary

The purpose of this chapter was to carry out an analysis for CFAR detectors without adaptive censoring. The results show that in the case of homogeneous noise background, all the CFAR detectors perform well. However, in non-homogeneous noise background, CA-CFAR detectors suffer rapid degradation. The performance of OS-CFAR, GO-CFAR and SO-CFAR highly depends on the number of interfering targets and position of clutter edge. Therefore, in the chapter 6, adaptive censoring technique is applied to the CFAR detectors.

# CHAPTER 6

# Adaptive CFAR Techniques for Non-Homogeneous Noise Background

## 6.1 Introduction

CFAR techniques are already adaptive in noise level estimation. In this chapter, adaptive censoring is added into CFAR techniques. Because some cells in reference window do not have the same noise level as CUT, they must be censored in noise level estimation. Figures 6.1 and 6.2 show the signal in reference window for a clutter transmission with CUT in clear region. In figure 6.1, the first four cells are covered by clutter region, so they are having different SNR with other cells. Therefore, in noise level estimation, these four cells should be censored.

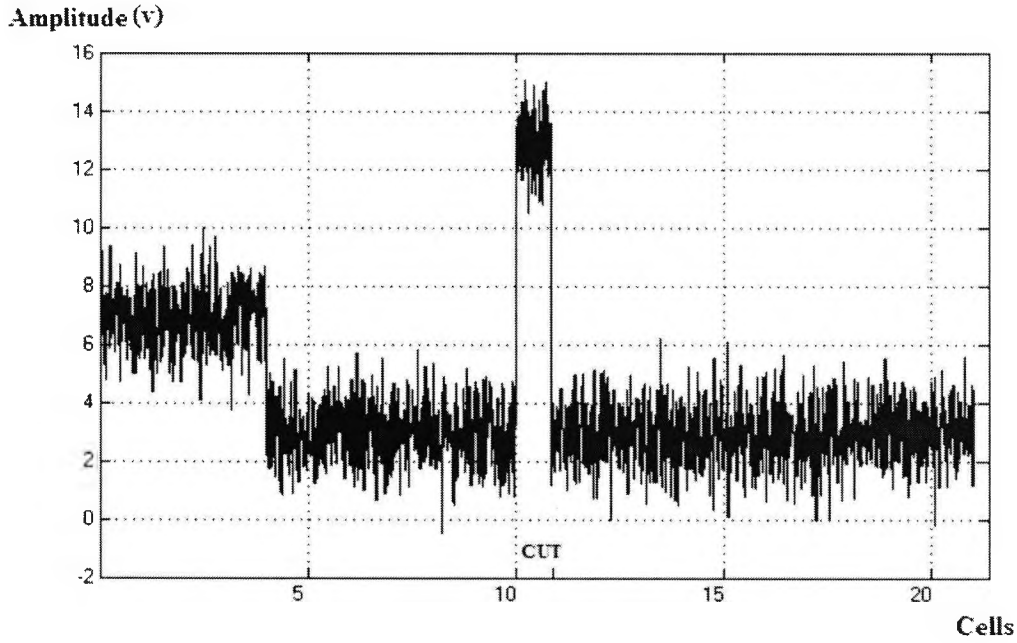


Figure 6.1: Signal in reference window for clutter transmissions, 4 cells are covered by the clutter region

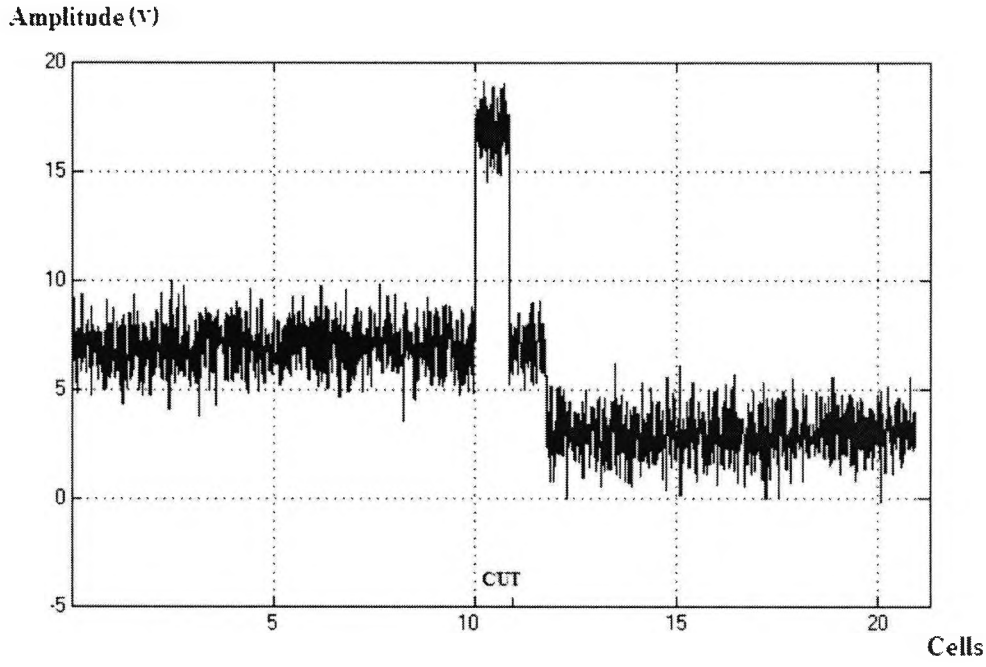


Figure 6.2: Signal in reference window for clutter transmission, 12 cells are covered by the clutter region

Figure 6.2 illustrates the situation that the CUT is covered by the clutter noise. In this situation, the left 12 cells including the CUT have same SNR, while the other 9 cells are with clutter-free SNR. Therefore, the noise level estimation, the 9 cells should be censored.

For transmission with interfering targets, it is like the situation in figure 6.1, because the interfering targets can be regarded as cells covered by clutter region and the CUT is not covered.

## 6.2 Adaptive censoring techniques

Objective of the adaptive censoring technique can be generally divided into two steps:

a) Find the clutter edge

b) Censor the cells on one side

In the first step, all the $N$ cells are first ranked as in equation (5.13) for OS-CFAR detectors.

$$X_{(1)} \leq X_{(2)} \leq \ldots \leq X_{(k)} \leq \ldots \leq X_{(N)}$$

The clutter-covered cells must be ranking higher than the other cells, especially for the high CNR. Therefore, assuming $X_{(k)}$ is the smallest cells that covered by clutter region. When $m < k$, $X_{(2)} - X_{(1)}$, $X_{(3)} - X_{(2)}$, ..., $X_{(m)} - X_{(m-1)}$ are I.I.D [20]. However, when it goes to $X_{(k)}$, there will be a sudden rise, and this can be used to find the clutter edge.

In the second step, if $k \leq N/2$, the CUT is considered to be in the clear region, otherwise, the CUT is decided to be in the clutter region. When the CUT is in the clear region, the clutter-covered cells must be censored, which refer to the cells from $X_{(k)}$ to $X_{(N)}$. When

the CUT is in the clutter region, the cells from $X_{(1)}$ to $X_{(k-1)}$ must be censored in noise level estimation.

### 6.2.1 Clutter edge detection

Clutter edge detection process is similar as PN code acquisition, while both of them are method of searching the cell higher power level.

To check if $X_{(k)}$ is the clutter edge, firstly the value of $S_{(k-1)} = X_{(1)} + X_{(2)} + \ldots + X_{(k-1)}$ is calculated as in CA-CFAR, then $S_{(k-1)} \times T_{(k-1)}$ is compared with $X_{(k)}$. If $S_{(k-1)} \times T_{(k-1)}$ is smaller than $X_{(k)}$, then $X_{(k)}$ is considered to be in the clutter region. Otherwise, it is from the clear region. The whole process starts from $X_{(1)}$, and if it is clear $X_{(2)}$ is to be tested, till the clutter edge is detected.

The hypothesis of null targets ($H_0$) and targets ($H_1$) are:

$$\begin{aligned} H_0 &: \lambda = u, \\ H_1 &: \lambda = u/(1+C) \end{aligned} \tag{6.1}$$

As shown in the equation, the clutter edge decision is made according to

$$X_{(k+1)} \underset{H_0}{\overset{H_1}{\gtrless}} S_k T_k; \qquad X_{(k+1)} \underset{H_0}{\overset{H_0}{\lessgtr}} S_k T_k; \tag{6.2}$$

The probability of false censoring $P_{fc}$ is the probability of detection under $H_0$, expressed in equation it is

$$P_{fc} = \Pr(R_k > 0 \mid H_0) \tag{6.3}$$

Where $R_k = X_{(k+1)} - S_k T_k$

$P_{fc}$ can be written as contour integral [52] given by

$$P_{fc} = -\frac{1}{2\pi i} \int_c \omega^{-1} \Phi R_k \mid H_0(\omega) d\omega \tag{6.4}$$

Where $\Phi R_k \mid H_0(\omega)$ is the MGF of equivalent test statistic $R_k$ under hypothesis of $H_0$, that is

$$\Phi R_k \mid H_0(\omega) = E[\exp(-R_k \omega)] \tag{6.5}$$

The joint MGF of order statistics $X_{(1)}, \ldots, X_{(k+1)}$ is defined to be

$$\Phi X_{(1)},\ldots, X_{(k+1)} \mid H_0(\omega_1,\ldots,\omega_{K+1}) = E\left[\exp\{-\sum_{j=1}^{K+1} \omega_j X_{(j)}\}\right] \tag{6.6}$$

By setting the

$$\omega_1 = \omega_2 = \ldots = \omega_k = -T_k \omega = -T_k \omega_{k+1} \tag{6.7}$$

The MGF of $R_k$ under hypothesis $H_0$ can be obtained as shown in Appendix B.

$$\Phi R_k \mid H_0(\omega) = \frac{N!}{(N-K+1)!} \prod_{j=1}^{k+1} \frac{1}{(N-j-1)+\omega[1-(k-j+1)T_k]} \tag{6.8}$$

Substituting equation (6.8) into (6.4), then the equation for $P_{fc}$ can be obtained by

$$P_{fc} = \binom{N}{K} \frac{1}{[1+T_k(N-K)]^K} \tag{6.9}$$

Then the $T_k$, $K$ =1, ...., $N$-1, for $N$ = 20 and $P_{fc} = 10^{-4}$ are presented in table 6.1.

Table 6.1: Scaling factor $T_k$ for clutter edge detection, $K$ = 1, 2, ..., 19

| K | 1 | 2 | 3 | 4 | 5 | 6 | 7 | 8 | 9 | 10 |
|---|---|---|---|---|---|---|---|---|---|---|
| $T_k$ | 10526 | 76.52 | 13.18 | 5.152 | 2.830 | 1.857 | 1.355 | 1.061 | 0.872 | 0.745 |
| K | | 11 | 12 | 13 | 14 | 15 | 16 | 17 | 18 | 19 |
| $T_k$ | | 0.655 | 0.592 | 0.547 | 0.518 | 0.503 | 0.506 | 0.534 | 0.616 | 0.901 |

The probability of edge detection ($P_{dc}$) can be derived from equation (6.9). All the cell under clear background may cause false clutter edge detection, and this is why $\binom{N}{K}$ exists in equation, but for correct detection, there is only one cell, so $\binom{N}{K}$ is deleted. And for correct clutter edge detection, the SNR of $X_{(k)}$ is lowered by clutter. Therefore the equation for $P_{dc}$ is shown as

$$P_{dc} = \frac{1}{[1+T_K(N-K)/(1+C)]^K} \tag{6.10}$$

The probability of clutter edge detection for the CFAR detector with 20 cells is shown in figure 6.3. Parameter $m$ denotes the number of clear cells.

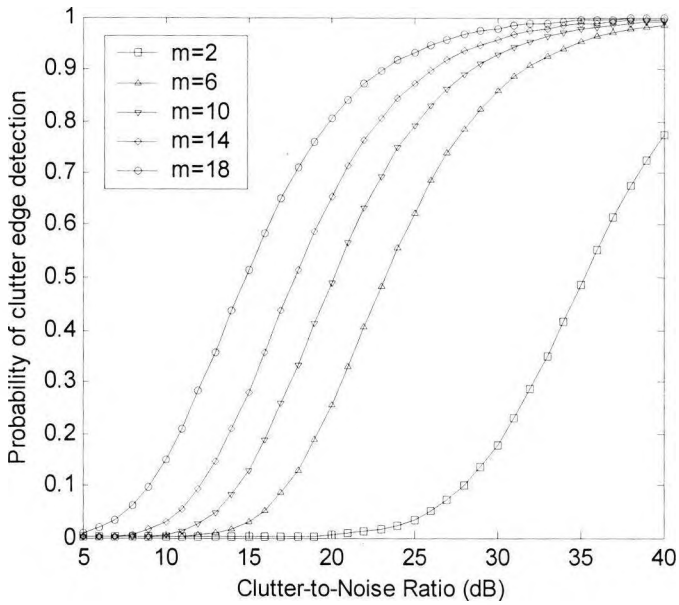


Figure 6.3: $P_{dc}$ for different number of cells covered by clutter, $m$ = 18, 14, 10, 6, 2

From figure 6.3, it can be seen that the number of cells in the clear is an important parameter for clutter edge detection, as it raises, the $P_{dc}$ raises efficiently. Another important parameter is the CNR, when it increases, the value of $P_{dc}$ increases.

## 6.3 CFAR detectors with adaptive censoring

The adaptive PN code detector named GO/SO-CFAR detector is firstly referred in the [20]. It is called GO/SO-CFAR, because in clutter transmission, it automatically selected the greatest or smallest *Z*, depending on the position of clutter edge. In multiple targets environment, the adaptive detector is named Automatic Censoring Mean Level Detector (ACMLD), and the smallest *Z* is selected for noise level estimation.

In this study, only GO/SO-CFAR detector is analysed, because ACMLD can be considered as GO/SO-CFAR detector with the CUT in clear.

### 6.3.1 Analysis of GO/SO-CFAR detector

In GO/SO-CFAR detector, if the CUT is from clear region ($K > N/2$), the lowest $K$ samples are used for noise level estimation.

$$Z = \sum_{i=1}^{k} X_{(i)} \tag{6.21}$$

By setting $K_{c1} = 0$ and $K = 0$ in (C.4) of appendix C, we can obtain that

$$\Phi_X(\omega) = \binom{N}{K} \prod_{j=1}^{K} \left[ \omega + \frac{N-j+1}{K-j+1} \right]^{-1} \qquad K > N/2 \tag{6.22}$$

The probability of false alarm can be calculated by (6.24) [20]

$$P_{fa} = \Phi_X[T/(1+C)] \tag{6.23}$$

Substitute (6.23) into (6.22), the equation for $P_{fa}$ can be written as

$$P_{fa} = \binom{N}{K} \prod_{j=1}^{K} \left[ T + \frac{N-j+1}{K-j+1} \right]^{-1} \qquad K > N/2 \tag{6.24}$$

If the CUT is covered by the clutter region ($K \leq N/2$), the cells from clear region must be censored, therefore, $Z$ can be calculated by

$$Z = \sum_{i=k+1}^{N} X_{(i)} \tag{6.25}$$

By setting $K_{c2} = 0$ and $K = 0$ in (C.4) of appendix C, we can obtain that

$$\begin{aligned} \Phi_X(\omega) &= \binom{N}{K} (1+\omega)^{-(N-K-1)} \\ &\cdot \sum_{j=0}^{K} \binom{K}{j} (-1)^j \left( 1 + \frac{j}{N-K} + \omega \right)^{-1} \qquad K \leq N/2 \end{aligned} \tag{6.26}$$

Substituting (6.26) into (6.23), the equation for $P_{fa}$ can be written as

$$\begin{aligned} P_{fa} &= \binom{N}{K} (1+T)^{-(N-K-1)} \\ &\cdot \sum_{j=0}^{K} \binom{K}{j} (-1)^j \left( 1 + \frac{j}{N-K} + T \right)^{-1} \qquad K \leq N/2 \end{aligned} \tag{6.27}$$

### 6.3.2 Results

To analyse the performance of GO/SO-CFAR detector, firstly, the $P_d$ of GO/SO-CFAR is compared with OS-CFAR and CA-CFAR in non-homogeneous noise background. Figures 6.4 and 6.5 compare the OS-CFAR, GO/SO-CFAR and CA-CFAR in $P_d$, when $K$ =18 and $r$ = 2. In these two figures $r \leq N$ - $K$, the OS-CFAR detector can obtain noise level without interfering. As shown in figure 6.4, the OS-CFAR has the highest detection probability. And with adaptive censoring, GO/SO-CFAR also performs well, with small difference to OS-CFAR. CA-CFAR is the worst, because any interfering targets will increase the threshold, especially for those with high INR.

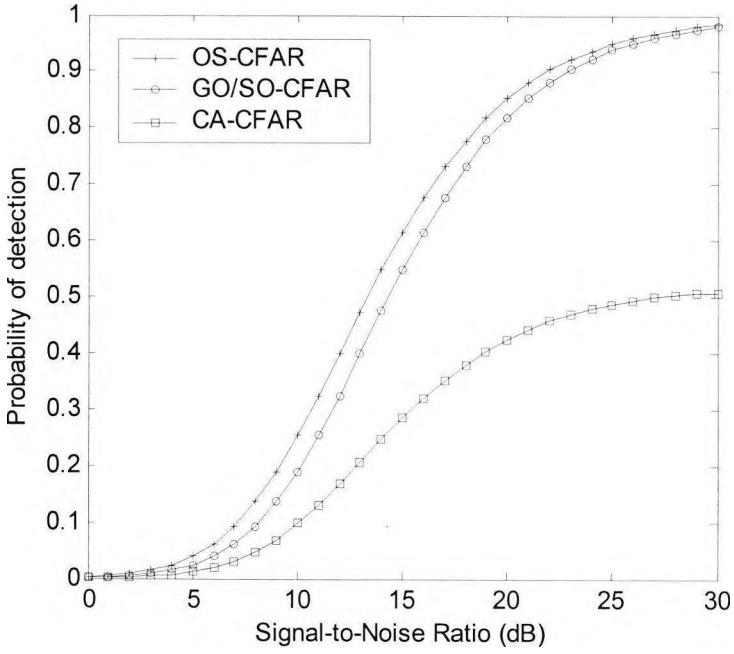


Figure 6.4: $P_d$ of GO/SO-CFAR, CA-CFAR and OS-CFAR, with $r$=2, $K$=18 and INR = 10dB

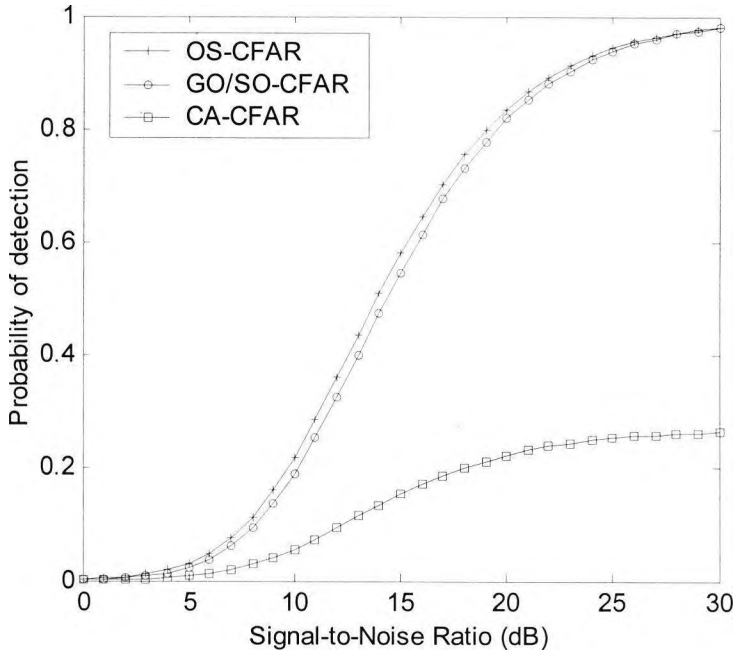


Figure 6.5: $P_d$ of GO/SO-CFAR, CA-CFAR and OS-CFAR, with $r$=2, $K$=18 and INR = 25dB

In figure 6.5, when the INR increases from 10 dB to 25 dB, it can be seen that the $P_d$ of OS-CFAR and GO/SO-CFAR have only little degradation. But the gap between them becomes smaller, this is because $P_{dc}$ is higher for increased INR. The advantage of using GO/SO-CFAR detector is not visible in figures 6.4 and 6.5, because there are only two interference targets existing, for OS-CFAR with $K$ = 18, the threshold obtaining can avoid the interference targets. Therefore, some simulations are done for more interfering targets, and the results are plotted in figures 6.6 and 6.7.

Figure 6.6 shows the $P_d$ for GO/SO-CFAR, CA-CFAR and OS-CFAR, when 4 interfering targets exist.

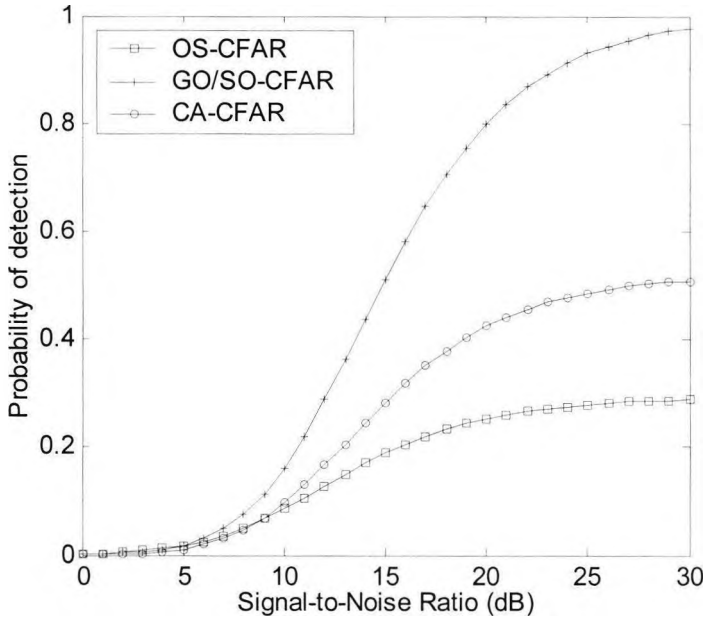


Figure 6.6: $P_d$ of GO/SO-CFAR, CA-CFAR and OS-CFAR, with $r$ = 4, $K$=18 and INR = 10 dB

With same INR, the $P_d$ of OS-CFAR suffers rapid degradation from 2 interfering targets to 4 interfering targets. The reason for the degradation is because the cell chosen for noise

level estimation is interfered by interfering targets, when $K < N - r$. For GO/SO-CFAR, the $P_d$ only decreased by a small amount compared with that in figure 6.4.

The advantage of using GO/SO-CFAR is more significant in figure 6.7 with INR = 25 dB. It can be seen that when the INR is higher, OS-CFAR and CA-CFAR will over estimate the threshold to a higher level, and this will lead to a very low $P_d$. However, in GO/SO-CFAR, for higher INR targets, they are more likely to be censored from the reference window. Therefore, the $P_d$ for GO/SO-CFAR with 4 interfering targets at INR = 25 only decreases slightly from that at INR = 10 dB.

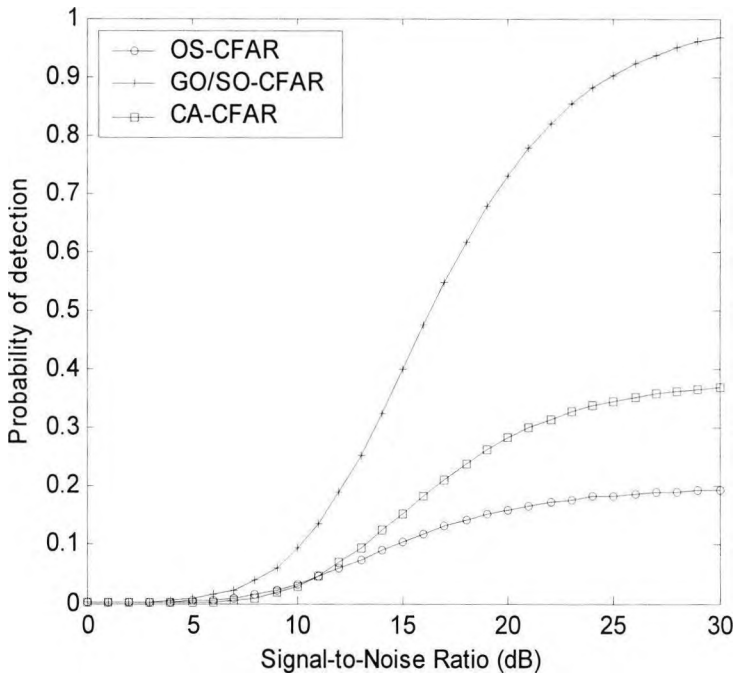


Figure 6.7: $P_d$ of GO/SO-CFAR, CA-CFAR and OS-CFAR, with $r$=4, $K$=18 and INR = 25 dB

At the following analysis, MAT is used as the parameter for comparison among the different CFAR techniques. Because CA-CFAR is not suitable for non-homogeneous noise background from the above results, it is no longer analysed in this chapter. OS-CFAR (20, 10) is used for comparison, as it is shown in chapter 5 with best average performance in MAT.

Figure 6.8 shows the MAT for GO/SO-CFAR, GO-CFAR, SO-CFAR and OS-CFAR, when SNR = INR = 10dB. It can be seen that, when the CUT is not within clutter region, the MAT for all kinds of CFAR detectors increases with the number of cells covered by clutter region. GO-CFAR is the one with much longer MAT than the other CFAR detectors. This is because in GO-CFAR, the side with clutter region is always selected for noise level estimation, and the threshold is higher over estimated with more cells covered by clutter region. This leads to lower $P_d$, thus longer MAT. SO-CFAR is the one with shortest MAT, as the side in clear region is always selected for noise level estimation.

When the CUT is covered, SO-CFAR becomes the one with longest MAT, and this is caused by the high $P_{fa}$ from low threshold estimation. In this situation, GO-CFAR becomes the one with shortest MAT, as it selects the side of reference window with higher noise level, and when CUT is covered, it is the correctly estimated. There are no significant differences between the MAT for GO/SO-CFAR and OS-CFAR (20, 10) in this figure.

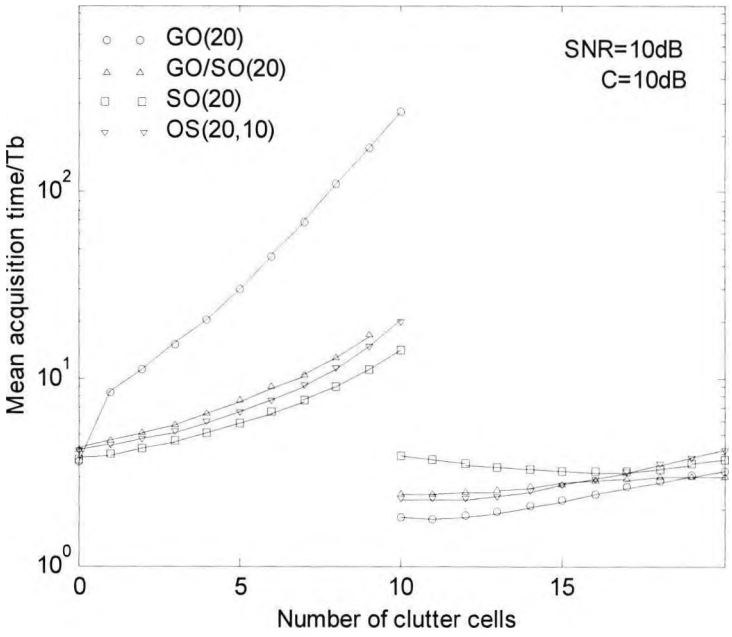


Figure 6.8: MAT of GO/SO-CFAR, GO-CFAR, SO-CFAR and OS-CFAR, SNR = CNR = 10dB

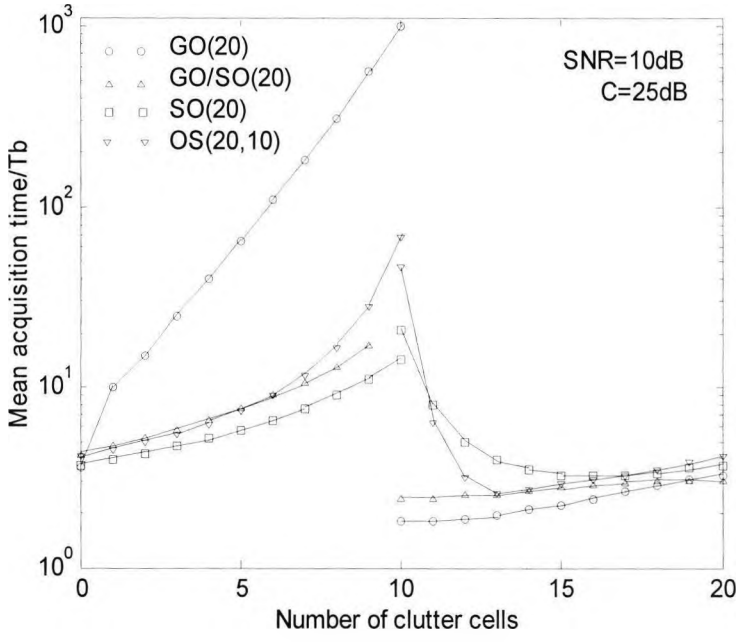


Figure 6.9: MAT of GO/SO-CFAR, GO-CFAR, SO-CFAR and OS-CFAR, SNR = 10dB, CNR = 25dB

In figure 6.9, the CNR is increased to check the difference among the MAT of the above four CFAR detectors. It can be seen that, when the CNR is high, OS-CFAR (20, 10) has long MAT when the clutter edge is near the CUT. But for GO/SO-CFAR, the MAT looks same as that in figure 6.8 with CNR= 10 dB, it still maintains at a short level.

In real mobile communication with clutter or multiple targets, as the number and strength of interfering targets are unknown and may be changing all the time. All the CFAR detectors except GO/SO-CFAR will suffer poor MAT at certain situations. Therefore, for better overall performance, GO/SO-CFAR is the best choice for unknown channel conditions.

## 6.4 Summary

In this chapter, GO/SO-CFAR technique with automatic censoring was analysed for non-homogeneous noise background. The equation for $P_d$ and $P_{fa}$ are derived for the proposed GO/SO-CFAR circuit. From the results, it was observed that with clutter edge detection, GO/SO-CFAR performs much better than the other CFAR techniques, especially for high CNR noise background. OS-CFAR (20, 10) can maintain the MAT at an average level for low CNR situation, but for high CNR, it suffers rapid degradation. GO-CFAR and SO-CFAR only perform well when the clutter edge is in certain position. However, in real mobile communications, the noise condition and clutter edge information are unknown for the receiver. Therefore, to ensure a short MAT, GO/SO-CFAR detector is a good choice. Also, other CFAR techniques with automatic censoring may do.

# CHAPTER 7

# Implementation of GO/SO-CFAR in FPGA

## 7.1 Introduction to FPGA

FPGA technique was invented by Xilinx in 1984. And since then, it has been developed from single glue logic chips to replacing custom application-specific integrated circuits (ASICs) and processors for signal processing and control applications. The FPGA market is expected to grow from $1.9 billion in 2005 to $2.75 billion by 2010 [53].

### 7.1.1 What is FPGA

At the highest level, FPGAs are reprogrammable silicon chips. Using pre-built logic blocks and programmable routing resources, you can configure these chips to implement custom hardware functionality without ever having to pick up a breadboard or soldering iron. You develop digital computing tasks in software and compile them down to a configuration file or bit stream that contains information on how the components should be wired together. In addition, FPGAs are completely reconfigurable and can instantly take on a brand new "personality" when you recompile a different bit stream.

### 7.1.2 Advantages of FPGA

a) Performance

Taking advantage of hardware parallelism, FPGAs exceed the computing power of DSP by breaking the paradigm of sequential execution and accomplishing more per clock cycle. BDTI, a noted analyst and benchmarking firm, released benchmarks showing how FPGAs can deliver many times the processing power per dollar of a DSP solution in some applications. Controlling Inputs and Outputs (I/O) at the hardware level provides faster response times and specialized functionality to closely match application requirements.

b) Time to market

FPGA technology offers flexibility and rapid prototyping capabilities in the face of increased time-to-market concerns. You can test an idea or concept and verify it in hardware without going through the long fabrication process of custom ASIC design. You can implement incremental changes to iterate on an FPGA design within hours instead of weeks. Commercial off-the-shelf (COTS) hardware is also available with different types of I/O already connected to a user-programmable FPGA chip. The growing availability of high-level software tools decrease the learning curve with layers of abstraction and often include valuable IP cores (pre-built functions) for advanced control and signal processing.

c) Cost

The nonrecurring engineering expense of custom ASIC design far exceeds that of FPGA-based hardware solutions. The large initial investment in ASICs is easy to justify for Original Equipment Manufacturers (OEMs) shipping thousands of chips per year, but many end users need custom hardware functionality for the tens to hundreds of systems in development. The very nature of programmable silicon means that there is no cost for

fabrication or long lead times for assembly. As system requirements often change over time, the cost of making incremental changes to FPGA designs are quite negligible when compared to the large expense of repinning an ASIC.

d) Reliability

While software tools provide the programming environment, FPGA circuitry is truly a "hard" implementation of program execution. Processor-based systems often involve several layers of abstraction to help schedule tasks and share resources among multiple processes. The driver layer controls hardware resources and the operating system manages memory and processor bandwidth. For any given processor core, only one instruction can execute at a time, and processor-based systems are continually at risk of time-critical tasks pre-empting one another. FPGAs, which do not use operating systems, minimize reliability concerns with true parallel execution and deterministic hardware dedicated to every task.

e) Long-term maintenance

As mentioned earlier, FPGA chips are field-upgradeable and do not require the time and expense involved with ASIC redesign. Digital communication protocols, for example, have specifications that can change over time, and ASIC-based interfaces may cause maintenance and forward compatibility challenges. Being reconfigurable, FPGA chips are able to keep up with future modifications that might be necessary. As a product or system matures, you can make functional enhancements without spending time redesigning hardware or modifying the board layout.

## 7.2 Matched Filter Implementation

As discussed in chapter 3, the critical path for the MF with direct form FIR structure is very long. Therefore, MF with transposed form FIR structure is selected, as it has critical path with only one multiplier and adder [35].

The coefficients of MF are input from PN code generator as shown in the figures 7.1 and 7.2. These figures show the detailed structure of MF with traditional and transposed form FIR.

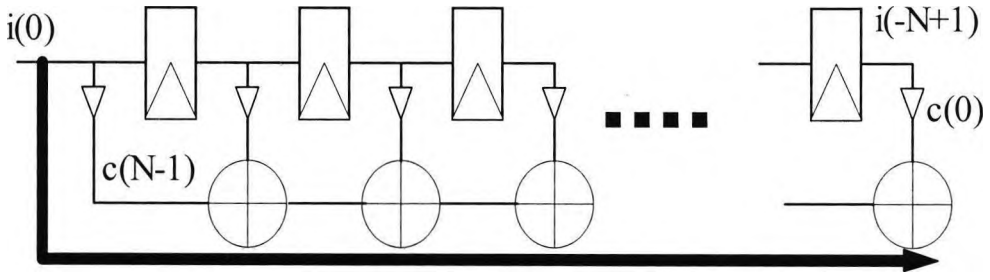


Figure 7.1: MF with traditional FIR structure

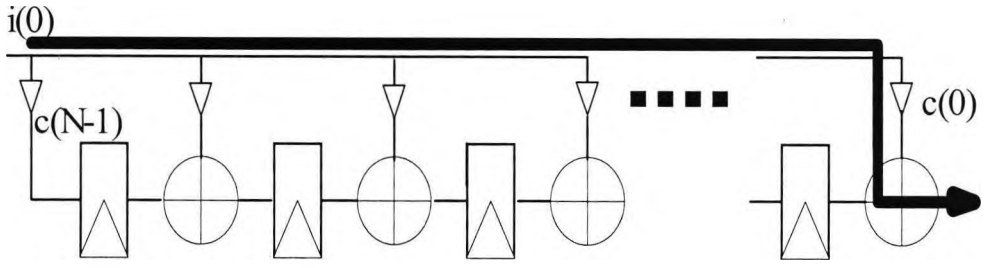


Figure 7.2: MF with transposed form FIR structure

In this thesis, MF with 256 coefficients is used in implementation, and input i(t) is sampled at 8 bits. The coefficients are used in the later part of this chapter.

### 7.2.1 Adders in MF

When adding two 2's components of B bits wide, the result may be B+1 bits. The carry out of Most Significant Bit (MSB), is to prevent the overflow [54]. Therefore, when $2^N$ numbers of $B$ bits wide components are added together, $N+B$ bits output is needed. Figure 7.3 illustrate the adders for MF with $2^N$ taps.

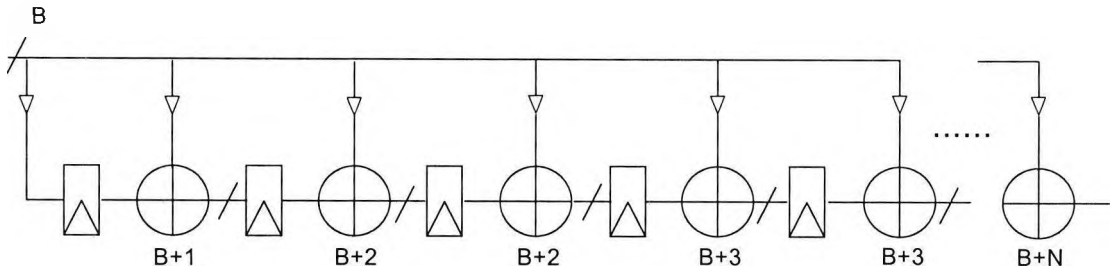


Figure 7.3: Bits of adders in MF with $2^N$ taps

In MF of 256 taps with initial input at 8 bits, the adders of different length needed is shown in table 7.1

Table 7.1: Adders with different length needed for implementation

| Bits of adder | 9 | 10 | 11 | 12 | 13 | 14 | 15 | 16 |
|---|---|---|---|---|---|---|---|---|
| Number of adders | 1 | 2 | 4 | 8 | 16 | 32 | 64 | 128 |

### 7.2.2 Multipliers in MF

XOR gates can be used for multiplier in MF. Table 7.2 shows the truth table of a two input XOR gate.

Table 7.2: Truth table for two input XOR gate

| Input A | Input B | Output C |
|---|---|---|
| 0 | 0 | 0 |
| 0 | 1 | 1 |
| 1 | 0 | 1 |
| 1 | 1 | 0 |

One carry-in bit is needed for the next adder stage, when it is 1, negation is applied. Figure 7.4 shows the detailed structure of a tap of MF. In MF with transposed form FIR, the one input of adder is always directly from the input, and another is from the pipeline of adder chains.

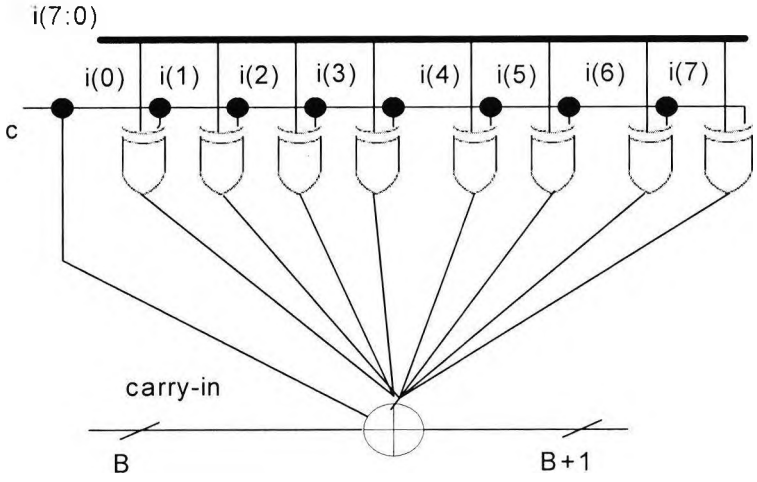


Figure 7.4: Structure of a tap in MF

## 7.3 GO/SO-CFAR Implementation

In this thesis, 20 reference cells are used in reference window, plus the CUT, there are totally 21 cells. All this cells are with same bit length as the output from MF, which is 16 bits.

For GO/SO-CFAR, comparators, adders, multipliers and memory for data storage are required.

a) Adders

Adders are needed to calculate the noise level. In the worst situation, when no cell is censored from the reference window, all the 20 cells are added for noise level estimation. Therefore, it will be 5 bits longer than the output of MF. Thus, the output of adder will be 21 bits, and a 21 bits adder is required [55].

b) Comparators

Comparators are needed for ranking process of GO/SO-CFAR detector. For 16 bits input, a 16 bits comparator is needed. And, decision process, a comparator with same bit length of the output is needed. Therefore, another 21 bits comparator is needed. Figure 7.5 shows the N bits comparator.

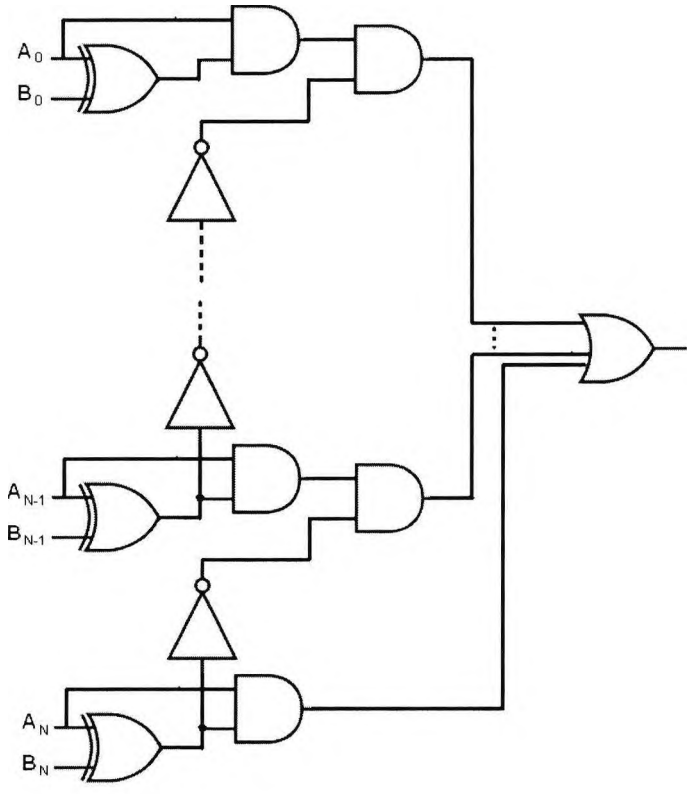


Figure 7.5: N bits comparator

c) Multiplier

Only 1 Multiplier is needed, which is used for threshold calculation for detector of clutter edge and code acquisition.

d) Memory for storage

When all the cells are ranked, they must be stored somewhere. Therefore a memory with 20 spaces and 16 bits in length is needed.

### 7.3.1 Simulations

Very High speed integrated circuit Description Language (VHDL) was used in programming for FPGA function description. The codes for MF and a tap of MF are coded in software ISE from Xlinx, and they are shown in Appendices D, and E.

In this thesis, MATLAB system generator was used for simulation, and both VHDL codes and block diagrams were used in Black box of MATLAB, like showing in figure 7.6. In this figure, PN code sequence with AWGN is designed as received signal, and block *Match filter* is linked to the VHDL codes in Appendices D and E. Threshold for detection is calculated by block of *CFAR detector*.

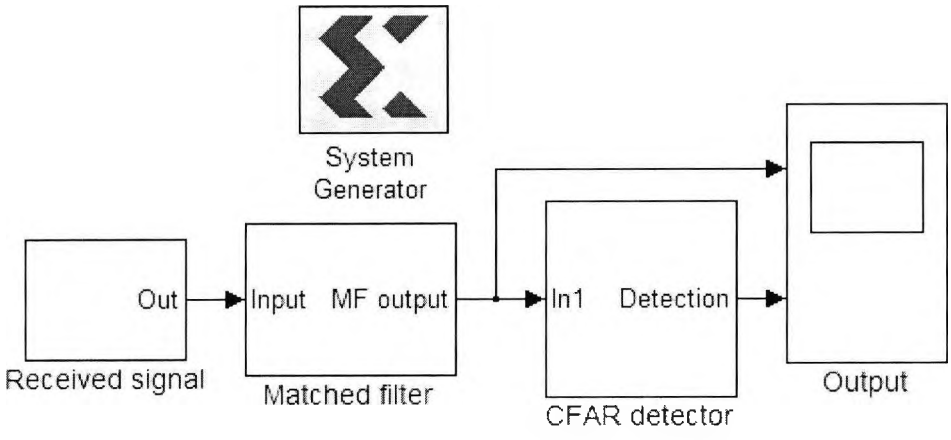


Figure 7.6: Simulation blocks in MATLAB

Figure 7.7 shows the MF and the detection output for the PN code with 256 chip length.

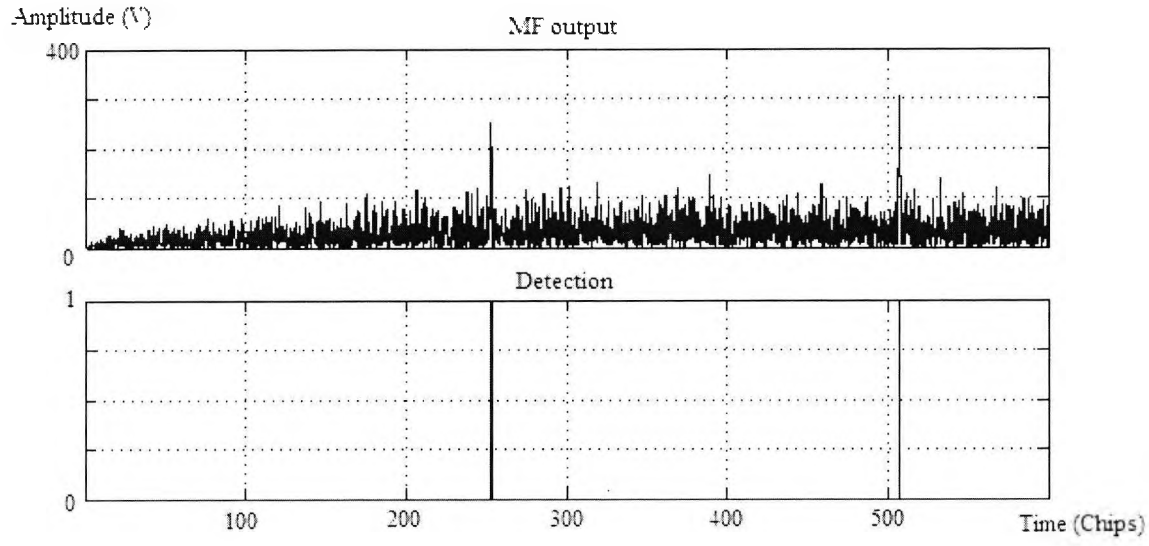


Figure 7.7: Simulation results for MF and detection output

After simulation in MATLAB, Modelsim was used as simulator for the pre-route and post-route design to verify the logic function and timing.

### 7.3.2 Hardware requirement for GO/SO-CFAR

After the simulations, the circuit of MF with GO/SO-CFAR detector was successfully laid out on "Virtex-E XCV600E" of Xilinx, which were used in my previous research for the lay out of a CA-CFAR detector. For the GO/SO-CFAR detector, 2638 slices out of total 6912 in the device is used, which is about 38.2% of the total and the delay is 4.933 ns. Compared with the requirement of CA-CFAR at 32.3% of the total slices and 4.799 ns delay [39] and that of OS-CFAR in [55], GO/SO-CFAR requires more hardware, and longer delay. However, the difference is slight.

## 7.4 Summary

In this chapter, the FPGA technique is introduced and the advantage of using it is listed. The components of MF and GO/SO-CFAR, like adders, multipliers and comparators are clearly introduced in structure. By using MATLAB, Modelsim and ISE in simulation, the implementation of GO/SO-CFAR is achieved in "Virtex-E XCV600E" of Xilinx. Compared with the requirement of implementing a CA-CFAR detector or OS-CFAR detector, GO/SO-CFAR detector needs a bit more hardware and has slightly longer delay.

# CHAPTER 8

## Conclusion and Future Works

### 8.1 Conclusion

The main aim of this thesis was to design a PN acquisition approach that can give good performance in a mobile communication with unknown noise condition. GO/SO-CFAR is a CFAR technique with automatic censoring. The results showed that with automatic censoring, the MAT for GO/SO-CFAR can remain short for varying non-homogeneous noise background, while other CFAR techniques suffers rapid degradation. This thesis provides the detailed information for the analysis of PN code acquisition in DSSS systems.

In chapter 1, a general introduction of mobile communications was presented. The history of mobile communications began from TDMA. Due to the capacity limitation of TDMA, it can not meet the growing number of users. Therefore, CDMA is developed as the alternative to solve this problem. Two important implementation areas of CDMA are power control and PN code synchronisation. In this thesis, PN code synchronisation is researched.

Chapter 2 produced a brief introduction about CDMA and SS systems. CDMA was defined as a multiple access technique based on SS principles. All the three types of SS

systems: THSS, FHSS and DSSS are studied and the comparison was made among them. The importance of PN code in SS systems was stated, and study of different types of PN code sequence was carried out. Autocorrelation and cross-correlation values were used the parameters to evaluate the PN sequences. It was stated that Gold s has better cross-correlation performance than M-Sequence, while M-Sequence has better autocorrelation property. Therefore, M-Sequence is suitable for PN code acquisition.

In chapter 3, the theory of PN code acquisition was presented. It was highlighted that PN code acquisition was the process of obtaining a rough estimate of delay in the received PN code signal. In operation, it can be described as searching for the peak of autocorrelation of two sets of code. Correlation could be performed with active or passive MF. The MF is preferred because it is faster in acquisition but it is more complex in implementation. Serial and parallel is another selection for correlator structure, while serial search scheme is preferred for less complexity. In chapter 3, it was shown that $P_d$, $P_{fa}$ and MAT are popular parameters for performance analysis of PN code acquisition circuits, and MAT is the most important one.

In chapter 4, the study of mobile communication channels was carried out. It was noted that the received signal was attenuated by the fading effect in the channel. Ricean fading channel is common in rural areas, and Rayleigh fading channel normally exist in sub-urban or urban areas. Also, depending on the noise in channel, homogeneous noise background and non-homogeneous noise background were introduced. Non-homogeneous noise background can be separated as multiple targets and clutter transmission. They are used in the analysis for CFAR detectors in chapters 5 and 6.

Chapter 5 presented an analysis of CFAR detectors. Firstly, it illustrated why adaptive threshold was needed for mobile communications by showing the limitations of fixed threshold in non-constant noise environment. The models for CA-CFAR, OS-CFAR, GO-CFAR and SO-CFAR are introduced by reviewing the literatures, and the equations for $P_d$, $P_{fa}$ were derived. The lengths of reference window and order parameter $K$ in OS-CFAR are both simulated to check how they will affect the performance. And then, for properly chosen parameters, the performance of CA-CFAR, OS-CFAR, GO-CFAR and SO-CFAR detectors were analysed for both homogeneous noise background and non-homogeneous noise background in terms of $P_d$, $P_{fa}$ and MAT. The results illustrated that in a homogeneous noise background, all the four types of CFAR detectors perform well with high $P_d$, and short MAT. However, in non-homogeneous noise background, they suffer rapid degradation, especially for CA-CFAR. OS-CFAR, GO-CFAR and SO-CFAR only may perform well in some situations, and can not maintain it.

Technique of clutter edge detection for clutter transmission, and in multiple targets communications was introduced in chapter 6. This was used for counting interfering targets. Simulation results illustrated that, when there was less clutter cells, the $P_{dc}$ was higher, and for clutter with higher CNR, the $P_{dc}$ was higher as well. With clutter edge detection technique, CFAR detectors could censor the cells with different SNR as the CUT. GO/SO-CFAR is one of the automatic censored CFAR techniques, and its performance was analysed in this chapter. It was observed that when CNR was not high, GO/SO-CFAR and OS-CFAR (20, 10) could keep MAT at a low level for all the possible positions of clutter edge. But for high CNR clutter, OS-CFAR (20, 10) suffered long MAT, when the clutter edge was near the CUT. Therefore, for a channel with unknown

noise condition, GO/SO-CFAR is a much better choice than the other non-automatic censoring CFAR detectors.

Chapter 7 illustrated the FPGA implementation of GO/SO-CFAR detector with MF. The detailed structures of MF and GO/SO-CFAR circuit are shown in the relevant figures clearly. MATLAB, ISE, and Modelsim were used for the simulator. After route and timing, the GO/SO-CFAR detector with MF was laid out on the Xilinx device "Virtex-E XCV600E". Considering the slices used in device and the delay, GO/SO-CFAR detector was slightly more complex than CA-CFAR and OS-CFAR detectors, and had a little long delay, which can be neglected. However, considering the significant advantage in MAT for channels with unknown noise conditions, GO/SO-CFAR is a good choice for implementation.

## 8.2 Future works

In this thesis, GO/SO-CFAR is suggested for application in mobile communications with unknown noise conditions. However, GO/SO-CFAR is not the only CFAR technique with automatic censoring. In GO/SO-CFAR detectors, all the uncensored cells are added, and the average value is estimated as the noise level. Considering OS-CFAR is used for noise level estimation after censoring, one cell can be selected from remaining cells for noise level estimation. The performance of OS-CFAR detector with automatic censoring should be better than non-automatic censoring CFAR detectors. But if it is compared with GO/SO-CFAR, the results are still unpredictable. Therefore, other CFAR techniques with automatic censoring will be an interesting topic for future research.

Also, in this thesis, single dwell is used in the detector structure. However, in some publications it is suggested that double-dwell detector which has a short first dwell and longer second dwell gives better performance. It is because the short dwell takes short time to find a possible phase of acquisition, and the longer dwell is used to check whether it is correctly detected or not. Later, I will do some research on this by myself.

## Appendix A: Probability of false alarm for GO-CFAR and SO-CFAR

In this appendix, the probability of false alarm for GO-CFAR and SO-CFAR are derived. From [56], it can be obtained that

$$\int_0^{\phi} y^m \exp(-qy)dy = m!q^{-(m+1)} \times \left\{1 - \sum_{j=0}^{m} (yq)^j \exp(-qy)/j!\right\} \tag{A.1}$$

Considering the case that $n = N/2$ cells in leading window contains noise power with $\lambda = \gamma_1$ in equation (5.1), and with $\lambda = \gamma_2$ in the lagging window. The PDF $f_i(y)$ and CDF $F_i(y)$ of $Z_1$ and $Z_2$ in equation (5.20) can be presented as

$$f_i(y) = \frac{1}{n}\gamma_i^{-n} y^{n-1} \exp(-y/\gamma_i)/(n-1)! \quad i = 1, 2 \tag{A.2}$$

$$F_i(y) = 1 - \frac{1}{n}\exp(-y/\gamma_i)\sum_{j=0}^{n-1}(y/\gamma_i)^j/j! \tag{A.3}$$

The MGF of $Z$ in equation (5.21) can be obtained as

$$\begin{aligned}
M_Z(T) &= \int_0^{\infty} f_Z(y)\exp(-Ty)dy \\
&= \int_0^{\infty} f_1(y)F_2(y)\exp(-Ty)dy \\
&+ \int_0^{\infty} f_2(y)F_1(y)\exp(-Ty)dy \\
&= (1+\gamma_1 T/n)^{-n} - \sum_{j=0}^{n-1}\binom{n+j-1}{j}\gamma_1^{-n}\gamma_2^{-j} \times \{1/\gamma_1 + 1/\gamma_2 + T/n\}^{-(n+j)} \\
&+ (1+\gamma_2 T/n)^{-n} - \sum_{j=0}^{n-1}\binom{n+j-1}{j}\gamma_2^{-n}\gamma_1^{-j} \times \{1/\gamma_1 + 1/\gamma_2 + T/n\}^{-(n+j)}
\end{aligned} \tag{A.4}$$

By setting $\gamma_1 = 1$ and $\gamma_2 = 1 + C$, the $P_{fa}$ for GO-CFAR in special case is shown in equation (5.37)

In general case, we can just let n cells in lagging window with $\lambda = \gamma_3$. And in leading window, let n-r cells with $\lambda = \gamma_1$ and r cells with $\lambda = \gamma_2$.

$$Z_1 = \frac{1}{n}\sum_{i=n+1}^{2n} X_i \sim CDF = G(n,\gamma_3) \tag{A.5}$$

$$Z_2 = \frac{1}{n}\sum_{i=1}^{n-r} X_i + \sum_{i=n-r+1}^{n} X_i = \frac{1}{n}(W_1 + W_2) \tag{A.6}$$

Where $W_1 \sim G(n-r,\gamma_1)$ and $W_2 \sim G(r,\gamma_2)$. The PDF of $Z_2$ can be given by

$$f_2(y) = \int_0^y f_{w_1(x)} f_{w_2(y-x)} dx \tag{A.7}$$

Where $f_{w_1}$ and $f_{w_2}$ are the PDF of $W_1$ and $W_2$. Using equation A.1, A.7 can be written as [17]

$$f_2(y) = A_0 \sum_{i=0}^{r-1} A_1(i)\{y^i \exp(-y/\gamma_2) - \sum_{m=0}^{n-2-i} y^{m+i}(1/\gamma_1 - 1/\gamma_2)^m \times \exp(-y/\gamma_1)/m!\} \tag{A.8}$$

where

$$A_0 = \{(r-1)!(n-r-1)!\gamma_1^{n-r}\gamma_2^r\}^{-1} \tag{A.9}$$

and

$$A_1(i) = \binom{r-1}{i} \frac{(n-2-i)!(-1)^{r-1-i}}{(1/\gamma_1 - 1/\gamma_2)^{n-1-i}} \tag{A.10}$$

The CDF of $Z_2$ can be obtained by integrating $f_2(y)$ and is given by [17]

$$F_2(y) = 1 - A_0 \sum_{i=0}^{r-1} A_1(i)\{i!\gamma_2^{i+1} \sum_{j=0}^{i} (y/\gamma_2)^j \times \exp(-y/\gamma_2)/j! - \sum_{mi=0}^{n-2-i} \frac{\gamma_1^{m+i+1}(m+i)!}{m!} \times (1/\gamma_1 - 1/\gamma_2)^m \sum_{k=0}^{m+i} (y/\gamma_1)^k \times \exp(-y/\gamma_1)/k!\} \tag{A.11}$$

The MGF of $Z$ can be written as

$$
\begin{aligned}
M_Z(T) &= \int_0^{\infty} f_Z(y)\exp(-Ty)dy \\
&= \int_0^{\infty} f_1(y)F_2(y)\exp(-Ty)dy + \int_0^{\infty} f_2(y)F_1(y)\exp(-Ty)dy \\
&\overset{\Delta}{=} I_1 + I_2
\end{aligned}
\tag{A.12}
$$

where

$$
\begin{aligned}
I_1 &= M_{Y_1}(T) - [A_0/(n-1)!]\gamma_3^{-n}\sum_{i=0}^{r-1} A_1(i) \\
&\times\{B_1(i)\sum_{j=0}^{i} B_2(j,T) - \sum_{m=0}^{n-2-i} B_3(m,i)\sum_{k=0}^{m+i} B_4(k,T)\}
\end{aligned}
\tag{A.13}
$$

and

$$
\begin{aligned}
I_2 &= M_{Y_2}(T) - A_0\sum_{i=0}^{r-1} A_1(i)\sum_{j=0}^{n-1} A_2(j) \\
&\times\{A_3(i,j,T) - \sum_{m=0}^{n-2-i} A_4(i,j,m,T)\}
\end{aligned}
\tag{A.14}
$$

where

$$M_{Y_1}(T) = (1+\gamma_3 T/n)^{-n}$$

$$M_{Y_1}(T) = (1+\gamma_1 T/n)^{r-n}(1+\gamma_2 T/n)^{-r}$$

$$A_2(j) = \gamma_3^{-j}/j!$$

$$A_3(i,j,T) = (i+j)!(1/\gamma_2 + 1/\gamma_3 + T/n)^{-(i+j+1)}$$

$$A_4(i,j,m,T) = \frac{(m+i+j)!(1/\gamma_1 - 1/\gamma_2)^m}{m!(1/\gamma_2 + 1/\gamma_3 + T/n)^{m+i+j+1}}$$

and

$$B_1(i) = i!\gamma_2^{i+1}$$

$$B_2(j,T) = \frac{(n+j-1)!}{j!\gamma_2^j(1/\gamma_2 + 1/\gamma_3 + T/n)^{n+j}}$$

$$B_3(m,i) = (m+i)!\gamma_1^{m+i+1}(1/\gamma_1 - 1/\gamma_2)^m/m!$$

$$B_4(k,T)=\frac{(n+k-1)!}{k!\gamma_1^k(1/\gamma_1+1/\gamma_3+T/n)^{n+k}}$$

If the CUT is covered by clutter region, then $\gamma_1=1$, $\gamma_2=1+C$, $\gamma_3=1+C$, otherwise, $\gamma_1=1$, $\gamma_2=1+C$, $\gamma_3=1$, and the $P_{fa}$ can be calculated by replacing $T$ with $T/(1+C)$.

In case of multiple targets communication, with r interfering targets, we can just let $\gamma_1=1$, $\gamma_2=1+I$ and $\gamma_3=1$ to calculated $P_{fa}$ and $P_d$.

# Appendix B: Probability of false censoring

In this appendix, the probability of false censoring is analysed. Considering $N$ independent identically distributed exponential samples are ranked as

$$X_{(1)} \le X_{(2)} \le \ldots \le X_{(N)} \tag{B.1}$$

Assuming the parameter of distribution of parent population of the order statistics are with equal unity. The joint MGF of $X_{(k_{c1}+1)},\ldots,X_{(k_{c1}+k+1)}$ is defend to be

$$\Phi_{X_{(K_{c1}+1)},\ldots,X_{(K_{c1}+K+1)}}(\omega_1,\ldots,\omega_{k+1}) = E\left[\exp\left\{-\sum_{j=1}^{K+1}\omega_j X_{(K_{c1}+j)}\right\}\right] \tag{B.2}$$

Equation (B.2) can be written as

$$\begin{aligned}
&\Phi_{X_{(K_{c1}+1)},\ldots,X_{(K_{c1}+K+1)}}(\omega_1,\ldots,\omega_{k+1}) \\
&= \int_{0<x_{K_{c1}+1}\le\ldots\le x_{k_{c1}+K+1}<\infty} dx_{k_{c1}+1}\ldots\int dx_{K_{c1}+K+1} \\
&\times f_{X_{(K_{c1}+1)},\ldots,X_{(K_{c1}+K+1)}}(x_{K_{c1}+1},\ldots,x_{K_{c1}+K+1}) \\
&\times \exp\left\{-\sum_{j=1}^{K+1}\omega_j x_{K_{c1}+j}\right\}
\end{aligned} \tag{B.3}$$

$f_{X_{(K_{c1}+1)},\ldots,X_{(K_{c1}+K+1)}}(x_{K_{c1}+1},\ldots,x_{K_{c1}+K+1})$ denotes the joint PDF of $X_{(K_{c1}+1)},\ldots,X_{(K_{c1}+K+1)}$ which is given by [57]

$$\begin{aligned}
&f_{X_{(K_{c1}+1)},\ldots,X_{(K_{c1}+K+1)}}(x_{K_{c1}+1},\ldots,x_{K_{c1}+K+1}) \\
&= \frac{1}{K_{c1}!(N-K_{c1}-K-1)!}\,per(A)
\end{aligned} \tag{B.4}$$

Where

$$per(A)=\begin{vmatrix} P(x_{K_{c1}+1}) & \cdots & P(x_{K_{c1}+1}) \\ \vdots & \ddots & \vdots \\ P(x_{K_{c1}+1}) & \cdots & P(x_{K_{c1}+1}) \\ p(x_{K_{c1}+1}) & \cdots & p(x_{K_{c1}+1}) \\ \vdots & \ddots & \vdots \\ p(x_{K_{c1}+K+1}) & \cdots & p(x_{K_{c1}+K+1}) \\ \overline{P}(x_{K_{c1}+K+1}) & \cdots & \overline{P}(x_{K_{c1}+K+1}) \\ \vdots & \ddots & \vdots \\ \overline{P}(x_{K_{c1}+K+1}) & \cdots & \overline{P}(x_{K_{c1}+K+1}) \end{vmatrix} \tag{B.5}$$

Where $p(.)$, $P(.)$, and $\overline{P}(.)$ denotes the density, the distribution and the reliability function of the sequence $X_1,...,X_N$.

Using equation (B.3) to (B.5), the joint MGF of $X_{(k_{c1}+1)},...,X_{(k_{c1}+k+1)}$ can be written as

$$\begin{aligned} &\Phi_{X_{(K_{c1}+1)},...,X_{(K_{c1}+K+1)}}(\omega_1,...,\omega_{k+1}) \\ &= \frac{N!}{K_{c1}!(N-K_{c1}-K-1)!}\int_{0<x_{K_{c1}+1}\le...\le x_{k_{c1}+K+1}<\infty} dx_{k_{c1}+1}... \\ &\times \int dx_{K_{c1}+K+1}[1-\exp(-x_{K_{c1}+1})]^{K_{c1}} \\ &\times \exp[-(N-K_{c1}-K-1)x_{K_{c1}+K+1}] \\ &\times \exp\left\{-\sum_{j=1}^{K+1}\omega_j x_{K_{c1}+j}\right\} \end{aligned} \tag{B.6}$$

Using binomial formula, $[1-\exp(-x_{K_{c1}+1})]^{K_{c1}}$ can be expended as

$$[1-\exp(-x_{K_{c1}+1})]^{K_{c1}} = \sum_{v=0}^{K_{c1}}\binom{K_{c1}}{v}(-1)^v \exp(-vx_{K_{c1}+1}) \tag{B.7}$$

Substituting (B.7) into (B.6), we can get

$$
\begin{aligned}
&\Phi_{X_{(K_{c1}+1)},\ldots,X_{(K_{c1}+K+1)}}(\omega_1,\ldots,\omega_{k+1}) \\
&= \sum_{v=0}^{K_{c1}} \binom{K_{c1}}{v} (-1)^v \frac{N!}{K_{c1}!(N-K_{c1}-K-1)!} \\
&\times \int_{0<x_{K_{c1}+1}\le\ldots\le x_{K_{c1}+K+1}<\infty} dx_{k_{c1}+1}\cdots \\
&\times \int dx_{K_{c1}+K+1} \exp(-vx_{K_{c1}+1}) \\
&\times \exp[-(N-K_{c1}-K-1)x_{K_{c1}+K+1}] \\
&\times \exp\left\{-\sum_{j=1}^{K+1}\omega_j x_{K_{c1}+j}\right\}
\end{aligned}
\tag{B.8}
$$

Using transformation

$$
\begin{aligned}
Y_1 &= X_{(K_{c1}+1)} \\
Y_2 &= X_{(K_{c1}+2)} - X_{(K_{c1}+1)} \\
&\vdots \\
Y_{K+1} &= X_{(K_{c1}+K+1)} - X_{(K_{c1}+K)}
\end{aligned}
\tag{B.9}
$$

Whose Jacobian is equal to unity. The random variables $Y_1,\ldots,Y_{K+1}$ are statistically independent.

$$
X_{(K_{c1}+j)} = \sum_{i=1}^{j} Y_i \tag{B.10}
$$

Substituting (B.10) into (B.6), we can obtain that

$$
\begin{aligned}
&\Phi_{X_{(K_{c1}+1)},\ldots,X_{(K_{c1}+K+1)}}(\omega_1,\ldots,\omega_{k+1}) \\
&= \frac{N!}{K_{c1}!(N-K_{c1}-K-1)!}\prod_{j=2}^{K+1}\left(\frac{1}{\beta_j+N-K_{c1}+1-j}\right) \\
&\times \sum_{v=0}^{K_{c1}}\binom{K_{c1}}{v}(-1)^v\left(\frac{1}{v+N-K_{c1}+\beta_1}\right)
\end{aligned}
\tag{B.11}
$$

Where

$$
\beta_j = \sum_{i=j}^{K+1}\omega_i \tag{B.12}
$$

If we define a statistics $R$ to be

$$R = X_{(K_{c1}+K+1)} - T(K \mid K_{c1}) \sum_{j=1}^{K+1} X_{(K_{c1}+j)} \tag{B.13}$$

For GO/SO-CFAR, with $R_k = X_{(k+l)} - S_k T_k$, if $K_{c1} = 0$, R is equivalent test statistics for the censoring procedures.

By using equation (6.7), the MGF of $R$ is obtained as

$$\begin{aligned} \Phi_{R(K|K_{c1})}(\omega) &= \frac{N!}{K_{c1}!(N - K_{c1} - K - 1)!} \\ &\cdot \prod_{j=2}^{K+1} \left( \frac{1}{\omega[1 - T(K \mid K_{c1})(K - j + 1)] + N - K_{c1} + 1 - j} \right) \\ &\cdot \sum_{v=0}^{K_{c1}} \binom{K_{c1}}{v} (-1)^v \left( \frac{1}{\omega[1 - KT(K \mid K_{c1})] + N + v - K_{c1}} \right) \end{aligned} \tag{B.14}$$

Substitute (B.14) into (6.4), the probability of false censoring can be calculated by

$$\begin{aligned} P_{fc} &= \left( \frac{N!}{K_{c1}!(N - K_{c1} - k)!(K - 1)!} \right) \\ &\cdot \left( \frac{1}{[1 + (N - K_{c1} - K)T(K \mid K_{c1})]^{K-1}} \right) \\ &\cdot \sum_{v=0}^{K_{c1}} \binom{K_{c1}}{v} (-1)^v \left( \frac{1}{v + K[1 + (N - K_{c1} - K)T(K \mid K_{c1})]} \right) \end{aligned} \tag{B.15}$$

## Appendix C: Probability of false alarm

In this appendix, $P_{fa}$ of detector is derived. Firstly, we define the statistic $X$ to be

$$X = \sum_{j=K_{c1}+1}^{N-K_{c2}} X_{(j)} \tag{C.1}$$

Where $X_{(1)},...,X_{(N)}$ is the order statistics of the I.I.D samples $X_1,...,X_N$. If $K_{c1}=0$, it is the estimator of noise level in GO/SO-CFAR detector when the CUT is in clear region. If $K_{c2}=0$, it is the estimator of noise level in GO/SO-CFAR detector when the CUT is in the clutter region.

The MGF of $X$ is defined to be

$$\Phi_X(\omega) = E[\exp(-\omega X)] \tag{C.2}$$

The joint MGF of $X_{(K_{c1}+1)},...,X_{(N-K_{c2})}$ can be obtained by

$$\Phi_{X_{(K_{c1}+1)},...,X_{(N-K_{c1})}}(\omega_{K_{c1}+1},...,\omega_{N-K_{c2}}) = E\left[\exp\left\{-\sum_{j=K_{c1}+1}^{N-K_{c2}} \omega_j X_j\right\}\right] \tag{C.3}$$

Set $\omega_j = \omega$, and $N-K_{c2} = K_{c1}+K+1$. Using (B.9), (C.1), (C.2) and (C.3), the MGF of $X$ can be written as

$$\begin{aligned}\Phi_X(\omega) &= \frac{N!}{K_{c1}!K_{c2}!} \\ &\times \prod_{j=2}^{K+1}\left(\frac{1}{\omega(N-K_{c1}-K_{c2}-j+1)+(N-K_{c1}-j+1)}\right) \\ &\times \sum_{v=0}^{K_{c1}}\binom{K_{c1}}{v}(-1)^v\left(\frac{1}{\omega(N-K_{c1}-K_{c2})+(N+v-K_{c1})}\right)\end{aligned} \tag{C.4}$$

# Appendix D: VHDL code for Matched Filter

```
library ieee ;
use ieee.std_logic_1164.all;
use ieee.numeric_std.all;

entity mf is
  generic(
    iInDataWidth    : integer := 8;
    iOutDataWidth   : integer := 16;
    iNumOfChips     : integer := 256
  );
  port(
    InCode : in  std_logic ;
    InData : in  std_logic_vector (iInDataWidth-1 downto 0);
    SysClk : in  std_logic;
    SysRst : in  std_logic;
    Result : out std_logic_vector (iOutDataWidth-1 downto 0)
  );
end mf ;

architecture virtex of mf is

  type ResultArray is array (iNumOfChips-1 downto 0)
    of std_logic_vector(iOutDataWidth-1 downto 0);

  signal Zero     : std_logic_vector(iOutDataWidth-1 downto 0);
  signal lOutCode : std_logic_vector(iNumOfChips-1 downto 0);
  signal lResult  : ResultArray;

  component mf_parallel_tap
    generic (
      iInDataWidth    : integer := 8;
      iOutDataWidth   : integer := 16;
      );
    port (
      InCode  : in  std_logic;
      InData  : in  std_logic_vector (iInDataWidth-1 downto 0);
      PrevTap : in  std_logic_vector (iOutDataWidth-1 downto 0);
      SysClk  : in  std_logic;
      SysRst  : in  std_logic;
      OutCode : out std_logic;
      Result  : out std_logic_vector (iOutDataWidth-1 downto 0)
      );
  end component;

begin

  Zero <= (others => '0');

  FirstTap : mf_parallel_tap
    generic map (
      iInDataWidth    => iInDataWidth,
      iOutDataWidth   => iOutDataWidth,
        )
    port map (
      InCode  => InCode,
      InData  => InData,
      PrevTap => Zero,
      SysClk  => SysClk,
```

```
      SysRst  => SysRst,
      OutCode => lOutCode(0),
      Result  => lResult(0)
    );

  InstTaps: for I in 1 to iNumOfChips-1 generate
    Taps : mf_parallel_tap
      generic map (
        iInDataWidth    => iInDataWidth,
        iOutDataWidth   => iOutDataWidth,
      )
    port map (
        InCode  => lOutCode(I-1),
        InData  => InData,
        PrevTap => lResult(I-1),
        SysClk  => SysClk,
        SysRst  => SysRst,
        OutCode => lOutCode(I),
        Result  => lResult(I)
      );
  end generate InstTaps;

  GenerateResult : Result <= lResult(iNumOfChips-1);

end virtex;
```

# Appendix E: VHDL code for a Matched Filter tap

```
library ieee ;
use ieee.std_logic_1164.all;
use ieee.numeric_std.all;

entity mf_parallel_tap is
  generic(
    iInDataWidth    : integer := 8;
    iOutDataWidth   : integer := 16;
  );
  port(
    InCode  : in  std_logic;
    InData  : in  std_logic_vector (iInDataWidth-1 downto 0) ;
    PrevTap : in  std_logic_vector (iOutDataWidth-1 downto 0) ;
    SysClk  : in  std_logic;
    SysRst  : in  std_logic;
    OutCode : out std_logic;
    Result  : out std_logic_vector (iOutDataWidth-1 downto 0)
  );
end mf_parallel_tap ;

architecture Virtex of mf_parallel_tap is

  signal sInData    : signed(iInDataWidth-1 downto 0);
  signal sPrevTap   : signed(iOutDataWidth-1 downto 0);
  signal sAddSubOut : signed(iOutDataWidth-1 downto 0);
  signal sPipe      : signed(iOutDataWidth-1 downto 0);
  signal lCodeData  : std_logic;

begin

  sInData  <= signed(InData);
  sPrevTap <= signed(PrevTap);

    SingleTap : process (SysClk, SysRst)
    begin
    if (SysRst = '1') then
      sAddSubOut <= (others => '0');
      lCodeData  <= '0';
    elsif (SysClk'event and SysClk = '1') then
      lCodeData <= InCode;
      if  (lCodeData = '0') then
        sAddSubOut <= sPrevTap + sInData;
      else
        sAddSubOut <= sPrevTap - sInData;
      end if;
    end if;
  end process SingleTap;

   GeneratePipeline : process (SysClk)
   begin
    if (SysClk'event and SysClk = '1') then
      sPipe <= sAddSubOut;
    end if;
  end process GeneratePipeline;

  FeedThruCode   : OutCode <= lCodeData;
  GenerateResult : Result  <= std_logic_vector(sPipe);
  end Virtex
```

# Published Works

[1] B. Wei, M. Sharif, A. Almaini, and T. Binnie, "PN Code Acquisition with a CA-CFAR Adaptive Matched Filter using FPGA", in *Proceeding of International Conference on Systems, Signals and Image Processing,* Budapest, Hungary, September 21-23, 2006, pp. 123-126

[2] B. Wei, M. Sharif, T. Binnie, and A. Almaini, "Adaptive PN Code Acquisition in Multi-path Spread Spectrum Communications using FPGA", in *Proceeding of International International Symposium on Signals, Circuits and Systems,* Iasi, Romania, July 12-13, 2007, pp. 573-576

# PUBLISHED PAPER(S) NOT INCLUDED WITH THESIS

# References

[1] *IEEE Personal Communications,* Special Issue on IMT-2000: Standards Efforts of the ITU.vol. 4, August 1997

[2] T. Ojanpera and R. Prasad, "An Overview of Air Interface Multiple Access for IMT-2000/UMTS, "*IEEE Communications Magazine,* vol. 36. No. 6 September 1998, pp. 82-95

[3] T. S. Rappaport, Wireless Communications: Principles and Practice,2nd ed., New York: Prentice Hall, 2002

[4] A. M. Viterbi and A. J. Viterbi, "Erlang Capacity of a power controlled CDMA Systems, "*IEEE Journal on Selected Areas in Communications,* vol. 11, no. 6, August 1993, pp. 892-900

[5] D. M. Dicarlo and C. L. Weber, "Multiple Dwell Serial Search: Performance and Application to Direct Sequence Code Acquisition," *IEEE Transactions on Communications,* vol. 31, no. 5, May 1983, PP. 650-659

[6] S. Glisic and B. Vucetic, *Spread Spectrum CDMA Systems for wireless Communications,* Artech House Publishers, 1997

[7] A. J. Viterbi, *CDMA: Principles of Spread Spectrum Communication,* Addison Wesley Publishing Company, 1995

[8] J.S. Lee and L.E. Miller, *CDMA Systems Engineering Handbook,* Artech House Publishers, 1998

[9] M. K. Simon, J. K. Omura, R. A. Scholtz, B.K. Levitt, *Spread Spectrum Communications Handbook,* McGraw-Hill, Inc., 2002

[10] I. A. Glover and P. M. Grant, *Digital Communications,* 2nd ed., Prentice-Hall, 2003

[11] S. Bregni, *Synchronisation of Digital Telecommunications Networks,* John Wiley and Sons, Ltd. 2002

[12] B. Mahafza, *Radar Systems Analysis and Design using Matlab,* Chapman and Hall/CRC, 2002

[13] T. –T. Van Cao, "A CFAR thresholding approach based on test cell statistics", *IEEE Proceeding of Radar Conference.* April 2004, pp. 349-354

[14] M. Shor and N. Levanon, "Performance of order statistics CFAR", *IEEE Transactions on Aerospace and Electronic Systems,* vol. 27, no. 2, March 1991, pp. 214-224

[15] J. Guan, Y.N. Peng, Y. He, X.W. Meng, "Three types of distributed CFAR detection based on local test statistic", *IEEE Transactions on Aerospace and Electronic Systems,* vol. 38, no. 1, January 2002, pp. 278-288

[16] L. Zhao, W.X. Liu, X. Wu, J. S. Fu, "A novel approach for CFAR processors design", *IEEE Proceedings of Radar Conference,* May 2001, pp. 284-288

[17] P.P. Gandhi and S.A. Kassam, "Analysis of CFAR processors in nonhomogeneous background" *IEEE Transactions on Aerospace and Electronic Systems,* vol. 24, no. 4, July 1988, pp. 427-445

[18] Y. He, "Performance of some generalised modified order statistics CFAR detectors with automatic censoring technique in multiple target situations", *IEE Proceeding of Radar, Sonar and Navigation,* vol. 141, no. 4, August 1994, pp. 205-212

[19] C.-M. Cho, M. Barkat, "Moving ordered statistics CFAR detection for nonhomogeneous backgrounds", *IEE Proceeding of Radar and Signal Processing,* vol. 140, no. 5, October 1993, pp. 284-290

[20] S. D. Himonas, M. Barkat, "Automatic censored CFAR detection for nonhomogeneous environments", *IEEE Transactions on Aerospace and Electronic Systems,* vol. 28, no. 1, January 1992, pp. 286-304

[21] R. L. Peterson, R. E. Ziemer, D. E. Borth, *Introduction to Spread Spectrum Communications,* Prentice-Hall, Inc., 1995

[22] H. Harada and R. Prasad, *Simulation and Software Radio for Mobile Communications,* Artech House, 2002

[23] T. Hattori, S. Ogose, and M. Shafi, *Wireless Communications in the 21st Century,* IEEE Series on Digital and Mobile Communications, March 2002

[24] W. L. Root, W. B. Davenport, *An Introduction to the Theory of Random Signals and Noise,* Wiley-IEEE press, October 1987

[25] K. S. Zigangirov, *Theory of Code Division Multiple Access Communications,* IEEE, Inc., 2004

[26] K. Leonhard, *Designing CDMA2000 Systems,* John Wiley and Sons Ltd, 2004.

[27] S. Lee, *Spread Spectrum CDMA: IS-95 and IS-2000 for RF Communications,* McGraw-Hill, 2002

[28] E. H. Dinan and B. Jabbari, "Spreading Codes for Direct Sequence CDMA and Wideband CDMA Cellular Networks," *IEEE Communications Magazine,* September 1998, pp. 48-54

[29] R. Gold, "Optimal Binary Sequences for Spread Spectrum Multiplexing," *IEEE Transactions on Information Theory,* vol.IT-13 Oct. 1967, pp. 619-621

[30] IR. J. Meel, *Spread Spectrum (Introduction),* IWT HOBU-fonds, 1999

[31] T. F. Wong, *Spread Spectrum & CDMA,* Chapter 2, 1999

[32] M. Katz, *Code Acquisition in Advanced CDMA NeTworks,* Dissertation of University of Oulu, December 2002

[33] S. S. Rappaport and D. M. Grieco, "Spread-Spectrum Signal Acquisition: Methods and Technology," *IEEE Communications Magazine,* vol. 22, No. 6, June 1984, pp.6-21

[34] G. L. Turin, "An Introduction to Matched Filters," *IRE Transactions on Information Theory,* vol. IT-6, June 1960, pp. 311-329

[35] K. Chapman, P. Hardy, A. Miller, and M. George, "*CDMA Matched Filter Implementation in Virtex Devices"*, Application notes of Xilinx Company, January 2001

[36] J. A. Obiebi, *Adaptive PN Code Synchronisation in DS-CDMA Systems,* Phd Thesis of Napier University, October 2005

[37] R. B. Ward, "Acquisition of Pseudo noise Signals by Sequential Estimation," *IEEE Transactions on Communications,* COM-13, December 1965, pp.475-483

[38] W. Zhuang, "Noncoherent Hybrid Parallel PN Code Acquisition for CDMA Mobile Communications," *IEEE Transactions on Vehicular Technology,* vol. 45, no. 4, Nov. 1996, pp. 643-656

[39] B. Wei, M. Sharif, A. Almaini, and T. Binnie, "PN Code Acquisition with a CA-CFAR Adaptive Matched Filter using FPGA", in *Proceeding of International Conference on Systems, Signals and Image Processing,* Budapest, Hungary, September 21-23, 2006, pp. 123-126

[40] M. Patzold, *Mobile Fading Channels,* John Wiley and Sons Ltd, 2002

[41] B. Sklar, *Digital Communications: Fundamentals and Applications,* 2ed Edition, Prentice-Hall, 2001

[42] J. G. Proakis, *Digital Communications,* 4th edition., McGraw-Hill, 1995

[43] M. Skolnik. *Introduction to Radar Systems*: Third Edition. McGraw-Hill, New York, 2001

[44] N.L. Jonhson, S. Kotz, N. Balakrishnan, *Continuous Univariate Distributions.* Volume 1, 2nd Edition. Wiley, New York, 1994

[45] Gini, Greco, and Farina, "Clairvoyant and adaptive signal detection in non-Gaussian clutter: a data-dependent threshold interpretation", *IEEE Transactions on Signal Processing,* June 1999

[46] R. N. McDonough, A. D. Whalen, *Detection of Signals in Noise,* Academic Press, 1995

[47] H. M. Finn and R. S. Johnson, "Adaptive detection mode with threshold control as a function of spatially sampled clutter estimates," *RCA Review,* vol. 29, no. 3, 1968, pp. 414-464

[48] V. G. Hansen, "Constant false alarm rate processing in search radars," In *Proceeding of IEE International Radar Conference,* 1973, pp. 325-332

[49] V. G. Hansen and J. H. Sawyers, "Detection loss due to greatest-of-selection in a cell-averaging CFAR," *IEEE Transaction on Aerospace and Electronics Systems,* vol. 16, 1980, pp. 115-118

[50] G. V. Trunk, "Range resolution of targets using automatic detectors," *IEEE Transaction on Aerospace and Electronics Systems,* vol. 14, no. 5, 1978, pp. 750-755

[51] H. Rohling, "Radar CFAR thresholding in clutter and multiple targets situations," *IEEE Transaction on Aerospace and Electronics Systems,* vol. 19, no. 4, 1983, pp. 602-621

[52] X. Y. Xou, N. Morigana and T. Namekawa, "Direct evaluation of radar detection probabilities," *IEEE Transaction on Aerospace and Electronics Systems,* vol. 23, no. 4, 1987, pp. 418-423

[53] National Instruments, *The Field-Programmable Gate Array (FPGA): Expanding Its Boundaries,* InStat Market Research, April 2006

[54] CK. H. Deng, "A Burst Mode PN Acquisition Processor for Direct Sequence Spread-Spectrum" *Master thesis of University of California,* 1998

[55] B. Wei, M. Sharif, T. Binnie, and A. Almaini, "Adaptive PN Code Acquisition in Multi-path Spread Spectrum Communications using FPGA", in *Proceeding of International International Symposium on Signals, Circuits and Systems,* Iasi, Romania, July 12-13, 2007, pp. 573-576

[56] M. Weiss, "Analysis of some modified cell-averaging CFAR processors in multiple-target situations", *IEEE Transaction on Aerospace and Electronics Systems,* vol. 18, 1982, pp. 102-113

[57] R. J. Vaughan and W. N. Venables " Permanent expressions for order statistical," *Journal of Royal Statistical Society B,* Vol. 34, 1972, pp. 308-310